Modelling Eddy Current Effects for Degaussing Systems

M. C. Mascini

Technische Universiteit Delft

TU Delft

Modelling Eddy Current Effects for Degaussing Systems

by

M. C. Mascini

to obtain the degree of Master of Science
at the Delft University of Technology,
to be defended publicly on Thursday 29 July 2021 at 14:30.

Student number:	4393333	
Project duration:	9 November 2020 – 29 July 2021	
Thesis committee:	Prof. dr. ir. A. W. Heemink,	TU Delft
	Prof. dr. ir. M. B. van Gijzen,	TU Delft
	Dr. ir. E. S. A. M. Lepelaars,	TNO - TU Delft
	Ir. A. R. P. J. Vijn,	TU Delft

This thesis is confidential and cannot be made public until 29 July 2021.

An electronic version of this thesis is available at `http://repository.tudelft.nl/`.

Cover image: 'La voix des airs' by Rene Magritte (The Solomon R. Guggenheim Foundation, Peggy Guggenheim Collection, Venice, 1976).

TU Delft

Preface

This graduation project was a challenge, in a challenging time, and would not have been possible without the support and guidance of many people, who I would like to thank here.

Where to begin but with my direct supervisors Aad and Eugene. Since working with you both during Advanced Modeling in the first year of the Applied Mathematics MSc programme, I have been continuously amazed with the ease and grace with which you have guided me through this monster of a project. Aad, thank you for your friendliness, reassurance, and relativism. Eugene, thank you for your wisdom, eye for detail, and enthousiasm. I greatly enjoyed our weekly meetings, which always gave me a new healthy dose of motivation to tackle the problems at hand. Prof. Heemink, thank you for your trust and advice during our monthly progress meetings.

The rest of the TNO team deserves praise as well: thank you for making me feel welcome and at home (despite being literally ... at home). It's a pity I did not get to spend more time with everyone in person, as I'm sure we would've become great colleagues.

Then, on a more personal note, I would like to thank my family for always being ready to listen and offer support, during this project but also in general. I highly doubt I'd be here if I didn't have such a loving home to fall back on.

Thank you to all my friends - you know who you are. Weekends (and weeknights ...) with you gave me the power to push through the weekdays. Thanks to the ones who call, and the ones who like being called, and the ones who send random messages of support, and also to the ones who don't, but are there for me nonetheless.

Ita, thanks for dealing with me when I was a pain, and thanks for offering me some distraction when necessary. I'll miss sharing our little loft with you but I'm happy to have escaped the noise of the washing machine.

In the final weeks of this project, my great uncle ir. C. Beverloo passed away. The only person in the family who seemed to actually understand what I was working on, and an inspiration in character and kindness. Thank you.

M. C. Mascini
Rotterdam, 22 July 2021

Abstract

Eddy currents are currents which are induced in a conducting object by a varying magnetic field. These currents generate a magnetic field of their own. Modelling this phenomenon constitutes a diverse and challenging set of problems, for which many applications exist. One such application is the degaussing system of a naval ship. To guarantee safety on missions, a ship uses a degaussing system to reduce its magnetic signature. Being able to model the effect of eddy current fields is necessary to improve the accuracy of future degaussing systems.

This thesis will examine how eddy current effects can be modeled, and how such a model can be validated. An analytical solution for a sphere is derived and investigated. A boundary element method (BEM) is implemented, which is able to numerically approximate the electromagnetic fields in terms of the modified magnetic vector potential $\boldsymbol{A}^*$ and the reduced magnetic scalar potential φ. The approximation using the BEM is compared to the analytical solution. The BEM shows promising results, being able to model the shape of the magnetic signature of a sphere accurately. The model is also applied to more realistic geometries resembling naval ships, making it a strong candidate for further development and potential implementation in a future degaussing system.

Contents

Notation

Vectors will be denoted in bold, e.g. the velocity $\boldsymbol{v}$. Electromagnetic fields in the time domain will be denoted in calligraphic capitals, with vector fields being denoted in bold, e.g. the magnetic flux density $\boldsymbol{\mathcal{B}}$. For any vector quantity, the magnitude of a vector will once again be denoted by a regular capital, i.e. $r = |\boldsymbol{r}|$. Unit vectors are denoted by a hat, i.e. $\hat{\boldsymbol{r}} = \boldsymbol{r}/|\boldsymbol{r}|$. Line integrals will be denoted by $\int \mathrm{d}\boldsymbol{l}$, and surface integrals by $\iint \mathrm{d}\boldsymbol{a}$.

The electromagnetic fields can be viewed in the frequency domain or in the time domain. To distinguish between these domains, the time domain field will be denoted by a calligraphic symbol (e.g. $\boldsymbol{\mathcal{B}}$) whereas the frequency domain field will be denoted by a regular symbol (e.g. $\boldsymbol{B}$).

Relevant SI units

An overview of the relevant physical quantities is given in Table 1. Where relevant, the symbol associated with the quantity is given as well. The units and their equivalent in SI base units are also given.

Measure	**Symbol**	**Unit name**	**Unit**	**SI units**
Time	t	second	s	-
Length	l	metre	m	-
Mass	m	kilogram	kg	-
Electric current	I	ampere	A	-
Charge	Q	coulomb	C	As
Force	F	newton	N	kgms^{-2}
Energy	E	joule	J	$\mathrm{kgm}^2\mathrm{s}^{-2}$
Frequency	f	hertz	Hz	s^{-1}
Magnetic flux density	$\boldsymbol{B}$	tesla	T	$\mathrm{kgs}^{-2}\mathrm{A}^{-1}$
Electrical conductance	$\mho$	siemens	S	$\mathrm{kg}^{-1}\mathrm{m}^{-2}\mathrm{s}^3\mathrm{A}^2$
Voltage	V	volt	V	$\mathrm{kgm}^2\mathrm{s}^{-3}\mathrm{A}^{-1}$
Power	P	watt	W	$\mathrm{kgm}^2\mathrm{s}^{-3}$
Electrical capacitance	C	farad	F	$\mathrm{kg}^{-1}\mathrm{m}^{-2}\mathrm{s}^4\mathrm{A}^2$
Electrical inductance	L	henry	H	$\mathrm{kgm}^2\mathrm{s}^{-2}\mathrm{A}^{-2}$
Electric field	$\boldsymbol{E}$	volt per metre	Vm^{-1}	$\mathrm{kgms}^{-3}\mathrm{A}^{-1}$
Magnetic field	$\boldsymbol{H}$	ampere per metre	Am^{-1}	Am^{-1}
Current density	$\boldsymbol{J}$	ampere per square metre	Am^{-2}	Am^{-2}
Magnetization	$\boldsymbol{M}$	ampere per metre	Am^{-1}	Am^{-1}
Permittivity	ϵ	farad per metre	Fm^{-1}	$\mathrm{kg}^{-1}\mathrm{m}^{-3}\mathrm{s}^4\mathrm{A}^2$
Magnetic permeability	μ	henry per metre	Hm^{-1}	$\mathrm{kgms}^{-2}\mathrm{A}^{-2}$
Electrical conductivity	σ	siemens per metre	Sm^{-1}	$\mathrm{kg}^{-1}\mathrm{m}^{-3}\mathrm{s}^3\mathrm{A}^2$
Charge density	ρ	coulomb per cubic metre	Cm^{-3}	$\mathrm{Am}^{-3}\mathrm{s}$
Magnetic moment	$\boldsymbol{m}$	ampere squared metre	Am^2	Am^2

Table 1: Overview or relevant physical quantities.

1 Introduction

1.1. Context and motivation

The history of naval warfare dates back over three millennia, to ancient civilizations such as the Phoenicians, the Egyptians, and the Greek. Of course, naval technology has come a long way from the triremes and galleys of old. An active area of research is the subject of signature reduction. The signature of a vessel consists of all the physical signals by which it is detectable and identifiable. Among others, this includes its optical signature, its acoustic signal, the pressure waves it produces underwater, and its magnetic signature. The subject of this research is the magnetic signature of the ship, which refers to the magnitude and shape of the magnetic field surrounding the ship. Signature reduction is crucial for vessel safety, in part because of the ever-present risk of magnetic influence mines. These mines incorporate advanced sensing technologies and decision-making algorithms to optimize mine usage. A clear magnetic signature, which reveals information about a vessel's size, class, heading, speed, and other properties, may trigger such a mine, with devastating consequences.

Before one can investigate how to reduce the magnetic signature, one must understand what causes it. There are four major contributions to a ship's magnetic signature [15]:

- Ferromagnetism, which is induced in the ferromagnetic steel of the ship by the Earth's magnetic field.
- Eddy currents, which is induced in any conducting material in the ship by the rolling, pitching and yawing of the ship in the Earth's magnetic field.
- Electric currents flowing into the sea from the ship due to its cathodic protection system.
- Stray currents from shipboard active circuits.

Ferromagnetism is the largest contributor to the magnetic signature. In general, ferrous steel is used for the construction of naval vessels. This includes the hull, bulkheads, engines, and various other equipment. Being ferromagnetic, these structures have a permanent magnetization. In addition to this permanent magnetization, they also generate an induced magnetic field in the homogeneous Earth magnetic field.

The second largest contributor to the magnetic signature are eddy currents. Eddy currents are electrical currents which are generated in conducting materials which are subjected to a varying magnetic field. Equivalently, they are generated as the conducting material rotates within a homogeneous background field. These electrical currents generate a magnetic field surrounding the object. In the case of naval vessels, this effect is strongest for rolling motions, which have a larger angular rotation rate than pitching or yawing motions [15].

The third contributor is the cathodic protection system. The ship, being made of multiple electrically conducting materials with a difference in electrochemical potential, forms a battery in the salty seawater. The steel of the ship's hull will act as the anode, and the nickel-aluminum-bronze of the propeller will act as cathode [16]. The currents running through this battery corrode the ship's hull, and therefore a cathodic protection system is installed, which sends a voltage into several sacrificial zinc bars welded to the surface of the hull. These zinc bars act as anode, protecting the hull from corrosion. The corrosion currents contribute to the magnetic signature, but the magnitude of this contribution is relatively small.

The smallest contribution to the magnetic signature are those of stray fields, which are caused by currents running through shipboard active circuits, such as electrical engines, distribution cables, and breakers. The contribution of these stray fields is also relatively small.

To reduce the magnetic signature of a vessel, it is logical to begin by considering the largest contributor, ferromagnetism. Reduction of the ferromagnetic signature can be achieved in various ways. Passive reduction is possible by choosing a non-ferrous material, such as aluminum or titanium, for the construction of the ship [17]. However, this is not always feasible or affordable, and moreover some internal structures such as the engine must still be constructed from steel. Therefore, active signature compensation systems have been designed. Supposing that one knows the magnetization of the ship, it is then possible to calculate the induced magnetization, which is a function of the Earth's magnetic field at the ship's location as well as the its orientation within that field. The magnetic signature can then be actively canceled by making use of a degaussing system. The degaussing system consists of several coils, looping around the interior of the hull of the vessel in the cardinal directions, and a controller which supplies the coils with a current. The current through each coil generates a magnetic field. The currents are controlled in such a way that the magnetic field they generate counteracts the magnetic disturbance caused by the steel ship, thereby reducing the magnetic signature of the vessel ([15], [17]). Ideally, the coils are controlled in such a way that the field they generate is equal in magnitude and shape, but of opposite polarity, to the uncompensated field, and as such the magnetic signature is annihilated [17].

In order to effectively reduce the magnetic signature, it is important to be able to accurately determine the necessary coil currents for a given situation. In classical (open loop) degaussing systems, this is done by using a linear model, which is determined from measurements at a testing facility. The linear model takes as input the current homogeneous background field (which is known for each location and heading on the surface of the Earth) and outputs the currents necessary to counteract the induced magnetisation. This is combined with the predetermined currents for reduction of the permanent magnetisation, and the result is sent to the controller. Figure 1.2 shows a flowchart of these steps for an open loop degaussing system on the left. There is, however, a problem with open loop degaussing. The permanent magnetisation of the ferromagnetic object is not constant over time, as the object experiences hysteresis. Therefore, the classical degaussing system loses accuracy over time. The system must be recalibrated with the new permanent magnetisation, and the object may also be depermed to bring it back to a required state of magnetisation. Deperming is shown in Figure 1.1. At a special deperming range, several electrical cables are looped around the ship. When a current is applied to this cables, the resultant magnetic field influences the permanent magnetisation of the ship.

Figure 1.1: USS Harry S. Truman (CVN 75), a United States Navy aircraft carrier, being depermed at the Lambert's Point Deperming Station in Virginia. Note the electrical cables looping around the hull. (Source: `https://commons.wikimedia.org/wiki/File:US_Navy_051115-N-2984R-123_The_Nimitz-class_aircraft_carrier_USS_Harry_S._Truman_(CVN_75)_undergoes_a_deperming_evolution_at_the_Lambert%27s_Point_Deperming_Station_in_Norfolk,_Va.jpg`, Public Domain.)

A beter degaussing system can be developed which takes into account the changing permanent magnetization of the object. Such a Closed-Loop Degaussing (CLDG) system makes use of continuous on-board measurements of the current magnetic field near the vessel. With these measurements, the current magnetisation of the vessel can be calculated. Combined with the background field, this is then used as input for a non-linear model which determines the optimal currents for reduction of the magnetic signature (see the flowchart in Figure 1.2).

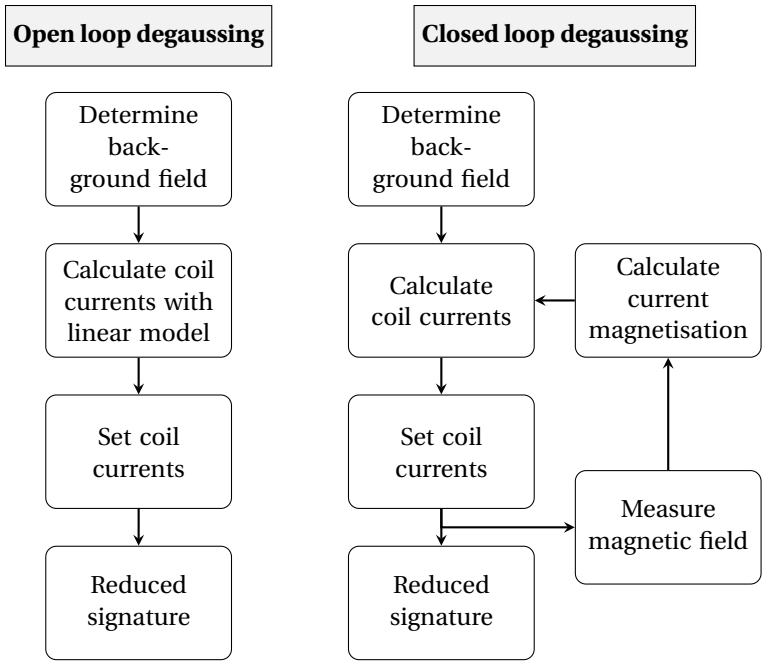

Figure 1.2: Overview of process steps in open loop degaussing (left) and closed loop degaussing (right).

A degaussing system as described above does not take into account the effects of eddy currents. This is because the magnitude of the eddy current fields is much smaller than the magnitude of the ferromagnetic field. However, technological advancements in both degaussing systems and magnetic influence mines may lead to increased importance of eddy current fields in the future. Degaussing systems are continuously improving the ability to hide the strong ferromagnetic signatures, and naval mines are becoming better at discerning faint signals from noise. Therefore, the magnetic field induced by eddy currents may become very important despite its smaller magnitude compared to the ferromagnetic signature. Additionally, for a closed-loop degaussing system, the eddy current fields influence the measurements from the on-board sensors.

This brings us to the main motivation for this research: **Being able to quickly and accurately calculate eddy current effects for naval vessels would be beneficial for future generations of degaussing systems. This increases the safety of future missions and deployments.**

1.2. State of the art

The problem under consideration is a vessel rolling in the Earth magnetic field. This periodic rolling motion causes eddy currents in the hull of the ship, which in turn generate a magnetic field. Figure 1.3 shows the magnetic field due to a steel cylindrical shell. At very low frequencies, there is no discernible eddy current effect: the magnetic field consists only of the induced magnetism of the steel shell. However, as the roll frequency increases, the magnetic field due to eddy currents becomes more apparent. Note that the eddy current field, in frequency space, is a complex field. The real part is referred to as the in-phase component, whereas the imaginary part is referred to as the quadrature component. The in-phase component, as the name implies, has the same phase as the roll frequency, whereas the phase of the quadrature component is offset by $\pi/2$, or a quarter cycle.

Investigating the eddy current field of an actual vessel is a much more complicated problem. The geometry is complex, consisting of internal structures such as bulkheads, as well as other large components such as the engine. One way of tackling this problem is by making use of commercial FEM packages such

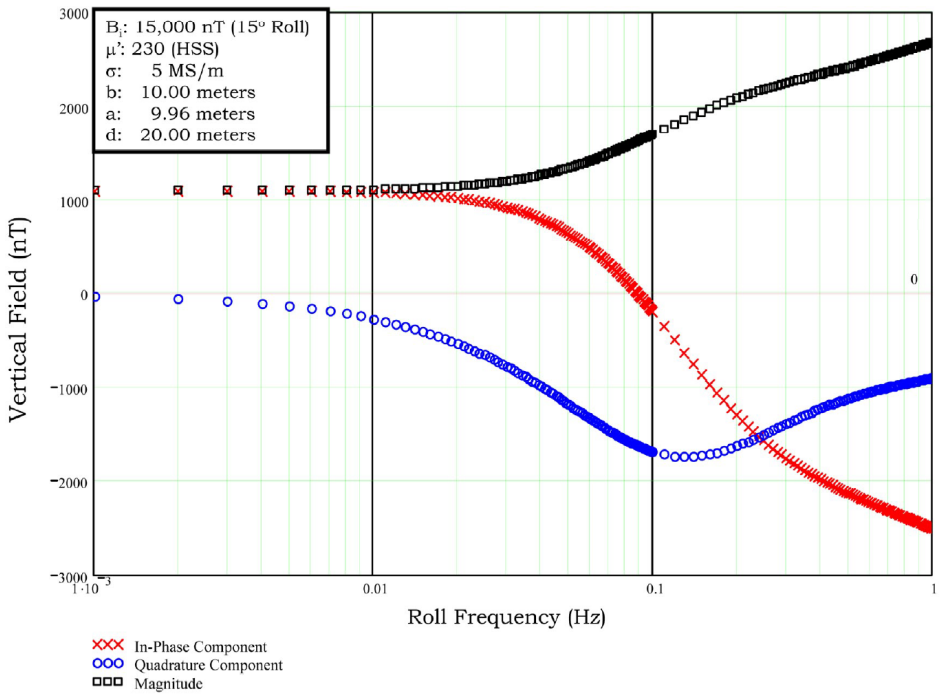

Figure 1.3: An example of the eddy current field generated by a two-dimensional steel (HSS) cylindrical shell (of outer diameter $b = 10$ m and inner diameter 9.96 m). The field at a depth of 20 m below the centre of the cylinder is shown. Note that the field consists of an in-phase component and a quadrature component. Image adapted from [17, p. 26].

as FLUX-3D or COMSOL. This was done by Birsan and Tan [6], for example. A finite element model of CFAV Quest, a Canadian vessel dedicated to research trials, was analyzed in FLUX-3D. The results were compared to measurements done during the international RIMPASSE trials [27], in which rolling motion was simulated in CFAV Quest at the Earth Field Simulator in Schirnau, Germany. This is a facility where a construction of coils surrounding the vessel can be used to create a chosen magnetic field strength and direction. There are two arrays of magnetic field sensors below the vessel which are used to measure the resultant fields. The result of this research is that the eddy current fields may have a significant contribution to a ship's signature, especially if the ship is degaussed. These results were corroborated by a similar trial with a scale model [31].

For the purposes of a degaussing system it is not desireable to depend on commercial software packages such as FLUX-3D. Instead, we would like to develop a model for the eddy current effect, which can then be implemented in the degaussing system. As such, it is necessary to dive into the physics governing the system, and determine an applicable method modelling and solving it.

The problem at hand is an eddy current problem. Eddy current problems find applications in many fields, and as such there has been much research into methods of modelling eddy currents. An everyday example is an induction stove, in which a coil supplied with an alternating current causes eddy currents in a pan, which in turn is heated by the resistive losses of the currents. Other applications include nondestructive examination of metal structures (such as aircraft parts and load-bearing steel structures), electromagnetic braking (e.g. for high-speed trains, or for power tools), and metal identification (e.g. for coins in vending machines, or for waste sorting). Eddy currents also emerge as an unwanted side effect which must be understood so it can be minimized. For example, alternating current power-lines are designed in such a way that losses due to eddy currents are minimized. Clearly, eddy current problems are a diverse collection, ranging from small geometries to very large geometries, and from low frequencies to very high frequencies. Each problem comes with its restrictions and requirements on the modelling method.

The most common approach for our subset of eddy current problems is to formulate the problem in terms of potentials, and then to make use of either a finite element method (FEM), or a boundary element method (BEM), or a hybrid model consisting of both methods. A relevant example is [46], in which a FEM model is used to determine the eddy current density in a ship. However, other approaches also exist. For example, a Partial Element Equivalent Circuit (PEEC) yields good results for shell-like geometries such as a car body

[22]. In particular, due to its circuit-like integral method, it works well for problems in which the geometry is coupled to an external electric circuit.

In summary: **there are islands of knowledge which must be bridged to achieve our research goals**. We must connect the demands of a degaussing system to the restrictions of a modelling method, taking into account the assumptions on the governing physics, as well as the knowledge gained from the results of experimental trials on marine vessels.

1.3. Research questions

The goal of this research project is to investigate and develop a modelling method for eddy current fields in the context of degaussing systems of naval vessels. Two main research questions arise from this:

- How can eddy current effects be modelled?
- How can the model be validated?

1.4. Report outline

The report is structured as follows. In Chapter 2 an overview of the relevant theory from the field of electromagnetics will be given. The Maxwell equations will be derived and discussed, and in conclusion an introduction to electromagnetic induction and thus eddy currents will be given. Subsequently, in Chapter 3, the eddy current problem is derived, which involves the quasi-magnetostatic approximation, and the time-harmonic Maxwell equations. An analytical solution for a magnetic and conducting sphere is then derived and analyzed. Having determined the problem which we would like to solve, we then focus on the different methods available for this in Chapter 4, at the end of which a motivated choice will be made for a boundary element method (BEM) implementation. This implementation will be fully described and derived in Chapter 5. Some prerequisite building blocks, such as the edge basis functions, are discussed in Chapter 6. With this, the model can be implemented and validated against the analytical model: this is done in Chapter 7. In this chapter, some approximations for other geometries will also be shown and discussed. Finally, the entire project will be discussed in the conclusion in Chapter 8. As this project marks a first exploration into the field of eddy current modelling, it offers many starting points for further research, which will also be discussed in this chapter.

2

Theory

The following sections contain the theoretical background of the physics and mathematics pertaining to electromagnetism. A short history of electromagnetism is given, which is adapted from the overview given in [11]. Following this, the derivation of Maxwell's equations is given, which is adapted from [14], [11] and [19].

2.1. From lodestones to electromagnets

The phenomenon of magnetism has been known and used since antiquity. Magnets occur naturally, for example in lodestones, which are magnetite-rich rocks magnetized by lightning strikes. These lodestones are common around the globe, and have been used by civilizations in Mesopotamia, Greece, China and America. Such lodestones were used to make a simple compass in China, which in turn allowed the Chinese to construct the street plans of certain towns in a grid-like layout. In these towns, areas built at different times are misaligned, since the horizontal component of Earth's magnetic field varies over time. In 1064, Zheng Gongliang discovered a technique with which iron could be permanently magnetized, leading to the first artificial magnets. With this, precise navigational compasses could be produced, allowing famous voyages such as those by Columbus and Cheng Ho to be completed.

It wasn't until 1600 that William Gilbert determined that the Earth itself was a magnet, as opposed to the common belief that it was the stars which attracted the compass's needle. In the 19^{th} century, many scientific breakthroughs contributed to a better understanding of magnetism. In 1820, Danish scientist Hans-Christian Ørsted accidentally discovered that a compass needle was deflected by a wire carrying a current, which was the first connection between magnetism and the young science of electricity. Mere weeks afterwards, André-Marie Ampère created the first electromagnet by winding a wire into a coil. Michael Faraday introduced the electric and magnetic fields, designed the electric motor in 1821, and connected magnetism to optics with the Faraday effect. All these discoveries and inventions were brought together in a unified theory by James Clerk Maxwell in 1864. These four equations, known as Maxwell's equations, will de derived in the following section.

By the beginning of the 20^{th} century, electricity and magnetism were used in many applications, such as street lighting and telegraph connections. Scientific research into magnetic theory was still being done, but some theories (such as Pierre Weiss's molecular field theory in 1907) challenged Maxwell's equations. The discrepancies were only explained once the theories of quantum mechanics and relativity were developed. The past century saw an ever-increasing understanding of the complexities of electromagnetism at the (sub)atomic level. Alongside these theoretical, an incredible amount of technological inventions have shaped our daily life. Still, it remains an active area of research, with new discoveries and inventions looming on the horizon.

2.2. Maxwell's Equations

2.2.1. Electrostatics

To derive Maxwell's equations, it is useful to begin by considering electrostatics, i.e. electric charges at rest. The field of interest here is the electric field, which will be described in steps. First, consider an electric point charge q (at position $\boldsymbol{r}_q$) and a test point charge Q (at position $\boldsymbol{r}_Q$), separated by a vector $\boldsymbol{r} = \boldsymbol{r}_Q - \boldsymbol{r}_q$. This

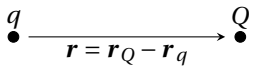

Figure 2.1: Two charges. The force on test charge Q can be computed using Coulomb's law.

situation is sketched in Figure 2.1. The units of charge are Coulomb (C) and the units of distance are meter (m). The force (in Newton (N)) on the test charge Q due to the charge q can be computed with Coulomb's Law:

$$\boldsymbol{F} = \frac{1}{4\pi\epsilon_0}\frac{qQ}{r^2}\hat{\boldsymbol{r}}, \tag{2.1}$$

where ϵ_0 is the permittivity of free space, which has a value of $8.85 \times 10^{-12}\,\mathrm{F\,m^{-1}}$, and the hat indicates a unit vector. Now suppose there is not one, but multiple point charges, and we are once again interested in the force that the test charge Q experiences due to these point charges. For multiple point charges $q_1, ..., q_n$ at various locations $\boldsymbol{r}_1, ..., \boldsymbol{r}_n$ from the test charge Q, the principle of superposition states that the total force on the test charge Q can be computed by

$$\boldsymbol{F} = \sum_{i=1}^{n} \boldsymbol{F}_i = \sum_{i=1}^{n} \frac{1}{4\pi\epsilon_0}\frac{q_i Q}{r_i^2}\hat{\boldsymbol{r}}_i. \tag{2.2}$$

Here, $r_i = |\boldsymbol{r}_i|$ is the distance from the test charge. To understand the effect of multiple point charges, it is useful to introduce the electric field $\boldsymbol{\mathcal{E}}(\boldsymbol{x})$ generated by the point charges, defined for this situation as:

$$\boldsymbol{\mathcal{E}}(\boldsymbol{x}) := \sum_{i=1}^{n} \frac{1}{4\pi\epsilon_0}\frac{q_i}{r_i^2(\boldsymbol{x})}\hat{\boldsymbol{r}}_i(\boldsymbol{x}), \qquad \boldsymbol{r}_i(\boldsymbol{x}) = \boldsymbol{x} - \boldsymbol{r}_{q_i}. \tag{2.3}$$

Note that $\boldsymbol{\mathcal{E}}$ is a function of position: physically, it is the force that a test charge would experience at a certain position. It has units $\mathrm{V\,m^{-1}}$. With this, the equation above becomes:

$$\boldsymbol{F} = Q\boldsymbol{\mathcal{E}}. \tag{2.4}$$

Extending this further, one can consider a continuous distribution of charges in a volume, having charge density at point $\boldsymbol{x}$ a charge density of $\rho(\boldsymbol{x})$ (in $\mathrm{C\,m^{-3}}$). The electric field produced by this volume is:

$$\boldsymbol{\mathcal{E}}(\boldsymbol{x}) = \frac{1}{4\pi\epsilon_0}\int \frac{\rho(\boldsymbol{x}')}{r(\boldsymbol{x})^2}\hat{\boldsymbol{r}}(\boldsymbol{x})\,\mathrm{d}\boldsymbol{x}', \qquad \boldsymbol{r}(\boldsymbol{x}) = \boldsymbol{x} - \boldsymbol{x}'. \tag{2.5}$$

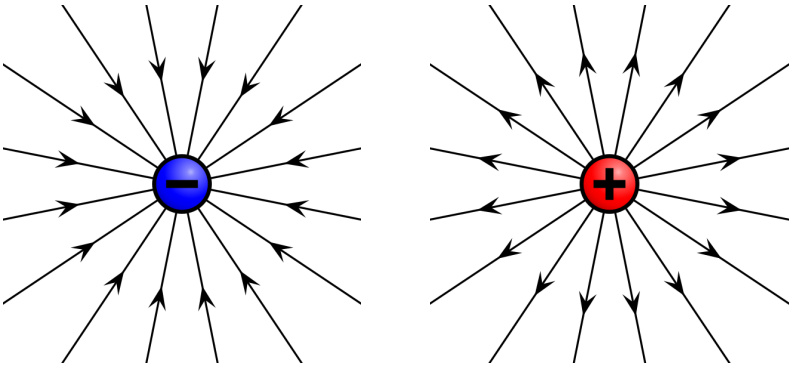

Figure 2.2: Field lines caused by a negative point charge (*left*) and a positive point charge (*right*). (Source: `https://commons.wikimedia.org/wiki/User:Geek3/VectorFieldPlot`, Creative Commons Attribution-Share Alike).

With this, it is possible to calculate the electric field strength and direction at a given position. It can be more informative to represent the electric field with field lines, instead of vector arrows. Field lines represent the strength (denser field lines corresponds to stronger field) and direction of the electric field. Field lines must have a beginning (at a positive charge) and an end (at a negative charge), and cannot cross (for this

would imply that the electric field has two different directions at the intersection). Figure 2.2 shows the field lines of a positive charge and a negative charge. The negative charge has a radial field line pattern, which field lines point into the charge, since a single positive test charge would experience a force towards the negative charge. Conversely, a single positive charge has radial field lines pointing outward, since it would repulse a positive charge (but attract a negative charge).

The fact that field lines always go from positive to negative charges, and do not cross, suggests that the flux through any closed surface is a measure of the total charge inside. This is in fact Gauss's law, which can be derived by first taking a surface integral over a closed spherical surface containing a single charge q at the origin:

$$\oiint \boldsymbol{\mathcal{E}} \cdot \mathrm{d}\boldsymbol{a} = \oiint \frac{1}{4\pi\epsilon_0}\frac{q}{r^2}\hat{\boldsymbol{r}} \cdot \mathrm{d}\boldsymbol{a} = \frac{1}{\epsilon_0} q. \tag{2.6}$$

Extending this to a surface containing multiple discrete point charges yields:

$$\oiint \boldsymbol{\mathcal{E}} \cdot \mathrm{d}\boldsymbol{a} = \sum_{i=1}^{n} \frac{1}{\epsilon_0} q_i. \tag{2.7}$$

Finally, considering a surface containing a continuous distribution of charges yields

$$\oiint \boldsymbol{\mathcal{E}} \cdot \mathrm{d}\boldsymbol{a} = \iiint \frac{\rho}{\epsilon_0} \mathrm{d}\boldsymbol{x}. \tag{2.8}$$

By the divergence theorem, the left-hand side can be rewritten to a volume integral of $\nabla \cdot \boldsymbol{\mathcal{E}}$. Since the integration volume was chosen arbitrarily, the integrands must be equal, leading to Gauss's law in differential form:

$$\nabla \cdot \boldsymbol{\mathcal{E}} = \frac{1}{\epsilon_0}\rho. \tag{2.9}$$

Figure 2.3 shows the field lines of multiple charges. Two opposite charges show field lines going from the positive charge to the negative charge, whereas two similar charges show field lines radiating outwards.

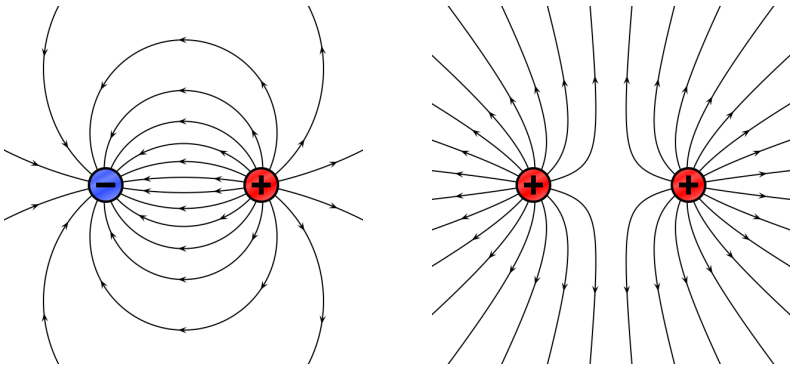

Figure 2.3: Field lines caused by two opposite point charges (*left*) and two identical point charges (*right*). (Source: `https://commons.wikimedia.org/wiki/User:Geek3/VectorFieldPlot`, Creative Commons Attribution-Share Alike).

Having found in Gauss's law an expression for the divergence of the field $\boldsymbol{\mathcal{E}}$, one might also be interested in an expression for the curl of the field $\boldsymbol{\mathcal{E}}$. This turns out to be rather simple. First consider a single charge q, located at the origin. The electric field due to this charge is

$$\boldsymbol{\mathcal{E}} = \frac{1}{4\pi\epsilon_0}\frac{q}{r^2}\hat{\boldsymbol{r}}. \tag{2.10}$$

Computing the line integral of $\boldsymbol{\mathcal{E}}$ between two points $\boldsymbol{a}$ and $\boldsymbol{b}$ yields

$$\int_{\boldsymbol{a}}^{\boldsymbol{b}} \boldsymbol{\mathcal{E}} \cdot \mathrm{d}\boldsymbol{l} = \int_{\boldsymbol{a}}^{\boldsymbol{b}} \frac{1}{4\pi\epsilon_0}\frac{q}{r^2} \cdot \mathrm{d}r \tag{2.11}$$

$$= \frac{1}{4\pi\epsilon_0}\left(\frac{q}{r_a} - \frac{q}{r_b}\right), \tag{2.12}$$

where we have made use of the transformation to spherical coordinates $\mathrm{d}\boldsymbol{l} = \mathrm{d}r\ \hat{\boldsymbol{r}} + r\ \mathrm{d}\theta\ \hat{\boldsymbol{\theta}} + r\sin\theta\ \mathrm{d}\varphi\ \hat{\boldsymbol{\varphi}}$, as described in Appendix A. For a closed path, this line integral is equal to zero, since $r_a = r_b$. Then, applying Stokes' theorem, this leads to

$$\nabla \times \boldsymbol{\mathcal{E}} = \mathbf{0}. \tag{2.13}$$

This also holds for multiple point charges and continuous distributions of charges. Note that this implies that the electric field $\boldsymbol{\mathcal{E}}$ can be described as the gradient of a scalar potential V:

$$\boldsymbol{\mathcal{E}} = -\nabla V. \tag{2.14}$$

For a more rigorous justification of the scalar potential, see Appendix C.

The expressions for the divergence and curl of the electric field $\boldsymbol{\mathcal{E}}$ are together known as Maxwell's equations for electrostatics:

$$\nabla \cdot \boldsymbol{\mathcal{E}} = \frac{1}{\epsilon_0}\rho, \tag{2.15}$$

$$\nabla \times \boldsymbol{\mathcal{E}} = \mathbf{0}. \tag{2.16}$$

2.2.2. Magnetostatics

When charges move steadily through a wire, this is called a steady current. The current is defined as the charge per unit time passing through a point in the wire, and is denoted by I, which has unit amperes (A). Note that the current is really a vector, since the charges are moving in a certain direction, but that given the fact that this direction is determined by the wire, it is generally not noted as a vector quantity explicitly. A steady current generates a magnetic field surrounding it. The magnetic flux density is denoted by $\boldsymbol{\mathcal{B}}$ and has units tesla (T). The magnitude and direction of the field (due to a current I running through a wire) at a certain position $\boldsymbol{x}$ can be computed by the Biot-Savart law:

$$\boldsymbol{\mathcal{B}}(\boldsymbol{x}) = \frac{\mu_0}{4\pi}\int \frac{I\ \mathrm{d}\boldsymbol{l}' \times \boldsymbol{r}}{|r|^3}. \tag{2.17}$$

In this equation, $\mathrm{d}\boldsymbol{l}'$ is a length along the wire, and μ_0 is the permeability of free space, which has a value of $4\pi \times 10^{-7}\,\mathrm{H\,m^{-1}}$. Figure 2.4 shows this situation: note that $\boldsymbol{r}$ is the vector from the source, i.e. the integration point along the wire, to the observation point $\boldsymbol{x}$.

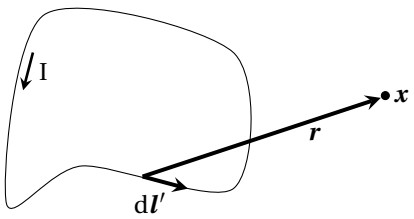

Figure 2.4: Sketch showing the wire with current I and its direction, the integration length $\mathrm{d}\boldsymbol{l}'$, and the vector $\boldsymbol{r}$.

With this, it is possible to calculate the strength of magnetic field generated by an infinite straight wire with a steady current I, at a distance of s from the wire, which turns out to be

$$B(s) = \frac{\mu_0 I}{2\pi s}. \tag{2.18}$$

The direction of the magnetic field at this point is such that it goes around the wire as would be expected from the right-hand rule (since there is a cross product in the Biot-Savart law). This is shown in Figure 2.5: an infinite wire, perpendicular to the page, produces a magnetic field which varies only with distance from the wire. The right-hand rule gives the direction: when the thumb points in the direction of the current, the fingers curl around the wire in the direction of the magnetic field.

This infinite wire example is illustrative in deriving an expression for the curl of $\boldsymbol{\mathcal{B}}$. Consider the line integral of a circular path at a distance s around the wire. Using the result obtained earlier, in Equation (2.18), one finds

$$\oint \boldsymbol{\mathcal{B}} \cdot \mathrm{d}\boldsymbol{l} = \oint \frac{\mu_0 I}{2\pi s}\,\mathrm{d}l = \frac{\mu_0 I}{2\pi s}\oint \mathrm{d}l = \mu_0 I. \tag{2.19}$$

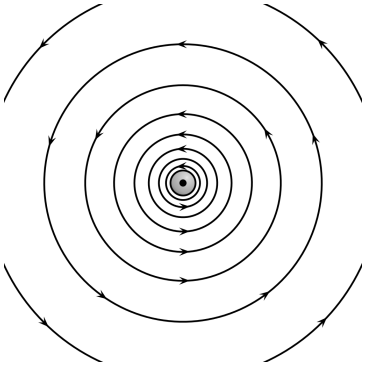

Figure 2.5: The magnetic field generated by a wire conducting a steady current. The wire is infinite and perpendicular to the page, the current is conducted out of the page. (Source: `https://commons.wikimedia.org/wiki/User:Geek3/VectorFieldPlot`, Creative Commons Attribution-Share Alike).

The chosen distance to the wire s does not appear in the answer. This is because the strength of the field decreases as the distance from the wire increases, and evidently these two effects cancel out so that the path integral yields the same result regardless of the distance s. In fact, it turns out that the path of the integral need not even be circular: any closed path around the wire would yield the same result.

By the principle of superposition, this equation extends simply to multiple infinite straight wires, each carrying a steady current $I_1, I_2, ..., I_n$. A line integral of a path around the bundle of wires would yield:

$$\oint \boldsymbol{\mathcal{B}} \cdot \mathrm{d}\boldsymbol{l} = \mu_0 (I_1 + ... + I_n). \tag{2.20}$$

Now, instead of considering multiple discrete wires, one could consider a continuous distribution of currents, with a volume current density $\boldsymbol{\mathcal{J}}$ (in $\mathrm{A/m^2}$). The enclosed current of this volume current density is $I = \int \boldsymbol{\mathcal{J}} \cdot \mathrm{d}\boldsymbol{a}$, where $\mathrm{d}\boldsymbol{a}$ is a surface integral element. This leads to

$$\oint \boldsymbol{\mathcal{B}} \cdot \mathrm{d}\boldsymbol{l} = \iint \mu_0 \boldsymbol{\mathcal{J}} \cdot \mathrm{d}\boldsymbol{a}. \tag{2.21}$$

Applying Stokes' theorem leads to

$$\iint (\nabla \times \boldsymbol{\mathcal{B}}) \cdot \mathrm{d}\boldsymbol{a} = \iint \mu_0 \boldsymbol{\mathcal{J}} \cdot \mathrm{d}\boldsymbol{a}, \tag{2.22}$$

which in turn yields

$$\nabla \times \boldsymbol{\mathcal{B}} = \mu_0 \boldsymbol{\mathcal{J}}. \tag{2.23}$$

This equation is called Ampère's law in differential form. It can in fact be derived directly from the Biot-Savart Law, and is therefore not limited to (bundles of) infinite straight wires, but is valid generally.

From the Biot-Savart law an expression for the divergence of the magnetic field can also easily be derived, which turns out to be zero:

$$\nabla \cdot \boldsymbol{\mathcal{B}} = 0. \tag{2.24}$$

This is interesting: it implies that magnetic field lines can not appear or disappear, but that they must form closed loops or extend to infinity. In other words, magnetic monopoles do not exist, and there is no such thing as magnetic charge. Figure 2.6 illustrates this: breaking a magnet into two parts does not leave one with a south and a north pole, but rather yields two magnets, each with a north and a south pole.

The fact that the magnetic field is divergence free implies that it can be described as the curl of a vector potential $\boldsymbol{A}$:

$$\boldsymbol{\mathcal{B}} = \nabla \times \boldsymbol{A}. \tag{2.25}$$

The justification for the vector potential is given in Appendix C. Note that the potential $\boldsymbol{A}$ is not unique, but must be fixed by way of a gauge.

The expressions for the divergence and curl of the magnetic field $\boldsymbol{\mathcal{B}}$ are together known as Maxwell's equations for magnetostatics:

$$\nabla \times \boldsymbol{\mathcal{B}} = \mu_0 \boldsymbol{\mathcal{J}}, \tag{2.26}$$

$$\nabla \cdot \boldsymbol{\mathcal{B}} = \boldsymbol{0}. \tag{2.27}$$

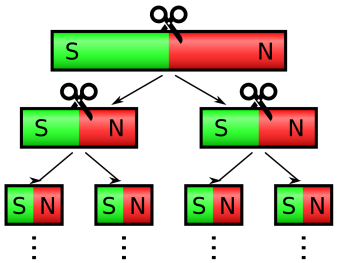

Figure 2.6: When a magnet is cut in half, the resulting pieces are smaller magnets, each with a north and south pole. It is impossible to separate these poles: magnetic monopoles don't exist. (Source: `https://commons.wikimedia.org/wiki/File:Repeated-cutting-a-magnet.svg`, Creative Commons Attribution-Share Alike)

2.2.3. Electrodynamics

When the charges are moving instead of stationary, the equations need to be adapted. Michael Faraday found that when the magnetic field changes, it induces an electric field. This is described by Faraday's law:

$$\nabla \times \boldsymbol{\mathcal{E}} = -\frac{\partial \boldsymbol{\mathcal{B}}}{\partial t}. \tag{2.28}$$

Note that Faraday's law agrees with the static equation for the curl of $\boldsymbol{\mathcal{E}}$ in case the magnetic field is static.

It is also necessary to adapt Ampère's law (equation (2.23) in the case of non-steady currents. The divergence of the left-hand side is always zero (since it is the divergence of a curl), but in the case of non-steady currents, the divergence of the right-hand side is generally not zero. This problem was fixed by Maxwell, who derived the following modification:

$$\nabla \times \boldsymbol{\mathcal{B}} = \mu_0 \boldsymbol{\mathcal{J}} + \mu_0 \epsilon_0 \frac{\partial \boldsymbol{\mathcal{E}}}{\partial t}. \tag{2.29}$$

The equations for curl and divergence of the electric and magnetic fields, with modifications to account for moving charges, are collectively known as Maxwell's equations, and are stated for completeness once more as a set:

$$\nabla \cdot \boldsymbol{\mathcal{E}} = \frac{1}{\epsilon_0}\rho, \qquad \text{Gauss's law,} \tag{2.30}$$

$$\nabla \times \boldsymbol{\mathcal{E}} = -\frac{\partial \boldsymbol{\mathcal{B}}}{\partial t}, \qquad \text{Faraday's law,} \tag{2.31}$$

$$\nabla \times \boldsymbol{\mathcal{B}} = \mu_0 \boldsymbol{\mathcal{J}} + \mu_0 \epsilon_0 \frac{\partial \boldsymbol{\mathcal{E}}}{\partial t}, \qquad \text{Ampères law with Maxwell's correction,} \tag{2.32}$$

$$\nabla \cdot \boldsymbol{\mathcal{B}} = 0. \tag{2.33}$$

Implicit in these equations is the continuity equation, which states that charge is conserved:

$$\nabla \cdot \boldsymbol{\mathcal{J}} = -\frac{\partial \rho}{\partial t}. \tag{2.34}$$

The continuity equation can be found by taking the divergence of Faraday's law, and filling into this the time-derivative of Gauss's law.

These equations govern the effect of charges and moving charges on the fields they produce. The converse, i.e. the force that a charge q, moving with velocity $\boldsymbol{v}$, experiences due to an electric field $\boldsymbol{\mathcal{E}}$ and a magnetic field $\boldsymbol{\mathcal{B}}$, is given by Lorentz force law:

$$\boldsymbol{F} = q(\boldsymbol{\mathcal{E}} + \boldsymbol{v} \times \boldsymbol{\mathcal{B}}). \tag{2.35}$$

An interesting result of the Lorentz force law is that magnetic forces never do any work on charges. Investigating the directions of the terms in the law show this. In other words, a magnetic force may change the direction of a charge, but it will not cause it to accelerate. This is surprising, because when a magnet lifts up a paperclip, something is clearly doing work, and it seems logical to assume it is the magnetic force. However, there are other forces involved here, as will be shown later when discussing electromagnetic induction.

2.2.4. Electric and magnetic fields in matter

When a non-conducting material (a dielectric) is placed in an electric field $\mathcal{E}$, the material becomes polarized. Neutral molecules will gain an induced electric dipole moment, and polar molecules will experience a torque. In both cases, the effect is that the dipoles align with the external field. This polarization is given by the field $\mathcal{P}$, which is defined as the electric dipole moment per unit volume. This polarization itself also produces an electric field. It turns out that the polarization causes bound charges $\rho_b = -\nabla \cdot \mathcal{P}$ within the dielectric (as well as surface charges σ_b). Within the dielectric, the total charge density can be written as the sum of these bound charges and all other charges, i.e. the free charge ρ_f. Filling this in in Gauss's Law (2.30) yields

$$\nabla \cdot \mathcal{E} = \frac{1}{\epsilon_0}(-\nabla \cdot \mathcal{P} + \rho_f). \tag{2.36}$$

By introducing the electric displacement $\mathcal{D} := \epsilon_0 \mathcal{E} + \mathcal{P}$, this can be rewritten as

$$\nabla \cdot \mathcal{D} = \rho_f. \tag{2.37}$$

When a material is placed in a magnetic field, the spin and orbit of the electrons in the material are affected. The electrons, which can be considered as magnetic dipoles due to their spin, experience torque, such that they line up with the external magnetic field. This causes paramagnetism. In many materials, this effect is neutralized by the electrons having opposing spin, so paramagnetism is most prevalent in atoms with an odd number of electrons. The orbits of an atom experience a different effect: in the presence of an external magnetic field, they are slowed down or sped up in such a way as to produce a new magnetic field which is oriented antiparallel to the original field. This effect is called diamagnetism. It is a weaker form of magnetism than paramagnetism, and as such occurs mainly in materials which do not experience much paramagnetism, such as atoms with an even amount of electrons. The last type of magnetism is the type that most people are familiar with, which is called ferromagnetism (since iron, in Latin *ferrum*, is the most well-known example of a ferromagnet). Ferromagnetism is the mechanism which underlies permanent magnets, and it is more complicated than paramagnetism or diamagnetism. Ferromagnetism will be discussed in the next section.

The mechanisms described above cause an object to become magnetized: the material contains many magnetic dipoles which are aligned in the same direction. This magnetization is denoted by the vector field $\mathcal{M}$, which is the magnetic dipole moment per unit volume. It turns out that (in the static case) the magnetization causes bound currents $\mathcal{J}_b = \nabla \times \mathcal{M}$, as well as surface currents $\boldsymbol{K}_b$. By splitting the current density $\mathcal{J}$ into the bound current $\mathcal{J}_b$ and the free current $\mathcal{J}_f$, Ampère's law (2.32) can be rewritten as

$$\nabla \times \mathcal{B} = \mu_0(\nabla \times \mathcal{M} + \mathcal{J}_f) + \mu_0\epsilon_0 \frac{\partial \mathcal{E}}{\partial t}. \tag{2.38}$$

This equation can be written in a more useful way by introducing the auxiliary field $\mathcal{H}$, defined as

$$\mathcal{H} := \frac{1}{\mu_0}\mathcal{B} - \mathcal{M}. \tag{2.39}$$

With this, Ampère's law becomes:

$$\nabla \times \mathcal{H} = \mathcal{J}_f + \epsilon_0 \frac{\partial \mathcal{E}}{\partial t}. \tag{2.40}$$

In the non-static case, when there are moving particles, the polarization current $\mathcal{J}_p$ which is due to moving charges must also be taken into account. The polarization current is given by

$$\mathcal{J}_p = \frac{\partial \mathcal{P}}{\partial t}. \tag{2.41}$$

Splitting the current density into three parts, i.e. $\mathcal{J} = \mathcal{J}_b + \mathcal{J}_f + \mathcal{J}_p$, and rewriting Ampère's law yields

$$\nabla \times \mathcal{H} = \mathcal{J}_f + \frac{\partial \mathcal{P}}{\partial t} + \epsilon_0 \frac{\partial \mathcal{E}}{\partial t}, \tag{2.42}$$

which by definition of $\mathcal{D}$ is equivalent to:

$$\nabla \times \mathcal{H} = \mathcal{J}_f + \frac{\partial \mathcal{D}}{\partial t}. \tag{2.43}$$

The time-derivative of $\mathcal{D}$ is also known as the displacement current.

This completes the derivation of Maxwell's equations in matter. The complete set of equations is:

$$\nabla \cdot \mathcal{D} = \rho_f, \qquad \text{Gauss's law,} \tag{2.44}$$

$$\nabla \times \mathcal{E} = -\frac{\partial \mathcal{B}}{\partial t}, \qquad \text{Faraday's law,} \tag{2.45}$$

$$\nabla \times \mathcal{H} = \mathcal{J}_f + \frac{\partial \mathcal{D}}{\partial t}, \qquad \text{Ampères law with Maxwell's correction,} \tag{2.46}$$

$$\nabla \cdot \mathcal{B} = 0. \tag{2.47}$$

2.2.5. Constitutive relationships

These equations were derived without concern for how the polarization and the magnetization of the material was created. To describe this, constitutive relationships are necessary. To relate the electric displacement field to the electric field, it is assumed that the material is such that the polarization is proportional to the electric field:

$$\mathcal{P} = \epsilon_0 \chi_e \mathcal{E}. \tag{2.48}$$

Here χ_e is a (dimensionless) property of the material called the electric susceptibility. For such a linear material, the displacement field is therefore related to the electric field by the following constitutive relationship:

$$\mathcal{D} = \epsilon_0(1+\chi_e)\mathcal{E} =: \epsilon \mathcal{E}. \tag{2.49}$$

The material parameter $\epsilon := \epsilon_0(1+\chi_e)$ is called the permittivity of the material. It has units $\mathrm{F\,m^{-1}}$. Sometimes a material is instead described using the dimensionless relative permittivity ϵ_r, which is defined as $\epsilon_r := 1+\chi_e$.

Now consider the relationship between the magnetic field and the magnetization of the material. For most paramagnetic and diamagnetic materials, the magnetization is linearly dependent on the magnetic field. For these linear materials, the dimensionless parameter χ_m is called the magnetic susceptibility, and it is defined in relation to $\mathcal{H}$ instead of $\mathcal{B}$:

$$\mathcal{M} = \chi_m \mathcal{H}. \tag{2.50}$$

For linear materials, the magnetic field $\mathcal{B}$ is also proportional to the field $\mathcal{H}$ by definition:

$$\mathcal{B} = \mu_0(1+\chi_m)\mathcal{H} =: \mu \mathcal{H}. \tag{2.51}$$

The parameter $\mu := \mu_0(1+\chi_m)$ is called the permeability of the material. It has units $\mathrm{H\,m^{-1}}$.

For linear materials, the following set of constitutive relationships has been derived:

$$\mathcal{D} = \epsilon \mathcal{E}, \tag{2.52}$$

$$\mathcal{H} = \frac{1}{\mu}\mathcal{B}. \tag{2.53}$$

Another class of magnets must also be mentioned, which display an interesting property called hysteresis. This type of magnetism is called ferromagnetism, and is the magnetism that most people refer to when they speak of magnets. Permanent magnets are ferromagnetic: they have magnetic memory, so to speak, and remain magnetized even after the external magnetic field is removed. The material is composed of many magnetic domains, within which the individual dipoles are aligned. When the material is exposed to an external magnetic field, the domain boundaries shift, causing the domains which align with the external field to grow, and the other domains to shrink. This process is not neatly reversible; when the magnetic field is removed, some domains will revert to an earlier state, but many will not, and thus the magnetization of the object has been changed. By exposing a ferromagnetic object to a very strong field, the object can become saturated, which means that it consist of one magnetic domain which covers the entire object.

This process of changing magnetization due to an external field is called hysteresis. It can be visualized by plotting the magnetization of the object against the internal magnetic field, as is done in Figure 2.7. The internal field is due to an external forcing field, which is varied. Start at point 0, the object has no magnetization and no internal magnetic field. Increasing the applied field strength causes the object to become magnetized, until it reaches saturation at point 1. When the applied field is decreased, the magnetic moment of the object decreases as well. However, at point 2, when there is no internal field, the object now does have a magnetic moment! It has retained some 'memory' of the magnetization. Subsequently, as a negative field is applied,

the magnetization decreases, until at point 3 the magnetization is zero once again. Following this, saturation is achieved at point 4, and upon increasing the field strength further one find that at point 5 the object has yet another magnetization while there is once again no applied field. Thus for a given field strength, multiple different magnetizations can be seen, depending on how the system arrived at that field strength.

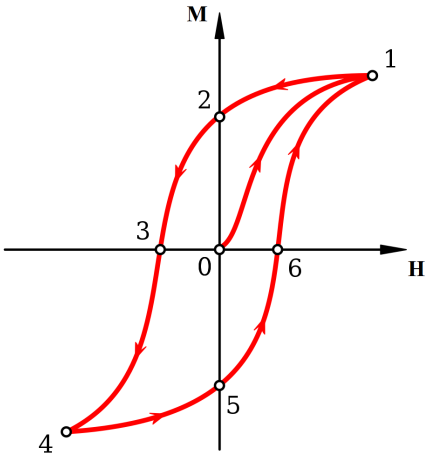

Figure 2.7: A sketch of a hysteresis loop. The applied background field $\mathcal{H}$ slowly varies, causing the magnetisation $\mathcal{M}$ of a ferromagnetic object to change as well. Note that multiple magnetisations are possible for a given applied field: the magnetisation depends on how the state was reached. (Source: Adapted from `https://commons.wikimedia.org/wiki/File:Hysteresis-from-unmagnetised-state.svg`, Creative Commons Attribute-Share Alike.)

Ferromagnetism introduces much additional complexity. It is the subject of much research, and several different models exist to describe it. In addition, magnetic objects need not be homogeneous (consisting of the same material or material parameters everywhere), nor need they be isotropic (containing identical direction-dependent properties everywhere). For the purpose of this project the objects under consideration will be linear, homogeneous, and isotropic materials, and therefore hysteresis and all the complicated factors stemming from it will be neglected.

2.2.6. Electromagnetic induction and eddy currents

Earlier, it was stated that Faraday found that a changing magnetic field induces an electric field. This is worth examining in detail, since it underlies the appearance of eddy currents. Begin by considering an electrical current, which by definition consists of moving charges. Some force must cause these charges to move. Generally, the current density $\mathcal{J}$ is proportional to this force $\mathbf{F}$. In the case of electromagnetics, the force can be calculated using the Lorentz force law, Equation (2.35). One thus finds that the current density is given by

$$\mathcal{J} = \sigma \boldsymbol{f} = \sigma(\mathcal{E} + \boldsymbol{v} \times \mathcal{B}), \tag{2.54}$$

where σ is the conductivity of the medium, and $\boldsymbol{f}$ is the force per unit charge. Good conductors, such as metals, have very high conductivity, whereas insulators have a very low conductivity. Note that in many cases, the velocity of the charges is very small, and therefore the second term in the equation is negligible, leading to the more familiar version of Ohm's law:

$$\mathcal{J} = \sigma \mathcal{E}. \tag{2.55}$$

For a simple electric circuit, such as a light powered by a battery, one finds that the current is the same everywhere in the circuit. This is surprising, since the current is only driven by the battery. Therefore, it could be expected that there is current only in the battery, and not in the rest of the circuit. The reason this is not the case is because the electric field of the charges helps the current flow: if charge would pile up somewhere, then this would cause an electric field at that point, which would 'push away' incoming charges, and 'pull back' outgoing charges, until the situation has evened itself out. This mechanism is self-regulating and works fast enough that the current can indeed be assumed to be the same everywhere. Thus one finds that there are really two components to the force which causes the particles to flow: the source $\boldsymbol{f}_s$, caused by a battery (for

example), and the electrostatic force $\boldsymbol{\mathcal{E}}$, which ensures that the current is the same everywhere:

$$\boldsymbol{f} = \boldsymbol{f}_s + \boldsymbol{\mathcal{E}}. \tag{2.56}$$

The effect of this is called the electromotive force (emf) of the circuit, denoted by $\mathscr{E}$, and it can be calculated by taking a line integral of $\boldsymbol{f}$ along the circuit:

$$\mathscr{E} = \oint \boldsymbol{f} \cdot \mathrm{d}\boldsymbol{l}. \tag{2.57}$$

In electrostatics, one has that $\oint \boldsymbol{\mathcal{E}} \cdot \mathrm{d}\boldsymbol{l} = 0$, and therefore one finds after splitting the components of $\boldsymbol{f}$ that the emf is caused solely by $\boldsymbol{f}_s$:

$$\mathscr{E} = \oint \boldsymbol{f}_s \cdot \mathrm{d}\boldsymbol{l}. \tag{2.58}$$

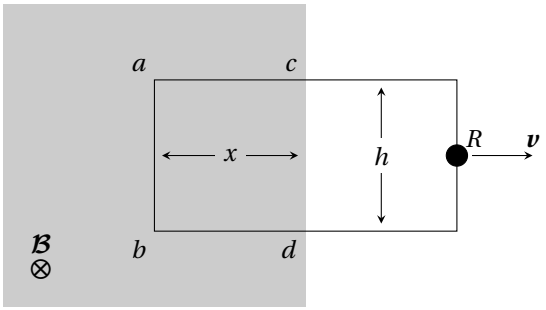

Figure 2.8: A sketch of a rigid rectangular circuit being pulled with a velocity $\boldsymbol{v}$ through a homogeneous magnetic field $\boldsymbol{\mathcal{B}}$ (which points into the page), indicated by the shaded region. By electromagnetic induction, a current will be driven, causing the light-bulb R to light up.

Now consider a different situation: a rigid rectangular circuit, with a light-bulb R at the center of one of the short sides, is pulled sideways through a uniform magnetic field $\boldsymbol{\mathcal{B}}$. This is sketched in figure 2.8: the shaded region represents the magnetic field, which points into the page, and the vector $\boldsymbol{v}$ shows the direction in which the circuit is pulled.

When the loop moves through the magnetic field, the charges in the segment ab experience a magnetic force. By the right-hand rule and Lorentz force law, one finds that the direction of this force is upward, and hence it causes a current to flow in the loop. The vertical component of this magnetic force is given by $\boldsymbol{F}_{\mathrm{mag}} = q\boldsymbol{v}B$, and thus the emf is

$$\mathscr{E} = \oint \boldsymbol{f}_{\mathrm{mag}} \cdot \mathrm{d}\boldsymbol{l} = vBh. \tag{2.59}$$

Note that there is no contribution from charges in the other segments of the loop within the shaded region, since the force on the particles is perpendicular to the wire on those segments, and hence does not drive current. It is also important to note that the magnetic force does not do any work, despite causing the emf. The work is in fact done by the force pulling the loop. It can be calculated that the work done per unit charge is exactly the emf.

There is another way to express the emf in this scenario. Consider Φ, the flux of $\boldsymbol{\mathcal{B}}$ through the loop:

$$\Phi = \iint \boldsymbol{\mathcal{B}} \cdot \mathrm{d}\boldsymbol{a}. \tag{2.60}$$

In the situation under consideration, the flux is $\Phi = xBh$. Because the loop is being pulled to the right, the area of the loop in the shaded region decreases, and thus the flux decreases as well. The rate of change of the flux is:

$$\frac{\mathrm{d}\Phi}{\mathrm{d}t} = Bh\frac{\mathrm{d}x}{\mathrm{d}t} = -vBh. \tag{2.61}$$

Note that this is exactly the negative emf. This nice result can in fact be applied to loops of any shape, which need not be fixed, moving through inhomogeneous magnetic fields, in any direction. It is called the flux rule for motional emf:

$$\mathscr{E} = -\frac{\mathrm{d}\Phi}{\mathrm{d}t}. \tag{2.62}$$

Note that it is necessary to be consistent in defining signs in these equation. In Equation (2.57), which direction should the loop integral be, and in Equation 2.60, which direction should the surface be taken to be? To determine this, make use of the right-hand rule: when the fingers of the right hand point around the positive direction of the loop, then the thumb points in the normal direction of the surface through which the flux is calculated. An easier way to determine the direction of the current is through Lenz's law: the direction of the current is such that the flux it produces opposes the change in flux it experiences. Or, as stated succinctly by Griffiths [14]: *"Nature abhors a change in flux."*

The above example shows a simple situation in which a magnetic field causes a current to flow. However, electromagnetic induction is not restricted to situations in which the loop moves through a field. Faraday showed this by performing three experiments, which can be described in very simple terms as:

- Moving a loop of wire through a magnetic field, as in the situation sketched earlier.
- Moving a magnet past a loop, while keeping the loop stationary.
- Placing a loop in a magnetic field, and keeping both stationary, while changing the strength of the magnetic field.

In all three situations, a current flowed through the loop. The first experiment is of course the exact experiment described above, and the flow of current is expected. The second experiment is not surprising either, since it is the relative movement which matters (although of course Faraday did not know anything about relativity quite yet). The result of the third experiment, however, is unexpected: there is no relative motion, and particles at rest do not experience a magnetic force, so the force causing the emf cannot be magnetic. If it is not a magnetic force, then it must be an electric force. Thus Faraday postulated that a changing magnetic field induces an electric field, and that the flux rule (Equation (2.62)) is valid whenever the magnetic flux through a loop changes, regardless of what causes the change in flux.

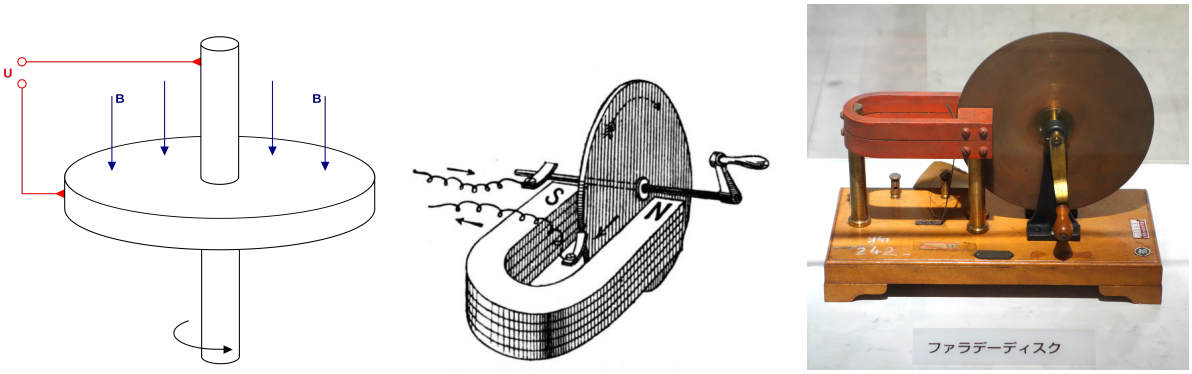

Figure 2.9: *Left*: a diagram of the working principle of a Faraday disk. The rotation of the disk through the uniform background field causes current to flow, leading to a potential difference U. (Source: `https://commons.wikimedia.org/wiki/File:Faraday_disc.svg`, Creative Commons Attribution Share-Alike). *Middle*: a sketch of a Faraday generator. A hand-cranked metal disk spins through the field generated by a permanent magnet, causing current to flow in the wires. (Source: [39], Creative Commons Public Domain, image from `https://commons.wikimedia.org/wiki/File:Faraday_disc_machine.png`). *Right*: a Faraday Generator. Note that this was not a very efficient generator, since counter-currents would flow in the part of the disk outside the magnet. (Source: National Museum of Nature and Science, Tokyo. Creative Commons Public Domain, photograph from `https://commons.wikimedia.org/wiki/File:Faraday_disk_-_National_Museum_of_Nature_and_Science,_Tokyo_-_DSC07366.JPG`).

Electromagnetic induction is not restricted to simple wire currents. See for example the Faraday disk, shown in Figure 2.9. This consists of a rotating metal disk in a uniform background field $\boldsymbol{\mathcal{B}}$. It is connected to a resistor R by a sliding contact on the rim of the disk and the vertical axle through the center of the disk. As the disk spins, an electrical current is induced in the disk. Calculating the emf using the flux law is difficult, since the path the current flows along is not well-defined. In fact, the current spreads out over the whole disk.

Eddy currents are loops of current induced in a conducting object due to a varying magnetic field. The same forces are at work as in the examples above, however the currents are now restricted to the object itself. The name 'eddy' derives from the fact that these currents are generally circular or vortex-like. The eddy currents experience resistance in the object, and therefore cause the temperature of the material to increase

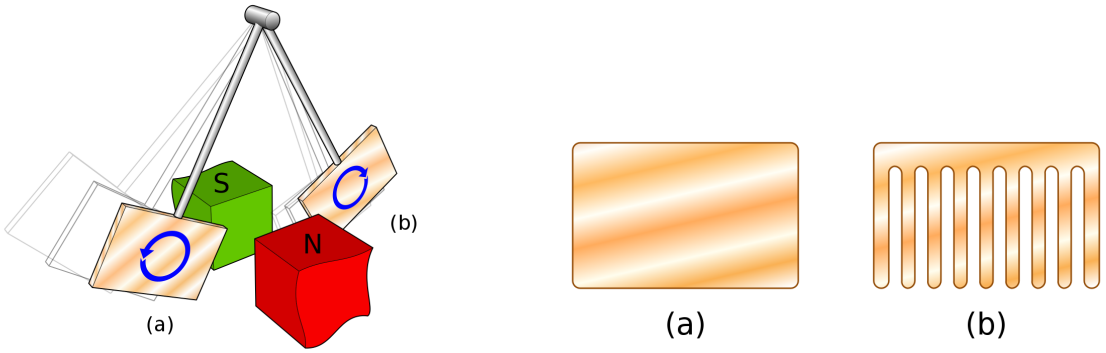

Figure 2.10: *Left*: Waltenhofen's pendulum. A conducting plate swinging in a magnetic field will experience a braking force due to the eddy currents generated in the plate. The direction of the currents is such that they cause a magnetic field which opposes the change in magnetic flux. (Source: `https://commons.wikimedia.org/wiki/File:Waltenhofen%27s-pendulum.svg`, Creative Commons Attribution Share-Alike). *Right*: When slots are introduced in the plate, it swings freely, since the eddy currents are greatly reduced. (Source: `https://commons.wikimedia.org/wiki/File:Waltenhofen%27s-pendulum-bobs.svg`, Creative Commons Attribution Share-Alike).

through Joule heating. In addition, the currents generate their own magnetic field. Eddy currents were first demonstrated by French physicist Leon Foucault, some twenty years after Faraday invented his generator, using a very similar set-up. Foucault placed a hand-cranked metal disk in the field generated by an electromagnet. He varied the strength of the magnetic field, and measured the torque necessary to turn the disk, as well as its temperature. Due to the resistive heating of the eddy currents, the temperature increases, and due to the magnetic field, the torque necessary to crank the disk increased as well.

A familiar experiment which shows the existence and effect of eddy currents, is that of Waltenhofen's pendulum, shown in Figure 2.10. A conducting metal plate is affixed to a pivot, and allowed to swing between the poles of a permanent magnet. The changing magnetic field experienced by the plate causes eddy currents to appear in the plate. Due to the eddy currents, the motion is damped, and the plate effectively experiences a braking force. When slots are cut into the plate, as shown in the second sketch, the plate swings freely, since the eddy currents are reduced. If a non-conducting material would be used, the plate would also not experience any braking force.

Eddy currents are notoriously difficult to calculate. They find many diverse applications. One common example is induction heating, which is found in many households today. The eddy currents produce Joule heating, which raises the temperature of the pan or skillet. Induction heating is also used for industrial purposes. Similarly, eddy currents are used for industrial metal melting. In this case, the fluid flow or metal deformation causes additional complexity. Another application is non-destructive testing of metals. A large metal object can be locally checked for flaws and defects by inducing eddy currents in the object, which will change when passing over a flaw. Of course, eddy currents also appear naturally, as a side-effect of other processes. The case at hand for this project is an example of this: the eddy currents are generated due to the periodic rolling motion of the vessel in the Earth magnetic field. Our goal is not to make use of this process, but to better understand it and to be able to model it, and so hopefully eliminate its effects.

3

The eddy current problem and its analytical solution for a sphere

3.1. Mathematical modelling of eddy currents

Eddy current problems are a subset of electromagnetic problems which are concerned with any process in which a varying magnetic field generates eddy currents in electrically conducting objects. The existence of these eddy currents was shown in the previous chapter. We are now interested in describing our eddy current problem and determining how it can be solved or approximated. This chapter will give an overview of the eddy current problem, and the assumptions and simplifications used to reach it. With this, an analytical solution for a simple geometry - the sphere - will be given and investigated. This analytical solution will then serve as validation for the numerical methods necessary for more complicated geometries.

3.1.1. Quasistatic approximation

The Maxwell equations in vacuum, as derived in Chapter 2, are:

$$\nabla \cdot \boldsymbol{\mathcal{E}} = \frac{1}{\epsilon_0}\rho, \qquad \text{Gauss's law,} \tag{3.1}$$

$$\nabla \times \boldsymbol{\mathcal{E}} = -\frac{\partial \boldsymbol{\mathcal{B}}}{\partial t}, \qquad \text{Faraday's law,} \tag{3.2}$$

$$\nabla \times \boldsymbol{\mathcal{B}} = \mu_0 \boldsymbol{\mathcal{J}} + \mu_0 \epsilon_0 \frac{\partial \boldsymbol{\mathcal{E}}}{\partial t}, \qquad \text{Ampères law with Maxwell's correction,} \tag{3.3}$$

$$\nabla \cdot \boldsymbol{\mathcal{B}} = 0. \tag{3.4}$$

along with the continuity equation

$$\nabla \cdot \boldsymbol{\mathcal{J}} = -\frac{\partial \rho}{\partial t}. \tag{3.5}$$

The Maxwell equations in matter were also derived:

$$\nabla \cdot \boldsymbol{\mathcal{D}} = \rho_f, \qquad \text{Gauss's law,} \tag{3.6}$$

$$\nabla \times \boldsymbol{\mathcal{E}} = -\frac{\partial \boldsymbol{\mathcal{B}}}{\partial t}, \qquad \text{Faraday's law,} \tag{3.7}$$

$$\nabla \times \boldsymbol{\mathcal{H}} = \boldsymbol{\mathcal{J}}_f + \frac{\partial \boldsymbol{\mathcal{D}}}{\partial t}, \qquad \text{Ampères law with Maxwell's correction,} \tag{3.8}$$

$$\nabla \cdot \boldsymbol{\mathcal{B}} = 0. \tag{3.9}$$

The Maxwell equations show the coupling between time-dependent electric and magnetic fields. A varying magnetic field causes an electric field through electromagnetic induction, and similarly a varying electric field causes a magnetic field. In some cases, the fields change slowly enough that one of the time-derivatives in the Maxwell equations can be neglected. This is called the quasistatic limit. When the source is a slowly varying charge density, the $\partial \boldsymbol{\mathcal{B}}/\partial t$ term is dropped, leading to the quasi-electrostatic approximation. Conversely,

when the source is a slowly-varying current density, the displacement currents $\partial \boldsymbol{\mathcal{D}}/\partial t$ are dropped, leading to the quasi-magnetostatic approximation. This is the situation at hand for eddy current problems. Below, a justification for the quasi-magnetostatic approach is given. It is adapted from [47, p.455-486].

Begin by considering a "slowly time-varying charge" in vacuum. To determine what constitutes a "slow" variation, an order-of-magnitude analysis is performed. The characteristic length of the system is given by l, and the characteristic time for a change in magnitude of the charge is given by T. In the case of a periodic source, with frequency ω, this leads to $T \sim 1/\omega$. With this, the dimensional estimates of the derivatives $\nabla \sim 1/l$ and $\partial/\partial t \sim 1/T \sim \omega$ can be made. Applying this to the continuity equation, and rearranging, one finds:

$$j \sim \omega l \rho, \tag{3.10}$$

where j is the magnitude of the current and ρ the magnitude of the charge. Note that the magnitude of the current density is proportional to j:

$$\mathcal{J} \sim j. \tag{3.11}$$

Using Helmholtz's theorem (Appendix B), the electric field $\boldsymbol{\mathcal{E}}$ can be decomposed into an irrotational part $\boldsymbol{\mathcal{E}}_G$ (satisfying Gauss's law) and a solenoidal part $\boldsymbol{\mathcal{E}}_F$ (satisfying Faraday's law). An order-of-magnitude estimate for these fields yields:

$$\mathcal{E}_G \sim \frac{l\rho}{\epsilon_0}, \tag{3.12}$$

$$\mathcal{E}_F \sim \omega B l. \tag{3.13}$$

By some algebra using the above results (detailed in [47, p.467]), one finds that

$$\frac{\mathcal{E}_F}{\mathcal{E}_G} \sim \frac{\omega^2 l^2}{c^2}, \tag{3.14}$$

where c is the speed of light, which is related to the permittivity and permeability of free space by the relation $c = 1/\sqrt{\mu_0 \epsilon_0}$. This implies that if ω is small, then the solenoidal part of the electric field is negligible, which means that the term $\partial \boldsymbol{\mathcal{B}}/\partial t$ can be dropped from Faraday's law. Thus the following condition on ω or l for a slowly-varying charge distribution is found:

$$\omega^2 \ll \frac{c^2}{l^2}. \tag{3.15}$$

This same analysis can be performed in matter instead of in vacuum: by the same process, but replacing the vacuum permittivity ϵ_0 and permeability μ_0 by the material properties ϵ and μ, the condition becomes

$$\omega^2 \ll \frac{1}{l^2 \mu \epsilon}. \tag{3.16}$$

Now consider a slowly time-varying current in vacuum. A similar approach will be used to determine the condition for "slow" in this case. Begin by temporarily neglecting the displacement current $\partial \boldsymbol{\mathcal{E}}/\partial t$ in Ampère's law, and let $\boldsymbol{\mathcal{B}}_A$ denote the resultant magnetic field. This leads to the following order-of-magnitude estimate:

$$\mathcal{B} \sim \mu_0 j l. \tag{3.17}$$

Note that this time-varying magnetic field induces an electric field by Faraday's law. This electric field, denoted by $\boldsymbol{\mathcal{E}}_F$, can be estimated to be:

$$\mathcal{E}_F \sim l\omega \mathcal{B}_A \sim \mu_0 \omega l^2 j. \tag{3.18}$$

The displacement current density $\boldsymbol{\mathcal{J}}_D$ corresponding to this field can similarly be estimated to be:

$$\mathcal{J}_D \sim \epsilon_0 \omega \mathcal{E}_F \sim \epsilon_0 \mu_0 \omega^2 l^2 j. \tag{3.19}$$

Rearranging this, and using $\mathcal{J} \sim j$ and $c = 1/\sqrt{\mu_0 \epsilon_0}$, one finds the following ratio between the displacement current density and the charge current density:

$$\frac{\mathcal{J}_D}{\mathcal{J}} \sim \frac{\omega^2 l^2}{c^2}. \tag{3.20}$$

This yields the same condition as was found for the electrostatic case above. The displacement current is negligible when

$$\omega^2 \ll \frac{c^2}{l^2}. \tag{3.21}$$

Note that, as before, one can also derive the condition for fields in matter, i.e. Equation (3.16).

An important part of quasistatic behaviour in metals is the concept of charge relaxation. Simply put: in a good conductor, charge will disappear from the interior of the object, and will only appear as surface charge. To see this, consider a conductor satisfying Ohm's law:

$$\boldsymbol{\mathcal{J}} = \sigma \boldsymbol{\mathcal{E}}. \tag{3.22}$$

Combining this with the continuity equation $\nabla \cdot \boldsymbol{\mathcal{J}} = -\partial \rho_f / \partial t$ and Gauss's law $\epsilon \nabla \cdot \boldsymbol{\mathcal{E}} = \rho_f$ yields a partial differential equation for the charge density:

$$\frac{\partial \rho_f}{\partial t} + \frac{\sigma}{\epsilon} \rho_f = 0. \tag{3.23}$$

Assuming that the conductivity σ is constant, this equation is solved by:

$$\rho_f(\boldsymbol{r}, t) = \rho_f(\boldsymbol{r}, 0) e^{-t/\tau_E}, \qquad \text{where } \tau_E := \epsilon/\sigma. \tag{3.24}$$

Thus it is found that charge disappears on a timescale τ_E. If the material has a high conductivity, this will occur very quickly. If the material has a very low conductivity, on the other hand, charge relaxation may be slow enough to permit a quasi-electrostatic. Effectively, this means that $\omega \gg 1/\tau_E$ is necessary for the quasi-electrostatic regime.

More interesting is the case of good conductors, since this leads to the quasi-magnetostatic approximation, which is what will be necessary for the eddy current problem. Strictly speaking, the solution given above (Equation (3.24)) is not valid when the conductivity is very large (see [47, p. 634] for a complete analysis). However, charge still disappears from the interior fast enough for the Coulomb effects to be non-discernable. Hence it may be assumed that there is no charge in the interior, so $\rho_f(\boldsymbol{r}, t) = 0$, and therefore by the continuity equation also $\nabla \cdot \boldsymbol{\mathcal{J}} = 0$. By an order-of-magnitude analysis ([47, p. 475]), one finds that the displacement currents can be neglected when

$$\mu\epsilon\omega^2 l^2 \ll 1 \qquad \text{and} \qquad \omega\tau_E \ll 1. \tag{3.25}$$

Quasi-magnetostatics can be applied to cases where electromagnetic induction is negligible, as well as to cases where it dominates. This stands in contrast with quasi-electrostatics, which has a more limited range of use.

For a rigorous justification of the eddy current problem and its neglection of displacement currents, see [9].

3.1.2. Time-harmonic problems: time-harmonic domain and frequency domain

For problems in which the sources are time-harmonic with a frequency $\omega = 2\pi f$, one expects the resulting fields to be time-harmonic as well. Therefore, it makes sense to consider the problem in the frequency domain instead of in the time domain. The simple way to do this is to assume a phasor convention with an angular frequency ω. With this, a field in the time-domain is rewritten using a Fourier transformation. For example, for the electric field $\boldsymbol{\mathcal{E}}$:

$$\boldsymbol{\mathcal{E}}(\boldsymbol{r}, t) = \mathrm{Re}\left(\boldsymbol{E}(\boldsymbol{r}) e^{j\omega t}\right). \tag{3.26}$$

Here, the phasor $\boldsymbol{E}$ is a complex vector. In the phasor domain, a time-derivative becomes a multiplication by $j\omega$:

$$\frac{\partial \boldsymbol{\mathcal{E}}(\boldsymbol{r}, t)}{\partial t} = \mathrm{Re}\left(j\omega \boldsymbol{E}(\boldsymbol{r}) e^{j\omega t}\right). \tag{3.27}$$

With this, the Maxwell equations in matter can be rewritten in their time-harmonic form. For example, applying the phasor convention to Faraday's law yields

$$\mathrm{Re}\left(\nabla \times \boldsymbol{E}(\boldsymbol{r}) e^{j\omega t}\right) = \mathrm{Re}\left(-j\omega \boldsymbol{B} e^{j\omega t}\right), \tag{3.28}$$

which is valid for all t if

$$\nabla \times \boldsymbol{E} = -j\omega \boldsymbol{B}. \tag{3.29}$$

By a similar process, the other Maxwell equations are transformed, leading to the time-harmonic Maxwell equations:

$$\nabla \cdot \boldsymbol{D} = \tilde{\rho}_f, \qquad \text{Gauss's law,} \tag{3.30}$$

$$\nabla \times \boldsymbol{E} = -j\omega \boldsymbol{B}, \qquad \text{Faraday's law,} \tag{3.31}$$

$$\nabla \times \boldsymbol{H} = \boldsymbol{J}_f + j\omega \boldsymbol{D}, \qquad \text{Ampères law with Maxwell's correction,} \tag{3.32}$$

$$\nabla \cdot \boldsymbol{B} = 0. \tag{3.33}$$

Note that $\tilde{\rho}_f$ represents the complex phasor, while ρ_f represented the time domain charge. For the other fields, the regular bold-faced font $\boldsymbol{E}, \boldsymbol{D}, \boldsymbol{B}, \boldsymbol{H}, \boldsymbol{J}$ represents the phasor domain, whereas the calligraphic bold-faced font represented the time domain fields $\boldsymbol{\mathcal{E}}, \boldsymbol{\mathcal{D}}, \boldsymbol{\mathcal{B}}, \boldsymbol{\mathcal{H}}, \boldsymbol{\mathcal{J}}$. Note that the opposite phasor convention (with $\exp(-j\omega t)$) is sometimes chosen. This leads to different Maxwell equations, since the sign of the derivative is flipped, but the solutions in the time domain will of course still be the same.

In principle, this is enough to work with. In problems in which a single frequency describes the system, such as problems involving an alternating current, the phasor convention suffices. However, it should be noted that a more rigorous approach is to consider the entire frequency domain, making use of the Fourier transform.

3.2. Analytical solution to the eddy current problem

For some simple geometries, the eddy current equations can be solved analytically. Such an analytical solution can be used to validate the numerical implementation. Phan et al. compare their BEM implementation against the analytical solution found in [23]. A complete derivation of the induced eddy currents due to a time-varying magnetic field for several simple geometries is given in [26]. The derivation for the eddy current problem in a sphere follows the derivation given in the appendix of [35]. However, it is given only for conductive objects, and not for magnetic objects, which is the situation at hand. For magnetic objects, the interface and boundary conditions need to be adapted somewhat. A full derivation for a three-dimensional magnetic sphere will be given below, following the same structure as is found in [26], but taking into account a magnetic object.

3.2.1. Derivation of analytical solution for a sphere

Consider a sphere Ω_1, with radius r_0. The sphere has uniform conductivity σ and permeability μ. It is located in a free air region Ω_0, for which the permeability is μ_0 and the conductivity is zero. The materials are governed by the constitutive relationships $\boldsymbol{B} = \mu \boldsymbol{H}$ and Ohm's law, $\boldsymbol{J} = \sigma \boldsymbol{E}$. Maxwell's equations, in frequency space and for the quasi-static approach in which displacement currents are ignored, are valid:

$$\begin{cases} \nabla \times \boldsymbol{E} = -j\omega \boldsymbol{B} \\ \nabla \times \boldsymbol{B} = \mu\sigma \boldsymbol{E}. \end{cases} \tag{3.34}$$

Since the material parameters are different for the two regions, the problem can not be solved directly. Instead, the problem will be reformulated with a vector potential $\boldsymbol{A}$ for each of the regions. A general solution for each of the regions will be determined, which subsequently will be made unique by way of the interface conditions.

By Gauss' law, $\nabla \cdot \boldsymbol{B} = 0$, so the magnetic flux density can be expressed as the curl of a vector potential $\boldsymbol{A}$:

$$\boldsymbol{B} = \nabla \times \boldsymbol{A}. \tag{3.35}$$

Appendix C gives a proof for the existence of the vector potential for rotation-free fields, as well as the scalar potential which will be used shortly. Filling this into Faraday's law, one finds:

$$\nabla \times (\boldsymbol{E} + j\omega \boldsymbol{A}) = \boldsymbol{0}, \tag{3.36}$$

which motivates the introduction of a scalar potential ϕ:

$$\boldsymbol{E} + j\omega \boldsymbol{A} = -\nabla\phi. \tag{3.37}$$

Filling this, and the expression for $\boldsymbol{B}$ in terms of the potential, into Ampere's law yields:

$$\nabla \times \nabla \times \boldsymbol{A} = \mu\sigma(-j\omega \boldsymbol{A} - \nabla\phi). \tag{3.38}$$

Making use of a vector identity then yields,

$$\nabla(\nabla\cdot\boldsymbol{A})-\nabla^2\boldsymbol{A}=\mu\sigma(-j\omega\boldsymbol{A}-\nabla\phi), \tag{3.39}$$

and after rewriting a Helmholtz equation for $\boldsymbol{A}$ emerges:

$$\nabla^2\boldsymbol{A}-j\omega\mu\sigma\boldsymbol{A}=\nabla(\nabla\cdot\boldsymbol{A}+\mu\sigma\phi). \tag{3.40}$$

Note that $\boldsymbol{A}$ is not yet uniquely specified. To do this, an appropriate gauge is chosen, i.e. a restriction on the divergence. By choosing $\nabla\cdot\boldsymbol{A}=-\mu\sigma\phi$, the right-hand side of the equation becomes zero. The left-hand side is rewritten using the wavenumber $k^2=-j\omega\mu\sigma$. Thus the following vector Helmholtz equation is finally found:

$$\nabla^2\boldsymbol{A}+k^2\boldsymbol{A}=0,\qquad k^2=-j\omega\mu\sigma. \tag{3.41}$$

With this equation, the source term is not explicitly found as forcing in the right-hand side. It will have to be incorporated using boundary conditions. Some special attention is needed for the wavenumber. Simply taking the square root yields two possible wavenumbers, which we temporarily denote by k_1 and k_2:

$$k_1=(1-j)\sqrt{\frac{\omega\mu\sigma}{2}},\quad\text{or}\quad k_2=-(1-j)\sqrt{\frac{\omega\mu\sigma}{2}}. \tag{3.42}$$

To determine which of these wavenumbers should be used, we consider the physics of the problem. Upon investigating the options, it becomes clear that one of the wavenumbers yields nonphysical results. Consider the fundamental solution of the vector Helmholtz equation. As is shown in Appendix D, this is

$$G(\boldsymbol{r},\boldsymbol{r}')=\frac{1}{4\pi|\boldsymbol{r}-\boldsymbol{r}'|}e^{jk|\boldsymbol{r}-\boldsymbol{r}'|}. \tag{3.43}$$

Were we to choose k_1, then this would yield

$$G(\boldsymbol{r},\boldsymbol{r}')=\frac{1}{4\pi|\boldsymbol{r}-\boldsymbol{r}'|}e^{(j+1)\sqrt{\omega\mu\sigma/2}|\boldsymbol{r}-\boldsymbol{r}'|}. \tag{3.44}$$

This exponential blows up as $|\boldsymbol{r}-\boldsymbol{r}'|$ increases. Physically, however, the Green's function is expected to decay. Based upon this, it seems that one should not use k_1. This is confirmed by also considering the Green's function, using k_1, transformed to the the time domain using the phasor convention in Equation (3.26):

$$\mathcal{G}(\boldsymbol{r},t)=\mathrm{Re}\left(\frac{1}{4\pi|\boldsymbol{r}-\boldsymbol{r}'|}e^{(1+j)\sqrt{\omega\mu\sigma/2}|\boldsymbol{r}-\boldsymbol{r}'|+j\omega t}\right) \tag{3.45}$$

$$=\frac{1}{4\pi|\boldsymbol{r}-\boldsymbol{r}'|}e^{\sqrt{\omega\mu\sigma/2}|\boldsymbol{r}-\boldsymbol{r}'|}\cos\left(\omega t+\sqrt{\omega\mu\sigma/2}|\boldsymbol{r}-\boldsymbol{r}'|\right) \tag{3.46}$$

The exponential term $e^{\sqrt{\omega\mu\sigma/2}|\boldsymbol{r}-\boldsymbol{r}'|}$ term once again blows up instead of decaying as would physically be expected. The cosine term $\cos\left(\omega t+\sqrt{\omega\mu\sigma/2}|\boldsymbol{r}-\boldsymbol{r}'|\right)$ also shows nonphysical behaviour: the wave propagates towards the source, instead of away from it. This can be seen by keeping the phase constant. If we let $\omega t+\sqrt{\omega\mu\sigma/2}|\boldsymbol{r}-\boldsymbol{r}'|=C$ for some constant C, then as t increases we find that $|\boldsymbol{r}-\boldsymbol{r}'|$ must decrease for the phase to remain constant. However, on grounds of the physics, one would expect the wave to propagate outwards. Choosing k_2 instead of k_1 solves these issues: the result is an exponentially decaying function, which propagates away from the source. Thus we choose

$$k=-(1-j)\sqrt{\frac{\omega\mu\sigma}{2}}. \tag{3.47}$$

The wavenumber k has units $[k]=\left([\omega][\mu][\sigma]\right)^{0.5}=\left(\mathrm{s}^{-1}\cdot\mathrm{kg\,m\,s^{-2}\,A^{-2}}\cdot\mathrm{m^{-3}\,kg^{-1}\,s^3\,A^2}\right)^{0.5}=\mathrm{m}^{-1}$. This makes sense, since the wavenumber is proportional to the reciprocal of the wavelength.

We are now ready to solve the vector Helmholtz equation. Let the source field be a time-varying field in the z-direction, i.e. $\boldsymbol{B}_s=B_0\hat{\boldsymbol{z}}$, at a frequency ω. This field excites the magnetic and conducting sphere. For the following derivation, it will prove useful to consider the potential in terms of the spherical coordinates. A point in space is represented in spherical coordinates as (r,θ,φ). Here r is the radial distance, θ the polar angle, and φ is the azimuthal angle, as shown in Figure 3.1. The vector identities for spherical coordinates are

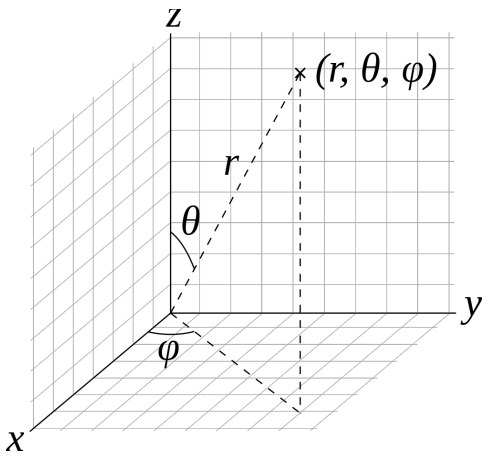

Figure 3.1: Spherical coordinate system (r,θ,φ) as used in physics (ISO 80000-2:2019 convention). Image from Wikimedia Commons (Public Domain)

given in Appendix A. The magnetic vector potential corresponding to this source field, expressed in spherical coordinates, is:

$$\boldsymbol{A}_s(r,\theta,\varphi) = \frac{1}{2} B_0 r \sin\theta \hat{\boldsymbol{\varphi}}. \tag{3.48}$$

This can be verified by checking $\nabla \times \boldsymbol{A}_s$, in spherical coordinates:

$$\nabla \times \boldsymbol{A}_s = \frac{1}{r\sin\theta}\left(\frac{\partial}{\partial\theta}\left(A_{s\varphi}\sin\theta\right) - \frac{\partial A_{s\theta}}{\partial\varphi}\right)\hat{\boldsymbol{r}} + \frac{1}{r}\left(\frac{1}{\sin\theta}\frac{\partial A_{sr}}{\partial\varphi} - \frac{\partial}{\partial r}\left(r A_{s\varphi}\right)\right)\hat{\boldsymbol{\theta}} + \frac{1}{r}\left(\frac{\partial}{\partial r}\left(r A_{s\theta}\right) - \frac{\partial A_{sr}}{\partial\theta}\right)\hat{\boldsymbol{\varphi}} \tag{3.49}$$

$$= \frac{1}{r\sin\theta}\left(\frac{\partial}{\partial\theta}\left(\frac{1}{2}B_0 r\sin^2\theta\right)\right)\hat{\boldsymbol{r}} + \frac{1}{r}\left(-\frac{\partial}{\partial r}\left(\frac{1}{2}B_0 r^2\sin\theta\right)\right)\hat{\boldsymbol{\theta}} \tag{3.50}$$

$$= B_0\cos\theta\hat{\boldsymbol{r}} - B_0\sin\theta\hat{\boldsymbol{\theta}} \tag{3.51}$$

$$= B_0\cos\theta\left(\sin\theta\cos\varphi\hat{\boldsymbol{x}} + \sin\theta\sin\varphi\hat{\boldsymbol{y}} + \cos\theta\hat{\boldsymbol{z}}\right) - B_0\sin\theta\left(\cos\theta\cos\varphi\hat{\boldsymbol{x}} + \cos\theta\sin\varphi\hat{\boldsymbol{y}} - \sin\theta\hat{\boldsymbol{z}}\right), \tag{3.52}$$

$$= B_0\left(\cos^2\theta + \sin^2\theta\right)\hat{\boldsymbol{z}}, \tag{3.53}$$

$$= B_0\hat{\boldsymbol{z}} = \boldsymbol{B}_s. \tag{3.54}$$

As expected, one finds $\boldsymbol{B}_s = \nabla\times\boldsymbol{A}_s$. Since $\boldsymbol{A}_s$ only has a $\hat{\boldsymbol{\varphi}}$-component, one finds that $\boldsymbol{A}$ is only excited in the azimuthal direction, and thus that $A_r = A_\theta = 0$. This greatly simplifies the vector Helmholtz equation (equation (3.41)). Since $A_r = A_\theta = 0$, the vector Laplacian $\nabla^2\boldsymbol{A}$ will also only have a $\hat{\boldsymbol{\varphi}}$-component. Making use of $\hat{\boldsymbol{\varphi}}$-component of the expression in Equation (A.19) and simplifying yields:

$$\left(\nabla^2 A_\varphi - \frac{A_\varphi}{r^2\sin^2\theta}\right) + k^2 A_\varphi = 0. \tag{3.55}$$

Making use of the expression for the Laplacian in spherical coordinates (Equation (A.18)), this yields the following partial differential equation for A_φ:

$$\frac{1}{r^2}\frac{\partial}{\partial r}\left(r^2\frac{\partial A_\varphi}{\partial r}\right) + \frac{1}{r^2\sin\theta}\frac{\partial}{\partial\theta}\left(\sin\theta\frac{\partial A_\varphi}{\partial\theta}\right) + \frac{1}{r^2\sin^2\theta}\frac{\partial^2 A_\varphi}{\partial\varphi^2} - \frac{A_\varphi}{r^2\sin^2\theta} + k^2 A_\varphi = 0. \tag{3.56}$$

Another useful result of the expression for the excitation field vector potential (Equation (3.48)) is that it reveals that the excitation field is not dependant on φ, and thus by symmetry one has that the φ-derivative is zero. Hence the final partial differential equation for $A_\varphi(r,\theta)$ is:

$$\frac{1}{r^2}\frac{\partial}{\partial r}\left(r^2\frac{\partial A_\varphi}{\partial r}\right) + \frac{1}{r^2\sin\theta}\frac{\partial}{\partial\theta}\left(\sin\theta\frac{\partial A_\varphi}{\partial\theta}\right) - \frac{A_\varphi}{r^2\sin^2\theta} + k^2 A_\varphi = 0. \tag{3.57}$$

This differential equation can be solved using conventional methods such as separation of variables, as is outlined in [2], section 9.4. Assuming that A_φ is separable, $A_\varphi(r,\theta) = R(r)\Theta(\theta)$, yields:

$$\frac{\Theta}{r^2}\frac{\partial}{\partial r}\left(r^2\frac{\partial R}{\partial r}\right) + \frac{R}{r^2\sin\theta}\frac{\partial}{\partial\theta}\left(\sin\theta\frac{\partial\Theta}{\partial\theta}\right) - \frac{R\Theta}{r^2\sin^2\theta} + k^2R\Theta = 0, \tag{3.58}$$

and, dividing by $R\Theta$, multiplying by r^2 and rearranging, one finds

$$\frac{1}{R}\frac{\partial}{\partial r}\left(r^2\frac{\partial R}{\partial r}\right) + k^2r^2 = -\frac{1}{\Theta\sin\theta}\frac{\partial}{\partial\theta}\left(\sin\theta\frac{\partial\Theta}{\partial\theta}\right) + \frac{1}{\sin^2\theta}. \tag{3.59}$$

The left-hand side consists only of functions depending on r, whereas the right-hand side consists only of functions depending on θ. Since these are independent variables, both sides can be equated to a constant λ:

$$\begin{cases} \dfrac{1}{R}\dfrac{\partial}{\partial r}\left(r^2\dfrac{\partial R}{\partial r}\right) + k^2r^2 = \lambda \\ -\dfrac{1}{\Theta\sin\theta}\dfrac{\partial}{\partial\theta}\left(\sin\theta\dfrac{\partial\Theta}{\partial\theta}\right) + \dfrac{1}{\sin^2\theta} = \lambda \end{cases}. \tag{3.60}$$

This can be rewritten, yielding two ordinary differential equations:

$$\begin{cases} \dfrac{1}{r^2}\dfrac{\mathrm{d}}{\mathrm{d}r}\left(r^2\dfrac{\mathrm{d}R}{\mathrm{d}r}\right) + k^2R - \dfrac{\lambda R}{r^2} = 0 \\ \dfrac{1}{\sin\theta}\dfrac{\mathrm{d}}{\mathrm{d}\theta}\left(\sin\theta\dfrac{\mathrm{d}\Theta}{\mathrm{d}\theta}\right) - \dfrac{\Theta}{\sin^2\theta} + \lambda\Theta = 0 \end{cases}. \tag{3.61}$$

First, consider the Θ equation. The equation is rewritten to:

$$\frac{\mathrm{d}^2\Theta}{\mathrm{d}\theta^2} + \frac{\cos\theta}{\sin\theta}\frac{\mathrm{d}\Theta}{\mathrm{d}\theta} - \frac{\Theta}{\sin^2\theta} + \lambda\Theta = 0. \tag{3.62}$$

This can be solved by changing the independent variable from θ to $t = \cos\theta$, which yields an equation for $P(\cos\theta) = P(t)$ instead of $\Theta(\theta)$:

$$\frac{\mathrm{d}^2P}{\mathrm{d}\theta^2} + \frac{\cos\theta}{\sin\theta}\frac{\mathrm{d}P}{\mathrm{d}\theta} - \frac{P}{\sin^2\theta} + \lambda P = 0. \tag{3.63}$$

The derivatives can be rewritten using the product rule:

$$\frac{\mathrm{d}P}{\mathrm{d}\theta} = \frac{\mathrm{d}P}{\mathrm{d}t}\frac{\mathrm{d}t}{\mathrm{d}\theta} = -\sin\theta\frac{\mathrm{d}P}{\mathrm{d}t}, \tag{3.64}$$

and

$$\frac{\mathrm{d}^2P}{\mathrm{d}\theta^2} = \frac{\mathrm{d}}{\mathrm{d}\theta}\left(-\sin\theta\frac{\mathrm{d}P}{\mathrm{d}t}\right) \tag{3.65}$$

$$= -\cos\theta\frac{\mathrm{d}P}{\mathrm{d}t} - \sin\theta\frac{\mathrm{d}^2P}{\mathrm{d}t\,\mathrm{d}\theta} \tag{3.66}$$

$$= -\cos\theta\frac{\mathrm{d}P}{\mathrm{d}t} + \sin^2\theta\frac{\mathrm{d}^2P}{\mathrm{d}t^2}. \tag{3.67}$$

Filling this in in the equation for $P(t)$ yields:

$$\sin^2\theta\frac{\mathrm{d}^2P}{\mathrm{d}t^2} - 2\cos\theta\frac{\mathrm{d}P}{\mathrm{d}t} - \frac{P}{\sin^2\theta} + \lambda P = 0. \tag{3.68}$$

Replacing $\cos\theta = t$, and $\sin^2\theta = 1 - t^2$ finally leads to the associated Legendre equation:

$$(1-t^2)\frac{\mathrm{d}^2P}{\mathrm{d}t^2} - 2t\frac{\mathrm{d}P}{\mathrm{d}t} - \frac{P}{1-t^2} + \lambda P = 0. \tag{3.69}$$

The associated Legendre equation is discussed in detail in chapter 15 of [2]. The general form of the associated Legendre equation is:

$$(1-t^2)\frac{\mathrm{d}^2P}{\mathrm{d}t^2} - 2t\frac{\mathrm{d}P}{\mathrm{d}t} - \frac{m^2}{1-t^2}P + \lambda P = 0. \tag{3.70}$$

Solving this equation, one finds that $\lambda = l(l+1)$, with l an integer and $l \geq m$, is a condition for nonsingular solutions in the range $-1 \leq t \leq 1$ (corresponding to the range $0 \leq \theta \leq \pi$). The regular solutions found in this way are called the associated Legendre functions (of the first kind), denoted by P_l^m. In the case at hand, $m = 1$. Thus one finds that Θ is some linear combination of associated Legendre functions $P_l^1(\cos\theta)$, with $l \geq 1$, and the separation constant λ is found to be of the form $\lambda = l(l+1)$. Note that if one relaxes the requirement for non-singular solutions, one finds a second set of solutions, called the associated Legendre functions of the second kind, denoted by Q_l^m. However, in the case at hand, regular solutions are required, and as such the associated Legendre functions of the second kind can be disregarded.

Having found a solution for the Θ equation, one can now continue with the R equation. The solution to Θ determines the parameter $\lambda = l(l+1)$, with integer coefficient $l \geq 1$. Thus the ordinary differential equation to be solved is:

$$\frac{1}{r^2}\frac{\mathrm{d}}{\mathrm{d}r}\left(r^2\frac{\mathrm{d}R}{\mathrm{d}r}\right) + k^2R - \frac{l(l+1)R}{r^2} = 0, \tag{3.71}$$

or, rewriting the derivatives and multiplying by r^2:

$$r^2\frac{\mathrm{d}^2R}{\mathrm{d}r^2} + 2r\frac{\mathrm{d}R}{\mathrm{d}r} + k^2r^2R - l(l+1)R = 0. \tag{3.72}$$

There are two situations at hand: outside the sphere, where $\sigma = 0$, one has $k^2 = 0$, and the equation reduces to the Laplace equation, whereas inside the sphere one has $k^2 = -j\omega\mu\sigma$. The first case is easier to solve: by the method of Frobenius, one finds that r^s is a complete solution. Substituting $R = r^s$ in the equation with $k^2 = 0$ yields:

$$s(s-1)r^s + 2sr^s - l(l+1)r^s = 0. \tag{3.73}$$

This equation has two solutions: $s = l$ and $s = -l-1$. Thus outside the sphere, the R solution for a given l is found to be

$$R(r) = Ar^l + Br^{-l-1}, \tag{3.74}$$

with A and B coefficients to be determined.

Now consider the case inside the sphere ($r \leq r_0$), with $k^2 = -j\omega\mu\sigma$. The equation is very similar to a Bessel equation, which in its general form is given by:

$$x^2\frac{\mathrm{d}^2y}{\mathrm{d}x^2} + x\frac{\mathrm{d}y}{\mathrm{d}x} + \left(x^2 - a^2\right)y = 0. \tag{3.75}$$

The difference between the equation at hand (Equation (3.72)) and the Bessel equation can be resolved by rewriting $R(r)$ as:

$$R(r) = \frac{Z(kr)}{(kr)^{1/2}}, \tag{3.76}$$

and changing the independent variable to $x = kr$. Note that, using the chain rule,

$$r\frac{\mathrm{d}R}{\mathrm{d}r} = r\frac{\mathrm{d}R}{\mathrm{d}x}\frac{\mathrm{d}x}{\mathrm{d}r} = kr\frac{\mathrm{d}R}{\mathrm{d}x} = x\frac{\mathrm{d}R}{\mathrm{d}x}, \tag{3.77}$$

and similarly,

$$r^2\frac{\mathrm{d}^2R}{\mathrm{d}r^2} = x^2\frac{\mathrm{d}^2R}{\mathrm{d}x^2}. \tag{3.78}$$

Filling this in in Equation (3.72) yields

$$x^2\frac{\mathrm{d}^2R}{\mathrm{d}x^2} + 2x\frac{\mathrm{d}R}{\mathrm{d}x} + x^2R - l(l+1)R = 0. \tag{3.79}$$

The derivatives can be written in terms of Z:

$$\frac{\mathrm{d}R}{\mathrm{d}x} = \frac{\mathrm{d}\left(Z(x)/\sqrt{x}\right)}{\mathrm{d}x} = \frac{\mathrm{d}Z}{\mathrm{d}x}x^{-1/2} - \frac{1}{2}Zx^{-3/2}, \tag{3.80}$$

and

$$\frac{\mathrm{d}^2 R}{\mathrm{d}x^2} = \frac{\mathrm{d}^2 Z}{\mathrm{d}x^2} x^{-1/2} - \frac{\mathrm{d}Z}{\mathrm{d}x} x^{-3/2} + \frac{3}{4} Z x^{-5/2}. \tag{3.81}$$

Rewriting the derivatives and simplifying yields a Bessel equation for Z:

$$x^2 \frac{\mathrm{d}^2 Z}{\mathrm{d}x^2} + x \frac{\mathrm{d}Z}{\mathrm{d}x} + \left(x^2 - \left(l + \frac{1}{2} \right)^2 \right) Z = 0. \tag{3.82}$$

This is solved by the Bessel functions of half-integer order. With an appropriate scaling factor, the solutions are known as spherical Bessel functions of the first and second kind, denoted by j_l and y_l respectively. A complete overview of these functions is given in [1, p. 436-456]. For our purposes, only the first two spherical Bessel functions of the first kind will be necessary. These are:

$$j_0(x) = \frac{\sin x}{x}, \tag{3.83}$$

$$j_1(x) = \frac{\sin x}{x^2} - \frac{\cos x}{x}. \tag{3.84}$$

Note the identity $j_1'(x) = j_0(x) - \frac{2}{x} j_1(x)$, which will be used to simplify the resultant expression later.

With this, the general solution to Equation (3.57) is found to be:

$$A_\varphi(r,\theta) = \sum_{l=1}^{\infty} P_l^1(\cos\theta) \cdot \begin{cases} C_{1,l}\, j_l(kr) + C_{2,l}\, y_l(kr), & (r \le r_0) \\ C_{3,l}\, r^l + C_{4,l}\, r^{-l-1}, & (r > r_0) \end{cases}, \tag{3.85}$$

where $C_{i,l}$ are constants, which can be determined from the boundary and interface conditions. The first condition is that the solution must be finite at $r = 0$. Since the spherical Bessel function of the second kind is undefined at $r = 0$, its coefficient must be $C_{2,l} = 0$. The second boundary condition is that the limit as $r \to \infty$ must converge to the source field, i.e.

$$\lim_{r\to\infty} A_\varphi(r,\theta) = \frac{1}{2} B_0 r \sin\theta. \tag{3.86}$$

Noting the identity $P_1^1(\cos\theta) = \sin\theta$, this condition implies that $l = 1$, and that $C_{1,1} = 1$ and $C_{3,l} = \frac{1}{2} B_0$. The simplified result is

$$A_\varphi(r,\theta) = \sin\theta \cdot \begin{cases} C_1\, j_1(kr), & (r \le r_0) \\ \frac{1}{2} B_0 r + C_4 r^{-2}, & (r > r_0) \end{cases}, \tag{3.87}$$

where the coefficients C_1 and C_4 are still to be determined. To determine these, the interface conditions at $r = r_0$ are used. The first interface condition is that the $\boldsymbol{A}$ field must be continuous at the interface. This is derived[1] in [14, p. 249], and more rigorously in [43]. The resultant interface condition is:

$$C_1\, j_1(kr_0) = \frac{1}{2} B_0 r_0 + C_4 r_0^{-2}. \tag{3.88}$$

The other condition on the interface is that the tangential component of the $\boldsymbol{H}$-field must be continuous. Noting that $\boldsymbol{H} = (1/\mu)\boldsymbol{B} = (1/\mu)\nabla \times \boldsymbol{A}$, this leads to the following equation:

$$\hat{\boldsymbol{r}} \times \left(\frac{1}{\mu_0} \nabla \times \boldsymbol{A} \right) \Bigg|_{r=r_0^+} = \hat{\boldsymbol{r}} \times \left(\frac{1}{\mu} \nabla \times \boldsymbol{A} \right) \Bigg|_{r=r_0^-}. \tag{3.89}$$

Here, r_0^+ and r_0^- denote the limit approaching r_0 from the outside and inside respectively. Using the formula's for the curl in spherical coordinates and applying the cross product, one finds that the following condition must hold:

$$\frac{1}{\mu_0} \left(-\frac{1}{r} \frac{\partial (r A_\varphi)}{\partial r} \right) \Bigg|_{r=r_0^+} = \frac{1}{\mu} \left(-\frac{1}{r} \frac{\partial (r A_\varphi)}{\partial r} \right) \Bigg|_{r=r_0^-}. \tag{3.90}$$

[1] Note that the proof for this seems to necessitate a Lorenz gauge, or to subtly imply that $\phi = 0$ everywhere, thereby reducing the gauge to a Lorenz gauge. This goes unnoted in the derivation in [26], but $\phi = 0$ will appear in the final analytical solution. However, [43] does show that continuity is also valid for the Lorenz gauge. In any case, continuity of the $\boldsymbol{A}$ potential is used in [26], and in eddy current BEM formulations such as [41], and as such will be used here as well.

Calculating the derivatives yields:

$$\frac{-1}{\mu_0 r}\sin\theta\left(r\left(\frac{1}{2}B_0-2C_4r^{-3}\right)+\frac{1}{2}B_0r+C_4r^{-2}\right)\Bigg|_{r=r_0^+}=\frac{-1}{\mu r}\sin\theta\left(rkC_1j_1'(kr)+C_1j_1(kr)\right)\Bigg|_{r=r_0^-}. \tag{3.91}$$

Filling in $r=r_0$ and simplifying yields the second condition:

$$\begin{aligned}\mu_r\left(B_0r_0-C_4r_0^{-2}\right)&=C_1\left(kr_0j_1'(kr_0)+j_1(kr_0)\right)\\&=C_1\left(kr_0j_0(kr_0)-j_1(kr_0)\right),\end{aligned} \tag{3.92}$$

where we have made use of the identity for $j_1'(x)$ mentioned earlier, and where $\mu_r=\mu/\mu_0$, the relative permeability.

Equations (3.88) and (3.92) form a linear system,

$$\begin{cases}C_1j_1(kr_0)=\dfrac{1}{2}B_0r_0+C_4r_0^{-2}\\ \mu_r\left(B_0r_0-C_4r_0^{-2}\right)=C_1\left(kr_0j_0(kr_0)-j_1(kr_0)\right)\end{cases} \tag{3.93}$$

which can be solved to find the coefficients C_1 and C_4:

$$C_1=\frac{3B_0r_0}{2\mu_r^{-1}kr_0j_0(kr_0)-2\mu_r^{-1}j_1(kr_0)+2j_1(kr_0)}, \tag{3.94}$$

$$\begin{aligned}C_4&=C_1j_1(kr_0)r_0^2-\frac{B_0r_0^3}{2}\\&=B_0r_0^3\left(\frac{3j_1(kr_0)}{2\mu_r^{-1}kr_0j_0(kr_0)-2\mu_r^{-1}j_1(kr_0)+2j_1(kr_0)}-\frac{1}{2}\right).\end{aligned} \tag{3.95}$$

Thus finally the following expression for the magnetic vector potential $\boldsymbol{A}$ is found:

$$\boldsymbol{A}(r,\theta)=\sin\theta\cdot\begin{cases}Cj_1(kr)\hat{\boldsymbol{\varphi}}, & (r\le r_0)\\ \left(\dfrac{1}{2}B_0r+\left(Cr_0^2j_1(kr_0)-\dfrac{B_0r_0^3}{2}\right)r^{-2}\right)\hat{\boldsymbol{\varphi}}, & (r>r_0),\end{cases} \tag{3.96}$$

with

$$C:=\frac{3B_0r_0}{2\mu_r^{-1}kr_0j_0(kr_0)-2\mu_r^{-1}j_1(kr_0)+2j_1(kr_0)}. \tag{3.97}$$

Earlier, the gauge condition $\nabla\cdot\boldsymbol{A}=-\mu\sigma\phi$ was chosen. However, upon taking the divergence of the above expression, one finds $\nabla\cdot\boldsymbol{A}=0$. This implies that the scalar potential ϕ is equal to zero. Thus one finds that the vector potential $\boldsymbol{A}$ and the electric field $\boldsymbol{E}$ are related by the simple expression $\boldsymbol{E}=-j\omega\boldsymbol{A}$. By Ohm's law, $\boldsymbol{J}=\sigma\boldsymbol{E}$, the following expression for the eddy currents in the sphere is finally found:

$$\boldsymbol{J}(r,\theta)=-j\omega\sigma\boldsymbol{A}=-j\omega\sigma\sin\theta Cj_1(kr)\hat{\boldsymbol{\varphi}},\quad(r\le r_0). \tag{3.98}$$

As a sanity check, let us check the units of this expression. Recall that $[k]=\mathrm{m}^{-1}$, and therefore kr (or kr_0) is dimensionless. Since μ_r is also dimensionless, the unit of C is simply $[C]=\mathrm{T\,m}$. Thus the unit of $\boldsymbol{J}$ is $[\boldsymbol{J}]=[\omega][\sigma][C]=\mathrm{s}^{-1}\cdot\mathrm{m}^{-3}\,\mathrm{kg}^{-1}\,\mathrm{s}^3\,\mathrm{A}^2\cdot\mathrm{kg\,s}^{-2}\,\mathrm{A}^{-1}\,\mathrm{m}=\mathrm{A\,m}^{-2}$, as expected.

An analytical relation for the magnetic field can now also be found. Using the relation $\boldsymbol{B}=\nabla\times\boldsymbol{A}$, and the expression for the curl in spherical coordinates (Equation (A.17)), one finds:

$$\boldsymbol{B}=\nabla\times\boldsymbol{A}=\frac{1}{r\sin\theta}\frac{\partial}{\partial\theta}\left(A_\varphi\sin\theta\right)\hat{\boldsymbol{r}}-\frac{1}{r}\frac{\partial}{\partial r}\left(rA_\varphi\right)\hat{\boldsymbol{\theta}}. \tag{3.99}$$

Inside the sphere, the magnetic field thus found is:

$$\boldsymbol{B}(r,\theta)=\frac{1}{r\sin\theta}\left(2\sin\theta\cos\theta Cj_1(kr)\right)\hat{\boldsymbol{r}}-\frac{1}{r}\left(krC\sin\theta j_0(kr)-C\sin\theta j_1(kr)\right)\hat{\boldsymbol{\theta}} \tag{3.100}$$

$$=2C\cos\theta r^{-1}j_1(kr)\hat{\boldsymbol{r}}-C\sin\theta r^{-1}\left(krj_0(kr)-j_1(kr)\right)\hat{\boldsymbol{\theta}}. \tag{3.101}$$

Similarly, the field outside the sphere is found to be:

$$\boldsymbol{B}(r,\theta) = \frac{1}{r\sin\theta}\left(2\sin\theta\cos\theta\left(\frac{1}{2}B_0 r + \left(Cr_0^2 j_1(kr_0) - \frac{B_0 r_0^3}{2}\right)r^{-2}\right)\right)\hat{\boldsymbol{r}} - \frac{1}{r}\left(\sin\theta\left(B_0 r - \left(Cr_0^2 j_1(kr_0) - \frac{B_0 r_0^3}{2}\right)\frac{1}{r^2}\right)\right)\hat{\boldsymbol{\theta}} \tag{3.102}$$

$$= \cos\theta\left(B_0 + \left(2Cr_0^2 j_1(kr_0) - B_0 r_0^3\right)r^{-3}\right)\hat{\boldsymbol{r}} - \sin\theta\left(B_0 - \left(Cr_0^2 j_1(kr_0) - \frac{B_0 r_0^3}{2}\right)r^{-3}\right)\hat{\boldsymbol{\theta}}. \tag{3.103}$$

With this, a complete analytical description of the magnetic field due to eddy currents in a magnetic object is found:

$$\boldsymbol{B}(r,\theta) = \begin{cases} 2C\cos\theta r^{-1} j_1(kr)\hat{\boldsymbol{r}} - C\sin\theta r^{-1}\left(kr\, j_0(kr) - j_1(kr)\right)\hat{\boldsymbol{\theta}}, & (r \le r_0) \\ \cos\theta\left(B_0 + \left(2Cr_0^2 j_1(kr_0) - B_0 r_0^3\right)r^{-3}\right)\hat{\boldsymbol{r}} - \sin\theta\left(B_0 - \left(Cr_0^2 j_1(kr_0) - \frac{B_0 r_0^3}{2}\right)r^{-3}\right)\hat{\boldsymbol{\theta}}, & (r > r_0). \end{cases} \tag{3.104}$$

Once again, let us check the units. With kr dimensionless, and $[C] = \mathrm{T\,m}$, one can easily check that $[B] = \mathrm{T}$.

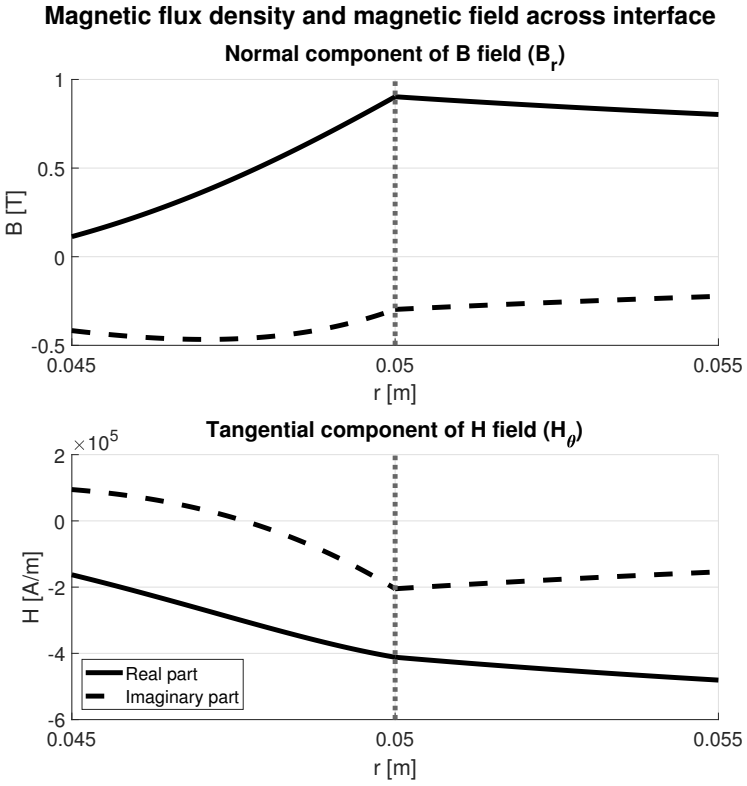

Figure 3.2: *Left:* The normal component of the magnetic flux density $\boldsymbol{B}$ across the interface $r = r_0$. *Right:* The tangential component of the magnetic field $\boldsymbol{H}$ across the interface. For both figures, the system parameters were chosen as in the base case described in 3.2.3. The radius r_0 is 0.05 m. The polar angle θ was chosen to be $\pi/3$ for this plot.

Let us also take a moment to verify that this expression satisfies the magnetic interface conditions, i.e. that the normal component of the $\boldsymbol{B}$ field is continuous, and that the tangential component of the $\boldsymbol{H}$ field is

continuous. Indeed, filling in $r = r_0$ for the $\boldsymbol{r}$-component in both regions yields:

$$2C\cos\theta r_0^{-1} j_1(kr) \stackrel{?}{=} \cos\theta\left(B_0 + \left(2Cr_0^2 j_1(kr_0) - B_0 r_0^3\right) r_0^{-3}\right) \tag{3.105}$$

$$\Rightarrow 2Cr_0^{-1} j_1(kr) \stackrel{?}{=} 2Cr_0^{-1} j_1(kr_0), \tag{3.106}$$

which is indeed satisfied. Similarly, for the tangential component, we require that $\boldsymbol{B}(\theta, r_0)/\mu_0$ approaching from inside the sphere is equal to $\boldsymbol{B}(\theta, r_0)/\mu$ approaching from outside the sphere:

$$-\frac{1}{\mu_0} C\sin\theta r_0^{-1}\left(kr_0 j_0(kr_0) - j_1(kr_0)\right) \stackrel{?}{=} -\frac{1}{\mu_1}\sin\theta\left(B_0 - \left(Cr_0^2 j_1(kr_0) - \frac{B_0 r_0^3}{2}\right) r_0^{-3}\right) \tag{3.107}$$

$$\Rightarrow Cr_0^{-1}\left(\mu_r^{-1} kr_0 j_0(kr_0) - \mu_r^{-1} j_1(kr_0)\right) \stackrel{?}{=} \frac{3B_0}{2} - Cr_0^{-1} j_1(kr_0) \tag{3.108}$$

$$\Rightarrow C\left(\mu_r^{-1} kr_0 j_0(kr_0) - \mu_r^{-1} j_1(kr_0) + j_1(kr_0)\right) \stackrel{?}{=} \frac{3B_0 r_0}{2} \tag{3.109}$$

$$\Rightarrow C \stackrel{?}{=} \frac{3B_0 r_0}{2\left(\mu_r^{-1} kr_0 j_0(kr_0) - \mu_r^{-1} j_1(kr_0) + j_1(kr_0)\right)}, \tag{3.110}$$

which is indeed satisfied by definition of C. Figure 3.2 shows the fields across the interface graphically, confirming that the interface conditions are satisfied.

3.2.2. Joule losses

The induced eddy currents heat the object by resistive heating. The energy involved in this process can be determined by deriving a conservation law. The desired law is called Poynting's theorem. For a derivation in the time domain, see [47, p. 507]. An important quantity is the Poynting vector:

$$\boldsymbol{\mathcal{S}} = \boldsymbol{\mathcal{E}} \times \boldsymbol{\mathcal{H}}, \tag{3.111}$$

which can be considered as the 'current density' of electromagnetic energy. The joule losses can be calculated by the surface integral:

$$\mathcal{P}_{\text{loss}} = -\oiint_{\partial\Omega_0} \boldsymbol{\mathcal{S}} \cdot \mathrm{d}\boldsymbol{a}. \tag{3.112}$$

Equivalent conservation laws can be found in the frequency domain as well. For a derivation of these, see [38, p. 58]. The complex Poynting vector is:

$$\boldsymbol{S} = \boldsymbol{E} \times \overline{\boldsymbol{H}}, \tag{3.113}$$

where the bar denotes the complex conjugate. The joule losses can be calculated by the surface integral:

$$P_{\text{loss}} = -\frac{1}{2}\,\mathrm{Re}\left(\oiint_{\partial\Omega_0} \boldsymbol{S} \cdot \mathrm{d}\boldsymbol{a}\right). \tag{3.114}$$

This can be applied to the analytical solution. On the boundary, we have $r = r_0$, so the electric field and the magnetic flux density, in the limit of r approaching r_0 from below, are given by:

$$\boldsymbol{E}(\theta) = -j\omega\sin\theta C j_1(kr_0)\hat{\boldsymbol{\varphi}}, \tag{3.115}$$

$$\boldsymbol{B}(\theta) = 2C\cos\theta r_0^{-1} j_1(kr_0)\hat{\boldsymbol{r}} - C\sin\theta r_0^{-1}\left(kr_0 j_0(kr_0) - j_1(kr_0)\right)\hat{\boldsymbol{\theta}}, \tag{3.116}$$

with

$$C = \frac{3B_0 r_0}{2\mu_r^{-1} kr_0 j_0(kr_0) - 2\mu_r^{-1} j_1(kr_0) + 2j_1(kr_0)}. \tag{3.117}$$

Thus the Poynting vector on the interface can be calculated:

$$\boldsymbol{S} = \boldsymbol{E} \times \frac{1}{\mu}\overline{\boldsymbol{B}} \tag{3.118}$$

$$= \left(-j\omega\sin\theta C j_1(kr_0)\right)\left(\frac{1}{\mu} 2\overline{C}\cos\theta r_0^{-1} j_1(\overline{k}r_0)\right)\hat{\boldsymbol{\theta}} - \left(j\omega\sin\theta C j_1(kr_0)\right)\left(\frac{1}{\mu}\overline{C}\sin\theta r_0^{-1}\left(\overline{k}r_0 j_0(\overline{k}r_0) - j_1(\overline{k}r_0)\right)\right)\hat{\boldsymbol{r}} \tag{3.119}$$

$$= \frac{-2j\omega}{\mu r_0} C^2 \sin\theta\cos\theta j_1(kr_0) j_1(\overline{k}r_0)\hat{\boldsymbol{\theta}} - \frac{j\omega}{\mu}\sin^2\theta C\overline{C} j_1(kr_0) r_0^{-1}\left(\overline{k}r_0 j_0(\overline{k}r_0) - j_1(\overline{k}r_0)\right)\hat{\boldsymbol{r}}. \tag{3.120}$$

This leads to the following expression for the joule losses for a sphere:

$$P_{\text{loss}} = -\frac{1}{2}\,\text{Re}\left(\oiint_{\partial\Omega_0}\left(\frac{-2j\omega}{\mu r_0}|C|^2\sin\theta\cos\theta\, j_1(kr_0)\,j_1(\overline{k}r_0)\hat{\boldsymbol{\theta}} + \frac{j\omega}{\mu}\sin^2\theta C^2\, j_1(kr_0)\,r_0^{-1}\left(\overline{k}r_0\, j_0(\overline{k}r_0) - j_1(\overline{k}r_0)\right)\hat{\boldsymbol{r}}\right)\cdot \mathrm{d}\boldsymbol{a}\right) \tag{3.121}$$

$$= -\frac{1}{2}\,\text{Re}\left(\int_0^{2\pi}\int_0^{\pi} -\frac{j\omega}{\mu}\sin^2\theta|C|^2\, j_1(kr_0)\,r_0^{-1}\left(\overline{k}r_0\, j_0(\overline{k}r_0) - j_1(\overline{k}r_0)\right) r^2\sin\theta\ \mathrm{d}\theta\ \mathrm{d}\varphi\right) \tag{3.122}$$

$$= \text{Re}\left(\frac{4j\omega\pi r_0}{3\mu}|C|^2\, j_1(kr_0)\left(\overline{k}r_0\, j_0(\overline{k}r_0) - j_1(\overline{k}r_0)\right)\right). \tag{3.123}$$

The units of this expression are $[P_{\text{loss}}] = [\omega][r_0][C]^2/[\mu] = \text{s}^{-1}\cdot\text{m}\cdot(\text{kg}\,\text{s}^{-2}\,\text{A}^{-1}\,\text{m})^2\cdot(\text{m}\,\text{kg}\,\text{s}^{-2}\,\text{A}^{-2})^{-1} = \text{kg}\,\text{m}^2\,\text{s}^{-3} = W$, as expected.

Being able to calculate the joule losses of the analytical solution is useful, since it represents an integral quantity for the entire sphere, which can be compared to the numerical approximation.

3.2.3. Qualitative investigation into the analytical solution

Using a MATLAB routine, the analytical solution was determined for various system parameters. We begin by investigating the results for a base case with the parameters as specified in [23]:

$$\begin{aligned} r_0 &= 0.05\,\text{m} \\ B_0 &= 1\,\text{T} \\ f &= 50\,\text{Hz} \\ \mu_r &= 20 \\ \sigma &= 10\,\text{MS}\,\text{m}^{-1} \end{aligned}$$

Recall that B_0 gives the magnitude of the magnetic field, which is oriented in the $\boldsymbol{z}$-direction, and is time-harmonic with an angular frequency of $\omega = 2\pi f$. The varying magnetic field induces eddy currents in the sphere, which in turn generate a magnetic field around the sphere.

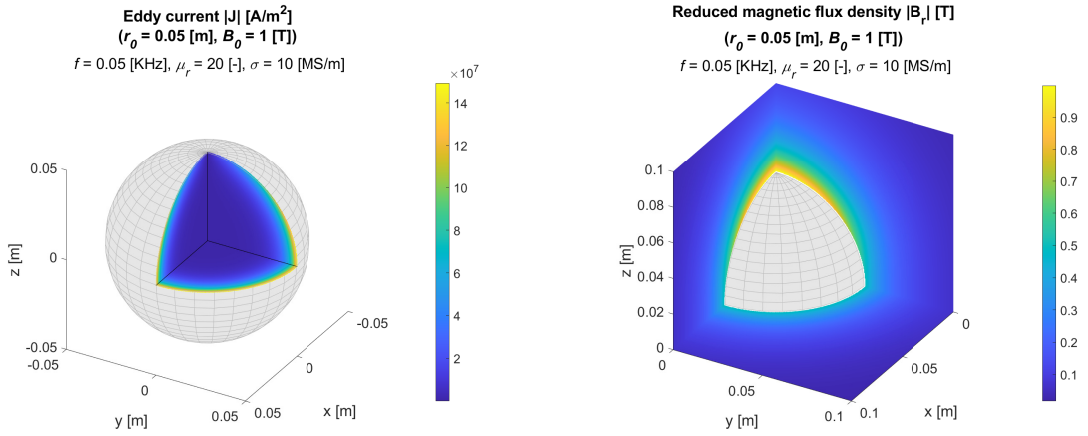

Figure 3.3: Eddy current distribution $\boldsymbol{J}$ inside sphere, and reduced magnetic flux density $\boldsymbol{B}_r$ around sphere.

Figure 3.3 shows the eddy current density on the left, and the reduced magnetic flux density (i.e. the magnetic flux density due to the eddy currents and magnetism, but without the excitation field $\boldsymbol{B}_0$) on the right. We can see that the eddy currents are concentrated very close to the surface of the sphere. This is called the skin effect. This effect, which is observable not just for eddy currents but for all alternating currents, increases with the frequency, the material conductivity and the material permeability. For a more detailed explanation of the skin effect, see [47, p. 477]. An important characteristic length is the skin depth δ:

$$\delta = \sqrt{2/(\omega\mu\sigma)}. \tag{3.124}$$

The skin depth is a measure of the depth at which the currents are concentrated. For these parameters, the skin depth is $\delta \approx 0.005\,\mathrm{m}$, which corresponds well to the results in the figure.

The eddy currents in the sphere are strongest around the $z = 0$ plane, or the 'equator' of the sphere. The reduced magnetic flux density which the eddy currents generate is strongest around the polar region of the sphere. This corresponds well with what one might expect: considering the eddy currents are loops of currents, the right hand rule would lead one to expect a dipole-like field extending above and below the loops. The reduced field ranges in strength from 0 T far from the sphere, to 1 T near the poles of the sphere.

Let us investigate the shape of the fields in some more detail. For the current density, we investigate a range of points between the centre of the sphere and its edge, along the $y = 0$, $z = 0$ axis. This range is shown in red in Figure 3.4. For the magnetic flux density, we investigate a range of points in the $y = 0$ plane, at a distance $r = 3r_0$ from the origin. This is shown in blue in Figure 3.4. These ranges are chosen since the fields show much characteristic variation along these paths. Due to symmetry of the solution, this tells us much about the solution everywhere.

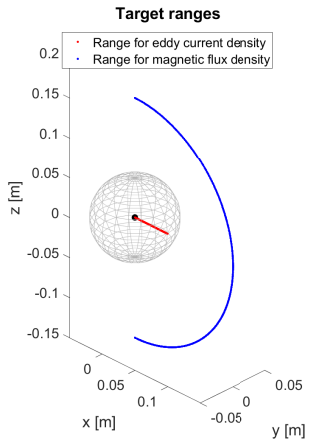

Figure 3.4: Target ranges for eddy current density (red) and magnetic flux density (blue). The red points lie on the $y = 0, z = 0$ axis. The blue points lie in the $y = 0$ plane, at a distance $r = 3r_0$ from the origin.

Figure 3.5 (left) shows the eddy current distribution in the sphere. Unsurprisingly, we see that for this range of points, there is only a $\boldsymbol{y}$-component, since this corresponds to the azimuthal component. The skin effect is also observable, as the strongest current density is near the edge of the sphere. This effect becomes more pronounced if the frequency is increased.

The magnetic flux density distribution near the sphere is shown in Figure 3.5 (right). Once again, we can see that the magnetic field is strongest near the poles (corresponding to a polar angle of $\theta = 0$ and $\theta = \pi$). There is an appealing symmetry to the real and imaginary parts of the components. However, the in-phase component is a bit stronger than the quadrature component.

3.2.4. Effect of varying permeability, conductivity and frequency

The eddy current distribution and the magnetic field it generates are related to the system parameters in a complex way. The permeability and conductivity of the object play an important role, as well as the generating frequency and the radius of the sphere. We will investigate the effects of the permeability, conductivity and frequency in detail.

Because of the complexity of the situation, let us begin by simplifying it somewhat by considering a non-conducting sphere ($\sigma = 0\,\mathrm{S\,m^{-1}}$). The reduced magnetic field near this sphere for a range of frequencies and relative permeabilities is shown in Figure 3.6. Since eddy currents cannot be induced in a non-conducting sphere, we see that the reduced magnetic field is constant for all frequencies (in the left-hand plot). This constant field is the induced magnetic field. In the right-hand plot, where the magnetic permeability is varied, we see that for $\mu_r = 1$ there is no field (since the sphere is not magnetic), and that as the permeability increases the strength of the induced magnetic field increases as well. Note that in both cases, the field only has a real component. Since it is an induced field, there is no imaginary component.

Now consider the case where the sphere is non-magnetic ($\mu_r = 1$). This means that the sphere is conduc-

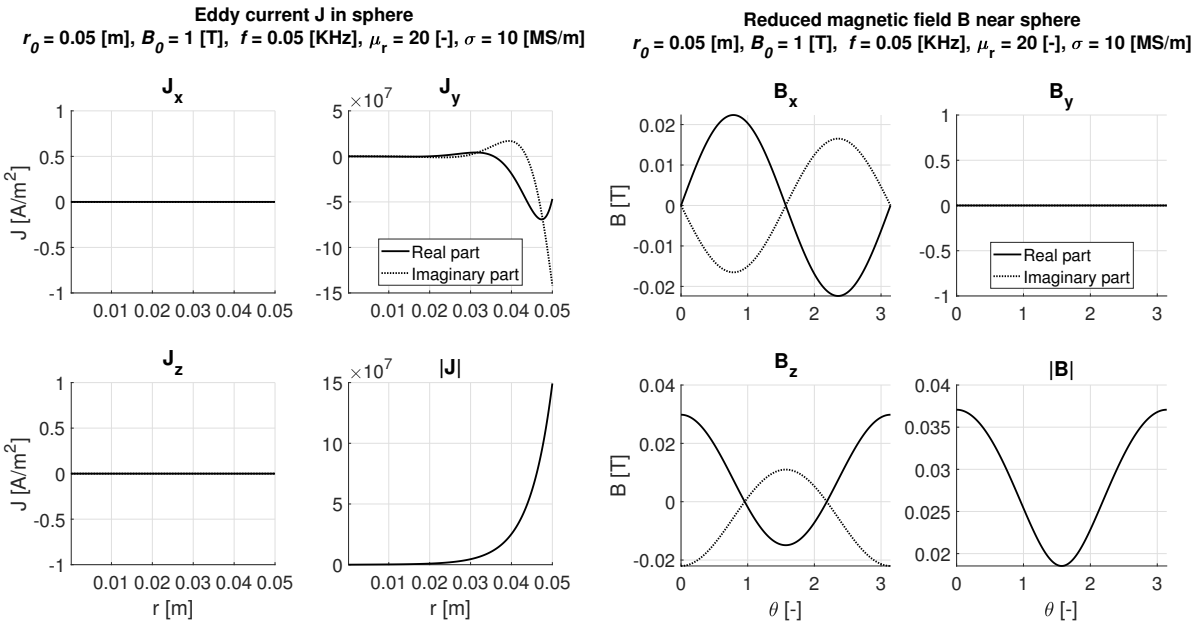

Figure 3.5: *Left:* Eddy current distribution for a range of points inside the sphere. *Right:* Reduced magnetic flux density for a range of points around the sphere. The target ranges for both plots are shown in Figure 3.4.

tive, and as such will contain eddy currents. The magnetic field generated by these currents for a range of frequencies and conductivities is shown in Figure 3.7. The two plots are very similar. Upon inspection of the analytical solution for the magnetic field, Equation (3.121), we find that the frequency and the conductivity both appear only in the wavenumber k, and as such their relationship to the magnetic field $\boldsymbol{B}$ is very similar. At low frequencies and conductivities, there is no magnetic field. The physical interpretation for this is that very low frequencies amount to a slowly-changing field, which is not enough to induce eddy currents and an eddy current field. On the other hand, a low conductivity of course implies an absence of currents, and hence no eddy current field.

As the frequency or conductivity increases, we begin to see an eddy current field. Initially, the field consists almost entirely of an imaginary component. This out-of-phase component increases, then reaches a maximum. From this point on, as the frequency or conductivity increases, the real part begins to dominate, until eventually the field is almost entirely real. A physical interpretation of this might be that as the frequency or conductivity increases, the eddy currents are pushed towards the surface (through the skin effect), and that therefore the eddy current field consists predominantly of a real (in-phase) component.

Now let us consider the case of a sphere which is both conducting and magnetic. Figure 3.8 shows the relevant fields for this case. Once again, the plots for varying frequency and conductivity are very similar. Interestingly, there is a region in which the induced magnetic field dominates (as in the left plot of Figure 3.6), and a region in which the field resembles the eddy current field of Figure 3.7. At low frequency or conductivity, eddy currents aren't generated, as shown in the earlier figures, so we see the induced magnetic field only. As the frequency or conductivity increases, eddy currents are generated. Recall that these eddy currents are oriented in such a way that they counteract the change in magnetic flux density. This might explain the decrease in the magnetic field as the eddy currents increase. The bottom plot, in which the magnetic permeability is varied, does not show the constant region seen in the other plots, as there is no induced magnetic field when the permeability is low. The behaviour of the field for the rest is the same as was seen for varying frequency and conductivity.

Finally, let us investigate the effect of the parameters on the joule losses. This is shown in Figure 3.9. As the strength of the background field B_0 increases, the joule losses increase monotonically. As can be seen from the derived expression, the relationship is in fact quadratic. Increasing frequency also leads to increasing joule losses. Upon inspecting the derived expression, we see that the relationship between frequency and joule losses is not as simple as was the case for B_0, since the frequency appears in the wavenumber k as well. However, the frequency appears as a factor ω in the equation, and this seems to dominate.

The material parameters μ_r and σ show more interesting behaviour: for both, there is a peak at which the

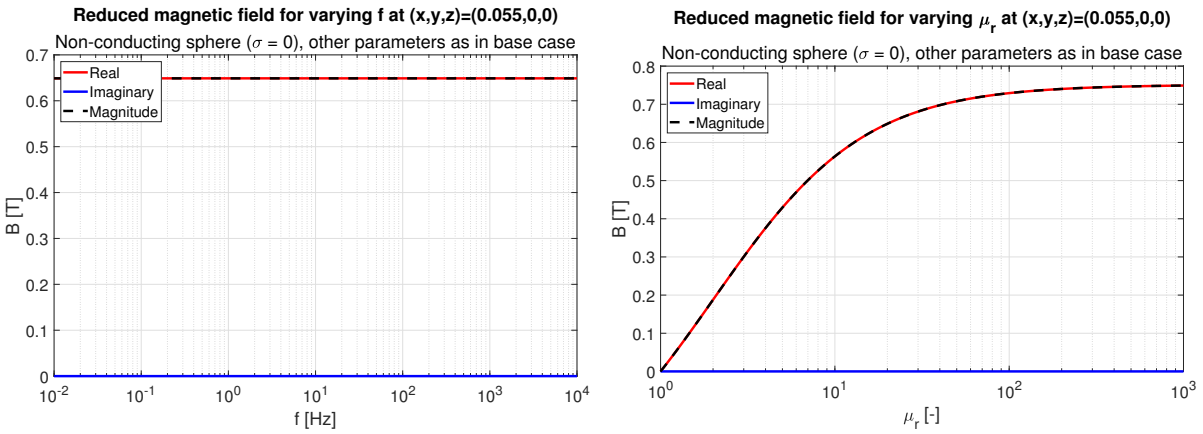

Figure 3.6: Effect of varying frequency (*left*) and magnetic permeablitiy (*right*) on the reduced magnetic field for a non-conducting sphere.

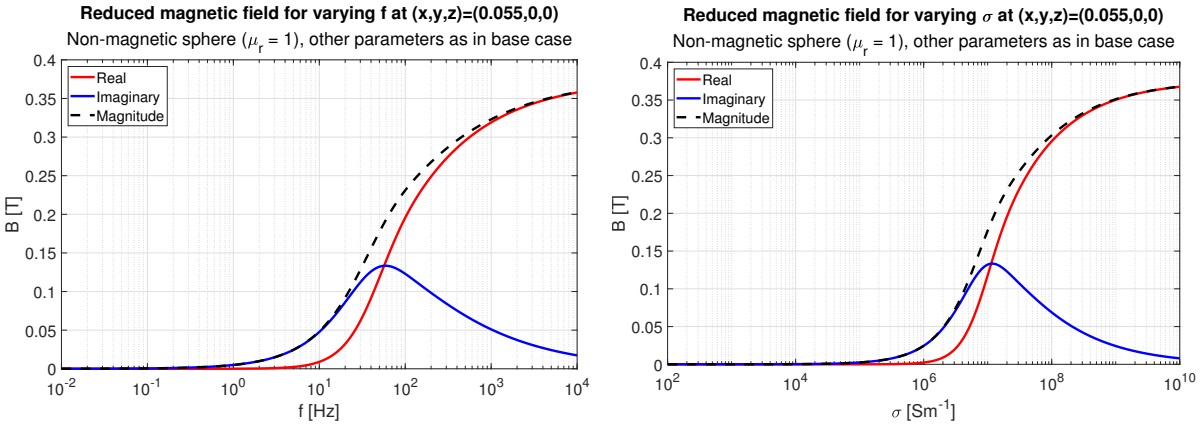

Figure 3.7: Effect of varying frequency (*left*) and conductivity (*right*) on the reduced magnetic field for a non-magnetic sphere.

joule losses are maximal. For the case of the conductivity σ, a possible interpretation might be that for high conductivities there is less resistance and hence less resistive heating. Thus we see joule losses only in the region where the conductivity is high enough to allow eddy currents to appear, but not so high that the eddy currents do not experience resistance.

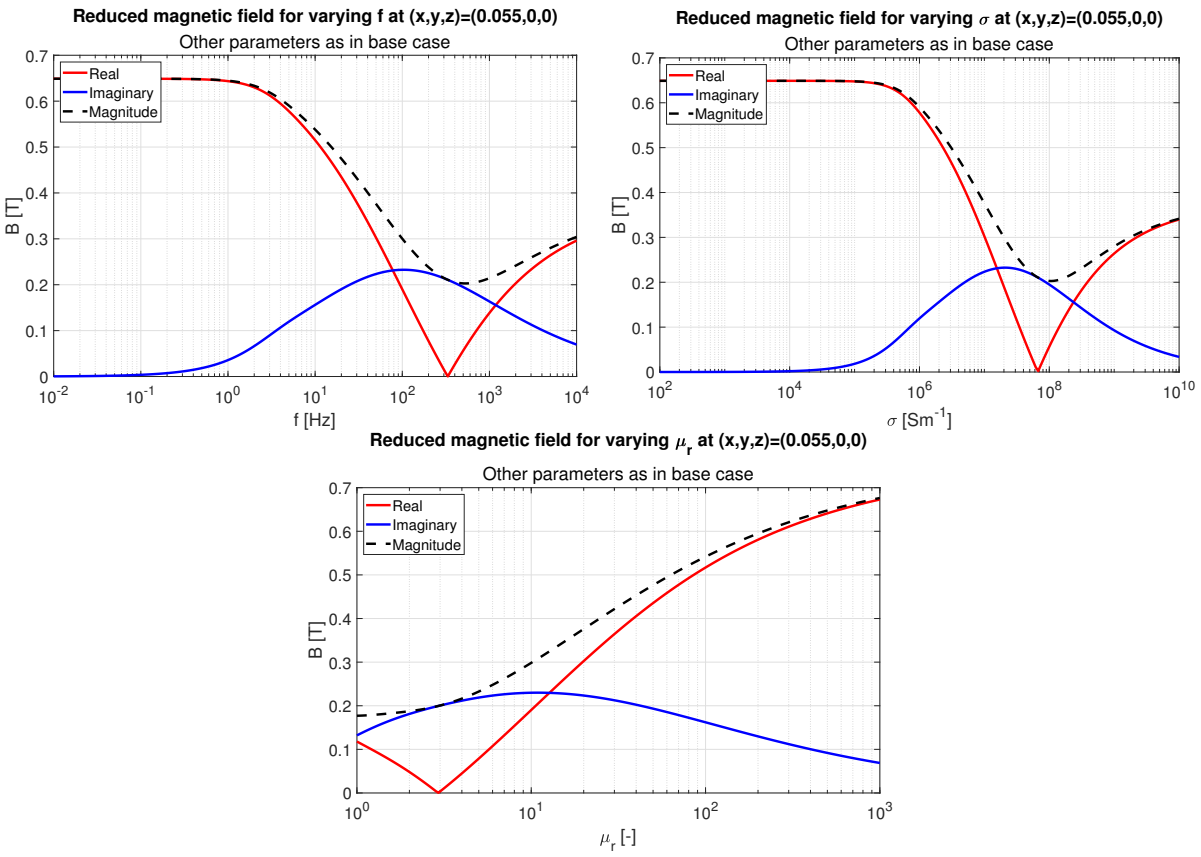

Figure 3.8: Effect of varying frequency (*left*), conductivity (*right*), and permeability (*bottom*) on the reduced magnetic field for a sphere.

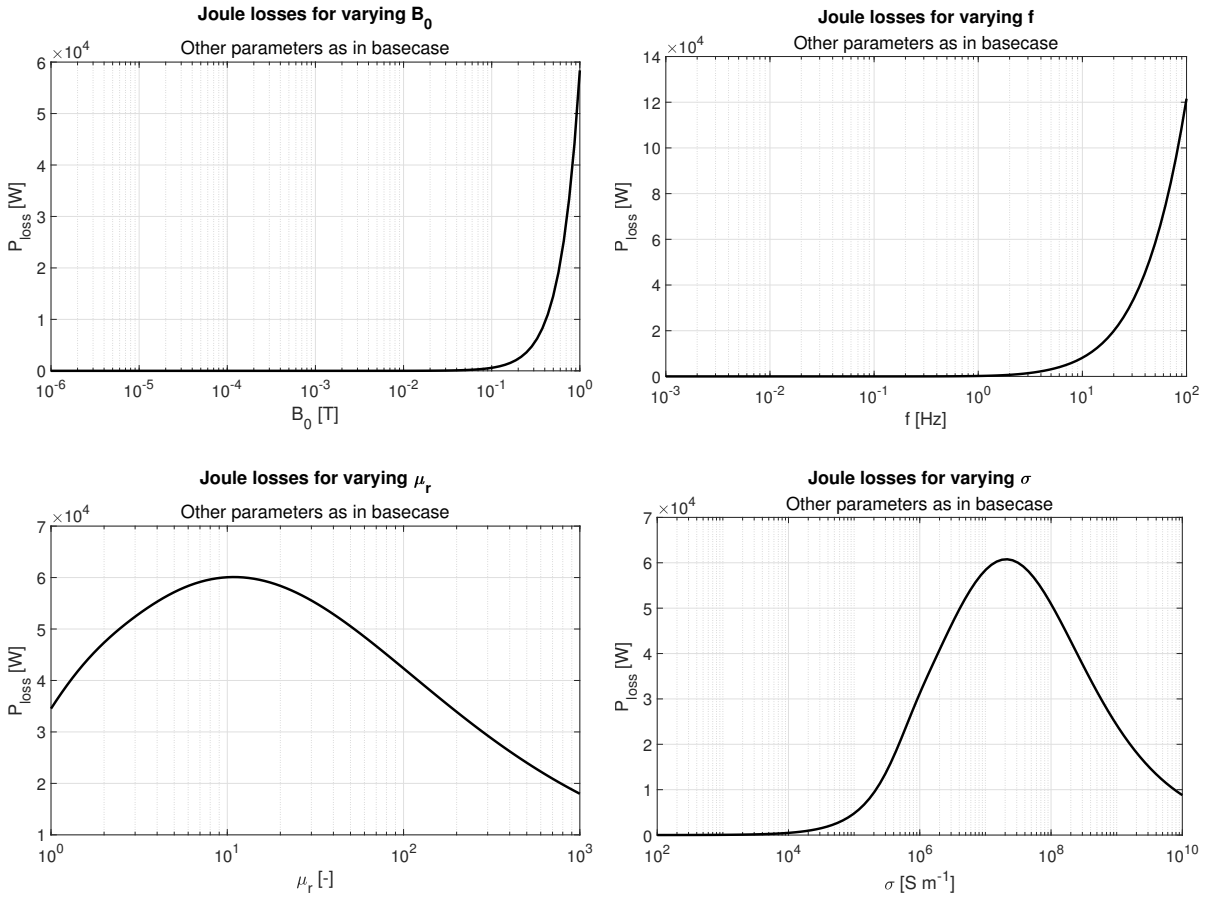

Figure 3.9: Effect of varying parameters on joule losses. *Top left:* varying background field B_0. *Top right:* varying frequency f. *Bottom left:* varying magnetic permeability μ_r. *Bottom right:* varying conductivity σ.

3.2.5. The eddy current field for a sphere as a magnetic dipole field

To gain a different understanding of the derived expressions, we will convert them back to Cartesian coordinates. We begin by considering the expression for the eddy currents in the sphere:

$$\boldsymbol{J} = -j\omega\sigma\boldsymbol{A} = -j\omega\sigma\sin\theta C j_1(kr)\hat{\boldsymbol{\varphi}}. \tag{3.125}$$

With the equations for the unit orthogonal vectors from Chapter A, this yields:

$$\begin{aligned}\boldsymbol{J} &= -j\omega\sigma\sin\theta C j_1(kr)\left(-\sin\varphi\hat{\boldsymbol{x}} + \cos\varphi\hat{\boldsymbol{y}}\right) &(3.126)\\ &= j\omega\sigma\sin\theta\sin\varphi C j_1(kr)\hat{\boldsymbol{x}} - j\omega\sigma\sin\theta\cos\varphi C j_1(kr)\hat{\boldsymbol{y}}. &(3.127)\end{aligned}$$

Using the relations between the Cartesian and spherical coordinate systems, e.g. $x = r\sin\theta\cos\varphi$, this can then be rewritten as:

$$\begin{aligned}\boldsymbol{J}(x,y,z) &= j\omega\sigma\frac{y}{r}C j_1(kr)\hat{\boldsymbol{x}} - j\omega\sigma\frac{x}{r}C j_1(kr)\hat{\boldsymbol{y}} &(3.128)\\ &= j\omega\sigma C\frac{y}{\sqrt{x^2+y^2+z^2}} j_1\left(k\sqrt{x^2+y^2+z^2}\right)\hat{\boldsymbol{x}} - j\omega\sigma C\frac{x}{\sqrt{x^2+y^2+z^2}} j_1\left(k\sqrt{x^2+y^2+z^2}\right)\hat{\boldsymbol{y}}. &(3.129)\end{aligned}$$

With this we have found the expression for the eddy currents inside the sphere, in Cartesian coordinates. Notably, there is no $\hat{\boldsymbol{z}}$ component, as expected since the currents only flow azimuthally.

By the same procedure, we can determine an expression for the magnetic flux density in the air region in Cartesian coordinates[2]. First, we substitute the local orthogonal spherical unit vectors by the Cartesian unit vectors:

$$\begin{aligned}\boldsymbol{B} &= \cos\theta\left(B_0 + \left(2Cr_0^2 j_1(kr_0) - B_0 r_0^3\right)r^{-3}\right)\hat{\boldsymbol{r}} - \sin\theta\left(B_0 - \left(Cr_0^2 j_1(kr_0) - \frac{B_0 r_0^3}{2}\right)r^{-3}\right)\hat{\boldsymbol{\theta}} &(3.130)\\ &= \cos\theta\left(B_0 + \left(2Cr_0^2 j_1(kr_0) - B_0 r_0^3\right)r^{-3}\right)\left(\sin\theta\cos\varphi\hat{\boldsymbol{x}} + \sin\theta\sin\varphi\hat{\boldsymbol{y}} + \cos\theta\hat{\boldsymbol{z}}\right)\\ &\quad - \sin\theta\left(B_0 - \left(Cr_0^2 j_1(kr_0) - \frac{B_0 r_0^3}{2}\right)r^{-3}\right)\left(\cos\theta\cos\varphi\hat{\boldsymbol{x}} + \cos\theta\sin\varphi\hat{\boldsymbol{y}} - \sin\theta\hat{\boldsymbol{z}}\right). &(3.131)\end{aligned}$$

This can be rearranged to:

$$\begin{aligned}\boldsymbol{B} &= \left(\cos\theta\sin\theta\cos\varphi\left(B_0 + \left(2Cr_0^2 j_1(kr_0) - B_0 r_0^3\right)r^{-3}\right) - \sin\theta\cos\theta\cos\varphi\left(B_0 - \left(Cr_0^2 j_1(kr_0) - \frac{B_0 r_0^3}{2}\right)r^{-3}\right)\right)\hat{\boldsymbol{x}}\\ &\quad + \left(\cos\theta\sin\theta\sin\varphi\left(B_0 + \left(2Cr_0^2 j_1(kr_0) - B_0 r_0^3\right)r^{-3}\right) - \sin\theta\cos\theta\sin\varphi\left(B_0 - \left(Cr_0^2 j_1(kr_0) - \frac{B_0 r_0^3}{2}\right)r^{-3}\right)\right)\hat{\boldsymbol{y}}\\ &\quad + \left(\cos^2\theta\left(B_0 + \left(2Cr_0^2 j_1(kr_0) - B_0 r_0^3\right)r^{-3}\right) + \sin^2\theta\left(B_0 - \left(Cr_0^2 j_1(kr_0) - \frac{B_0 r_0^3}{2}\right)r^{-3}\right)\right)\hat{\boldsymbol{z}}. &(3.132)\end{aligned}$$

Gathering terms and making use of trigonometric identities then yields:

$$\begin{aligned}\boldsymbol{B} &= \cos\theta\sin\theta\cos\varphi\left(3Cr_0^2 j_1(kr_0) - \frac{3B_0 r_0^3}{2}\right)r^{-3}\hat{\boldsymbol{x}} + \cos\theta\sin\theta\sin\varphi\left(3Cr_0^2 j_1(kr_0) - \frac{3B_0 r_0^3}{2}\right)r^{-3}\hat{\boldsymbol{y}}\\ &\quad + \left(B_0 + (3\cos^2\theta - 1)\left(Cr_0^2 j_1(kr_0) - \frac{B_0 r_0^3}{2}\right)r^{-3}\right)\hat{\boldsymbol{z}}. &(3.133)\end{aligned}$$

[2] We could of course also do this for the magnetic field inside the conductor, but this is of lesser interest to our purposes, and as such will be omitted.

Finally, replacing the variables yields:

$$\begin{aligned}\boldsymbol{B}(x,y,z) &= \left(3Cr_0^2 j_1(kr_0) - \frac{3B_0 r_0^3}{2}\right)\frac{xz}{r^5}\hat{\boldsymbol{x}} + \left(3Cr_0^2 j_1(kr_0) - \frac{3B_0 r_0^3}{2}\right)\frac{yz}{r^5}\hat{\boldsymbol{y}} \\ &\quad + \left(B_0 + \left(3\frac{z^2}{r^2} - 1\right)\left(Cr_0^2 j_1(kr_0) - \frac{B_0 r_0^3}{2}\right)r^{-3}\right)\hat{\boldsymbol{z}} \qquad (3.134) \\ &= \left(3Cr_0^2 j_1(kr_0) - \frac{3B_0 r_0^3}{2}\right)\frac{xz}{\left(x^2+y^2+z^2\right)^{5/2}}\hat{\boldsymbol{x}} \\ &\quad + \left(3Cr_0^2 j_1(kr_0) - \frac{3B_0 r_0^3}{2}\right)\frac{yz}{\left(x^2+y^2+z^2\right)^{5/2}}\hat{\boldsymbol{y}} \\ &\quad + \left(B_0 + \left(3\frac{z^2}{\left(x^2+y^2+z^2\right)^{5/2}} - \frac{1}{\left(x^2+y^2+z^2\right)^{3/2}}\right)\left(Cr_0^2 j_1(kr_0) - \frac{B_0 r_0^3}{2}\right)\right)\hat{\boldsymbol{z}}. \qquad (3.135)\end{aligned}$$

Rewriting this somewhat allows us to recognize the components of the field:

$$\boldsymbol{B}(x,y,z) = B_0\hat{\boldsymbol{z}} + \left(Cr_0^2 j_1(kr_0) - \frac{B_0 r_0^3}{2}\right)\left(\frac{3xz\hat{\boldsymbol{x}} + 3yz\hat{\boldsymbol{y}} + 3z^2\hat{\boldsymbol{z}}}{\left(x^2+y^2+z^2\right)^{5/2}}\right) - \frac{Cr_0^2 j_1(kr_0) - \frac{B_0 r_0^3}{2}}{\left(x^2+y^2+z^2\right)^{3/2}}\hat{\boldsymbol{z}}. \qquad (3.136)$$

In the first term, we recognize the excitation field $B_0\hat{\boldsymbol{z}}$. The other terms can in fact be rewritten to the form of a magnetic dipole. The magnetic flux density at a point $\boldsymbol{r} = (x,y,z)$ due to a magnetic dipole with magnetic dipole moment $\boldsymbol{m}$ is:

$$\boldsymbol{B}_{\text{dip}}(\boldsymbol{r}) = \frac{\mu_0}{4\pi}\left(\frac{3\boldsymbol{r}(\boldsymbol{m}\cdot\boldsymbol{r})}{|\boldsymbol{r}|^5} - \frac{\boldsymbol{m}}{|\boldsymbol{r}|^3}\right). \qquad (3.137)$$

Defining the magnetic moment $\boldsymbol{m}$ as

$$\boldsymbol{m} = \frac{4\pi}{\mu_0}\left(Cr_0^2 j_1(kr_0) - \frac{B_0 r_0^3}{2}\right), \qquad (3.138)$$

we find that the magnetic dipole field describes the remaining terms of the analytical solution exactly. Thus the reduced magnetic field due to the eddy currents for the sphere is found to be the field of a magnetic dipole, periodically varying with the forcing frequency.

4

Survey of methods for eddy current approximation

This chapter will give an overview of the formulations and methods available for solving the eddy current problem. After discussing the problem, the various potential formulations, and the different numerical techniques for solving these problems, an overview of several candidate methods will be given, of which one will be chosen to be implemented.

4.1. The eddy current problem and the various ways it can be solved

4.1.1. The eddy current problem

We begin by considering eddy current problems in general. Several formulations and techniques for the modelling of three-dimensional eddy current effects exist, which will be discussed here. The general setting under consideration is a conductive (and possibly magnetic) object in a domain of free air. Under the quasi-static assumption and in the frequency domain, as derived in Chapter 3.1, the system is governed by the Maxwell equations:

$$\begin{cases} \nabla \times \boldsymbol{H} &= \sigma_1 \boldsymbol{E}, \\ \nabla \times \boldsymbol{E} &= -j\omega \boldsymbol{B}, \\ \nabla \cdot \boldsymbol{B} &= 0, \\ \nabla \cdot \boldsymbol{D} &= \rho_f. \end{cases} \tag{4.1}$$

Here $\boldsymbol{D}$ is the electric displacement field (in $\mathrm{C\,m^{-2}}$), $\boldsymbol{E}$ is the electric field (in $\mathrm{V\,m^{-1}}$), $\boldsymbol{H}$ is the auxiliary field (in $\mathrm{A\,m^{-1}}$), $\boldsymbol{B}$ is the magnetic induction field (in T), ρ_f denotes the free charge density (in $\mathrm{C\,m^{-3}}$), and $\boldsymbol{J}_f$ denotes the free current density (in $\mathrm{A\,m^{-2}}$). These equations are supplemented by constitutive relations which relate $\boldsymbol{D}$ to $\boldsymbol{E}$, and $\boldsymbol{H}$ to $\boldsymbol{B}$. These constitutive relations may be linear or non-linear. For eddy current calculations, the constitutive relations will generally be assumed linear:

$$\boldsymbol{D} = \epsilon \boldsymbol{E} \tag{4.2}$$

$$\boldsymbol{H} = \frac{1}{\mu} \boldsymbol{B}. \tag{4.3}$$

Here ϵ is the permittivity of the material (in $\mathrm{F\,m^{-1}}$) and μ is the magnetic permeability of the material (in $\mathrm{H\,m^{-1}}$). Finally, Ohm's Law relates the electric field to the free current density:

$$\boldsymbol{J} = \sigma \boldsymbol{E}, \tag{4.4}$$

where σ is the electrical conductivity of the material (in $\mathrm{S\,m^{-1}}$).

4.1.2. Formulations using various potentials

Due to the nature of the governing equations, it is often preferable to solve eddy current problems using a formulation with potentials, as opposed to solving for the current density or magnetic field directly. The form

of the Maxwell equations allows us to express the magnetic and electric fields with various vector and scalar potentials (see Appendix C for a justification of these potentials). Carpenter [10] gives an overview of several formulations in a seminal paper from 1977. The formulations discussed can be split into two categories: those making use of a magnetic vector potential $\boldsymbol{A}$, and those making use of an electric vector potential $\boldsymbol{T}$. Within these categories, various other potentials can be constructed for the other fields, which are also differentiated by their choice of divergence, as well as their behaviour across interfaces. Robert et al. [34] mentions, for example, the formulations $\boldsymbol{A}-\boldsymbol{\Omega}$, $\boldsymbol{T}-\boldsymbol{\Omega}$, $\boldsymbol{A}^*-\boldsymbol{\Omega}$, $\boldsymbol{A}-\boldsymbol{\Phi}-\boldsymbol{\Omega}$, $\boldsymbol{E}-\boldsymbol{\Omega}$, and $\boldsymbol{H}-\boldsymbol{\Omega}$. Each has its advantages and disadvantages for specific types of problems.

Many contemporary methods (e.g. [29], [30], [36]) make use of the magnetic vector potential $\boldsymbol{A}$: inside the conductor, the magnetic flux density can be expressed as

$$\boldsymbol{B} = \nabla \times \boldsymbol{A}. \tag{4.5}$$

Filling this in in Faraday's equation, one finds that the electric field can be expressed as

$$\boldsymbol{E} = -j\omega\boldsymbol{A} - \nabla\phi, \tag{4.6}$$

where ϕ is the electric scalar potential. To make this potential unique, a gauge must be chosen. Common choices are the Coulomb gauge

$$\nabla \cdot \boldsymbol{A} = 0, \tag{4.7}$$

and the Lorenz gauge

$$\nabla \cdot \boldsymbol{A} = -\mu\sigma\phi, \tag{4.8}$$

which was seen in the analytical solution in the previous chapter. Biro and Preis [5] give a very detailed overview of the various formulations which can be constructed from the magnetic vector potential $\boldsymbol{A}$.

An important variant is introduced by Emson and Simkin [12] and will be discussed in some detail here. It is called the modified magnetic vector potential method, and denoted by $\boldsymbol{A}^*$. They claim that it requires the minimum degrees of freedom and is numerically stable. By doing away with the electric scalar potential in the conductor, and by making use of a magnetic scalar potential in the non-conductor, it requires only three degrees of freedom in the conductor, and only one degree of freedom in the non-conductor [1]. The modified magnetic scalar method is derived by defining:

$$\boldsymbol{A}^* = \boldsymbol{A} + \frac{\nabla\phi}{j\omega}, \tag{4.9}$$

and noting that $\nabla \times \boldsymbol{A}^* = \nabla \times \boldsymbol{A} = \boldsymbol{B}$, one finds that the system inside the conductor is governed by

$$\begin{cases} \boldsymbol{A} = -j\omega\boldsymbol{A}^* \\ \nabla \times \boldsymbol{A}^* = \boldsymbol{B}. \end{cases} \tag{4.10}$$

The modified vector potential is made unique by choosing the Coulomb gauge $\nabla \cdot \boldsymbol{A}^* = 0$. Outside the conductor, the field is irrotational. The magnetic field $\boldsymbol{H}$ can be decomposed into the source field $\boldsymbol{H}_s$ and the field generated by the eddy currents $\boldsymbol{H}_m$, which can be expressed as the gradient of a scalar potential φ:

$$\boldsymbol{H}_m = -\nabla\varphi. \tag{4.11}$$

This reduced magnetic scalar potential satisfies the Laplace equation. With the appropriate interface conditions (continuity of the tangential component of the $\boldsymbol{H}$ field, and continuity of the normal component of the $\boldsymbol{B}$ field) leads to the final $\boldsymbol{A}^* - \phi$ formulation. The derivation will be done in more detail in Chapter 5.

4.1.3. Finite elements, boundary elements, and edge elements

Once the problem is expressed in a suitable formulation, one must decide how to go about solving the problem. A common approach is to make use of a finite element method (FEM). The domain is discretized into volume elements, and the solution is assumed to be composed of a linear combination of basis functions defined on these elements. Using variational methods, a system of equations is assembled, which when solved

[1] In contrast, they state that although the methods using the electric vector potential $\boldsymbol{T}$ only makes use of a single degree of freedom outside the conductor, but that this comes at the cost of needing four degrees of freedom within the conductor, as well as the difficulties introduced by the discontinuity in $\boldsymbol{T}$ across the interface.

yields the coefficients of the basis functions. When the test functions are chosen to be the same as the basis functions, this is referred to as Galerkin's method. An example of Galerkin's approach is the formulation by Xu and Simkin [46], which makes use of the total and reduced magnetic vector potential and the electric scalar potential. This method gives good results for their test problems, one of which, interestingly, is a ship.

Making use of a FEM involves meshing the entire domain, which is computationally expensive. However, FEM leads to sparse matrices, for which fast solving methods exist. It also has as a drawback that it is not very versatile, if one for example wishes to know the fields at a point outside the domain. Thus problems with unbounded domains are less suitable for FEM. This can be overcome by making use of a boundary element method (BEM). The idea behind this method is to find a relation between the fields in the unbounded region and the values of the potentials on the boundary itself. Note that BEM leads to full matrices, in contrast to the sparse matrices found by FEM. Hybrid methods wherein the conductor is meshed using volume elements, and the boundary is meshed using boundary elements, have been applied with great success (e.g. [33],[36],[29] [21]). A very detailed introduction to the coupled BEM-FEM method is given in [8]. An overview of BEM methods for eddy currents is given by Ren et al. [32].

The choice of basis functions merits some thought as well. The most common choice is to use linear nodal basis functions. For each node of the mesh, the corresponding nodal basis function is defined such that it has value 1 at that node, value 0 on each other node, and is linear on each element (and thus piecewise linear on the entire domain). One might expect that these nodal shape functions can also be used to approximate a vector-valued unknown, by simply using three nodal shape functions (one for each component). In many cases this works well, however for eddy current problems it turns out that this may lead to nonphysical solutions [7, p. 108].

An alternative shape function which is appropriate for eddy current problems is the edge element (or edge shape function). The edge shape function is associated with an edge of an element, and is defined such that its circulation along that edge is 1, and its circulation along any other edge is 0. A more detailed investigation into the properties of edge functions will be given in Chapter 6. Much has been written about the motivation and rationale for edge functions; see for example [8], [25], or the cheerfully named [45]. In effect, the main advantage of edge elements is this: they enforce tangential continuity, but place no restriction on normal discontinuity, and are thus useful for modelling electromagnetic fields along interfaces between two different media. Edge elements are used in almost every formulation discussed above.

4.2. Choosing a method to be implemented

Having discussed the various tools which we have at our disposal in solving the eddy current problem, a choice must be made concerning the approach used in this project. For this, the following criteria are taken into account:

- For now, the geometry will be assumed to be simply connected, however eventually the method will be applied to a multiply connected domain.
- It should be possible to calculate the electromagnetic fields everywhere in the free air region.
- A method which can be incorporated with method-of-moments code is preferable.

A shortlist of four methods was determined. The methods under consideration were:

1. $\boldsymbol{A}^* - \varphi$ BEM-FEM. Detailed overview can be found in [29]. Coupled BEM-FEM method for simply connected object.
2. $\boldsymbol{A}^* - \varphi$ BEM. Detailed overview can be found in [30]. Pure BEM method for simply connected object (but can be extended to multiple objects).
3. Total and reduced vector potential. Detailed overview can be found in [46]. Pure FEM method for simply connected objects.
4. Unstructured-PEEC. Detailed overview can be found in [22]. Circuit-like integral method which is well-suited for thin media and systems with coupled external electric circuits.

Method (3) is the 'oldest' method under consideration. It is included because the paper explicitly shows good results for a ship geometry. However, as a pure FEM method, it involves meshing the entire domain, and

thus it is not easy to calculate the electromagnetic fields everywhere in the free air region. Hence this method will not be implemented.

Method (4) seems to be a good fit for the problem under consideration, as it is applicable to thin shells. However, the method is very complicated due to its choice of potentials (using vector and scalar potentials for both the conducting and non-conducting region) which leads to many degrees of freedom, as well as making use of circuit theory. This method is therefore deemed out of the scope of this research project, although it remains an interesting topic for further research.

Methods (1) and (2) are similar, making use of the same potential formulation, but differing in their discretisation method. Based on the degree of detail in the papers, method (2) appeared more feasible to implement, since it contained explicit equations for the system matrix. It also requires no volume meshing, but only surface meshing, which reduces meshing complexity and reduces the amount of unknowns in the system. As a further benefit, it can be extended to problems with multiple material regions. As such, it was chosen to implement the $\boldsymbol{A}^* - \varphi$ BEM method described in [30].

5

Derivation of BEM method

In this chapter, a complete derivation of the BEM method as outlined in [30] is given. Only the situation with a single conductive region will be considered, for which an explicit system of equations will be described, as well as methods for approximating the (singular) integrals involved.

5.1. Eddy current problem and potential formulation

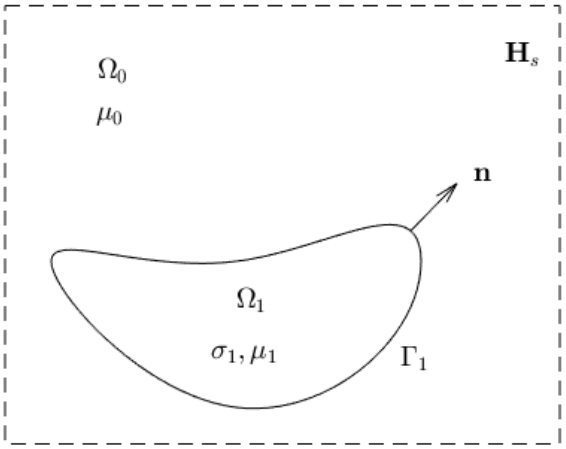

Figure 5.1: Schematic overview of a magnetic conductor Ω_1 in a free air region Ω_0 being excited by a periodically varying background field $\boldsymbol{H}_s$.

Consider a three-dimensional region Ω_1 (bounded by the surface Γ_1 and outward normal $\boldsymbol{n}$) which is magnetic (with permeability μ_1) and conductive (with conductivity σ_1). It is located in a free air domain Ω_0 which has permeability μ_0. The system is excited by an external magnetic source coil, which causes the exciting magnetic source field $\boldsymbol{H}_s$. The situation is sketched in Figure 5.1. As has been the case in the earlier derivations, displacement currents are neglected, and the problem is solved in the frequency domain. Under these quasi-static assumptions, the magnetic and electric fields in the conductor are governed by the following set of equations:

$$\begin{cases} \nabla \times \boldsymbol{H} = \sigma_1 \boldsymbol{E}, \\ \nabla \times \boldsymbol{E} = -j\omega \boldsymbol{B}, \end{cases} \tag{5.1}$$

where j is the imaginary unit, and ω is the frequency of the source field $\boldsymbol{H}_s$. The modified magnetic vector potential $\boldsymbol{A}^*$ will be used to find a system of differential equations. The modified vector potential $\boldsymbol{A}^*$ is derived [12] as follows. First, consider the region inside the conductor. Recall that the magnetic flux density $\boldsymbol{B}$ inside the conductor can be expressed with a magnetic vector potential $\boldsymbol{A}$:

$$\boldsymbol{B} = \nabla \times \boldsymbol{A}. \tag{5.2}$$

Filling this in in the equation for $\nabla \times \boldsymbol{E}$ above yields:

$$\nabla \times \boldsymbol{E} = -j\omega \nabla \times \boldsymbol{A}. \tag{5.3}$$

Taking everything to the left hand side, one finds:

$$\nabla \times \left(\boldsymbol{E} + j\omega \boldsymbol{A}\right) = \boldsymbol{0}. \tag{5.4}$$

This implies that the quantity on the left hand side can be expressed as the gradient of a scalar potential ϕ:

$$\boldsymbol{E} + j\omega \boldsymbol{A} = -\nabla \phi, \tag{5.5}$$

or, equivalently, that the electric field $\boldsymbol{E}$ inside the conductor can be expressed with $\boldsymbol{A}$ and a scalar potential ϕ:

$$\boldsymbol{E} = -j\omega \boldsymbol{A} - \nabla \phi. \tag{5.6}$$

This motivates the definition of the modified magnetic vector potential $\boldsymbol{A}^*$:

$$\boldsymbol{A}^* = \boldsymbol{A} + \frac{\nabla \phi}{j\omega}, \tag{5.7}$$

so that $\boldsymbol{E} = -j\omega \boldsymbol{A}^*$. Physically, since $\boldsymbol{E}$ is proportional to $\boldsymbol{A}^*$, this implies that the potential $\boldsymbol{A}^*$ must not leave the sphere. Therefore, the condition $\boldsymbol{n} \cdot \boldsymbol{A}^* = 0$ will be imposed. Also, note that $\nabla \times \boldsymbol{A}^* = \nabla \times \boldsymbol{A} = \boldsymbol{B}$, in other words, the modified magnetic vector potential has the same curl as the original vector potential $\boldsymbol{A}$. Thus the system inside the conductor is described by

$$\begin{cases} \boldsymbol{E} = -j\omega \boldsymbol{A}^*, \\ \nabla \times \boldsymbol{A}^* = \boldsymbol{B}. \end{cases} \tag{5.8}$$

By setting the Coulomb gauge, $\nabla \cdot \boldsymbol{A}^* = 0$, the modified magnetic vector potential is made unique. Combining these two equations, one finds that the modified magnetic scalar potential must satisfy the following equation:

$$\nabla \times \nabla \times \boldsymbol{A}^* + j\omega \sigma_1 \mu_1 \boldsymbol{A}^* = \boldsymbol{0}. \tag{5.9}$$

This equation is equivalent to the Helmholtz equation, since one has the vector identity $\nabla \times \nabla \times \boldsymbol{A}^* = \nabla(\nabla \cdot \boldsymbol{A}^*) - \nabla^2 \boldsymbol{A}^*$, and the Coulomb gauge, which together yield:

$$-\nabla^2 \boldsymbol{A}^* + j\omega \sigma_1 \mu_1 \boldsymbol{A}^* = \boldsymbol{0}. \tag{5.10}$$

With this, the governing equation for the region inside the conductor has been found.

Now consider the free air region Ω_0. In this region, a different approach is used. Denote the magnetic field caused by the eddy currents with $\boldsymbol{H}_m$, which, together with the source field $\boldsymbol{H}_s$, forms the total magnetic field:

$$\boldsymbol{H} = \boldsymbol{H}_s + \boldsymbol{H}_m. \tag{5.11}$$

The source field $\boldsymbol{H}_s$ is known. The magnetic field caused by the eddy currents ($\boldsymbol{H}_m$) is irrotational, and thus it can be expressed as the gradient of a scalar potential φ:

$$\boldsymbol{H}_m = -\nabla \varphi. \tag{5.12}$$

This leads to the following formulation, which is called the reduced magnetic scalar potential formulation:

$$\boldsymbol{H} = \boldsymbol{H}_s - \nabla \varphi. \tag{5.13}$$

From magnetostatics, it is known that the magnetic field is solenoidal, from which it follows that the scalar potential φ is governed by a Laplace equation:

$$\Delta \varphi = 0. \tag{5.14}$$

5.2. Interface conditions

Having found a description of the system in terms of a magnetic vector potential inside the conductor and a reduced scalar potential in the free air region, what remains is to determine the boundary conditions at the interface. Using a suitable infinitesimal volume (the *Gaussian pillbox*, [19, p. 16]) and the Maxwell equations, the following interface conditions are found:

$$\begin{cases} (\boldsymbol{n}\times\boldsymbol{H})|_{\Omega_1} = (\boldsymbol{n}\times\boldsymbol{H})|_{\Omega_0}, \\ \mu_1(\boldsymbol{n}\cdot\boldsymbol{H})\big|_{\Omega_1} = \mu_0(\boldsymbol{n}\cdot\boldsymbol{H})\big|_{\Omega_0}, \end{cases} \tag{5.15}$$

where the subscripts denote the domain to which the quantity belongs. The quantities on the left-hand side refer to the conductive domain Ω_1, while the quantities on the right-hand side belong to the free air domain Ω_0. In effect, the first boundary condition states that the tangential component of the magnetic field $\boldsymbol{H}$ must be continuous, while the second boundary condition states that the normal component of the magnetic flux density $\boldsymbol{B}$ must be continuous. These quantities can be expressed in terms of the formulated potentials: in Ω_1, the magnetic field $\boldsymbol{H}$ can be rewritten as:

$$\boldsymbol{H} = \frac{1}{\mu_1}\boldsymbol{B} = \frac{1}{\mu_1}\nabla\times\boldsymbol{A}^*. \tag{5.16}$$

In Ω_0, the magnetic field $\boldsymbol{H}$ can be rewritten using the reduced magnetic scalar potential formulation (Equation (5.13)), i.e. $\boldsymbol{H} = \boldsymbol{H}_s - \nabla\varphi$. Thus the boundary conditions are rewritten to express the relationship between $\boldsymbol{A}^*$ and φ at the interface:

$$\begin{cases} \boldsymbol{n}\times\left(\nabla\times\boldsymbol{A}^*\right) &= \mu_1\left(\boldsymbol{n}\times\boldsymbol{H}_s - \boldsymbol{n}\times\nabla\varphi\right), \\ \boldsymbol{n}\cdot\left(\nabla\times\boldsymbol{A}^*\right) &= \mu_0\left(\boldsymbol{n}\cdot\boldsymbol{H}_s - \boldsymbol{n}\cdot\nabla\varphi\right). \end{cases} \tag{5.17}$$

5.3. Integral form and Green's functions

The system hereby obtained, governed by the Helmholtz equation (5.10) for $\boldsymbol{A}^*$ and Laplace equation (5.14) for φ, can be restated in an integral equation by making use of the Green's functions for the equations. A complete overview of the motivation behind the Green's functions, and their derivation, is given in Appendix D. For the Helmholtz equation, the Green's function is found as the the solution of

$$\Delta G_1(\boldsymbol{r},\boldsymbol{r}') - j\omega\mu_1\sigma_1 G_1(\boldsymbol{r},\boldsymbol{r}') + \delta(\boldsymbol{r},\boldsymbol{r}') = 0, \tag{5.18}$$

where $\boldsymbol{r}'$ is the integration point, $\boldsymbol{r}$ is the observation point, and δ is a Dirac function. One might note that the term $\nabla\times\nabla\times\boldsymbol{A}^*$ has been replaced by a the negative Laplacian. This is valid, since $\nabla\times\nabla\times\boldsymbol{A}^* = \nabla(\nabla\cdot\boldsymbol{A}^*) - \nabla^2\boldsymbol{A}^*$, and $\nabla\cdot\boldsymbol{A}^* = 0$ by the Coulomb gauge. The equation is solved by

$$G_1(\boldsymbol{r},\boldsymbol{r}') = \frac{1}{4\pi|\boldsymbol{r}-\boldsymbol{r}'|}e^{-jk|\boldsymbol{r}-\boldsymbol{r}'|}, \tag{5.19}$$

where

$$k = (1-j)\sqrt{\frac{\omega\mu_1\sigma_1}{2}}. \tag{5.20}$$

For the modified vector potential, the following vector analogue of the Green's function must hold [42]:

$$\begin{aligned} \int_{\Omega_1}\Big(\left(\nabla\cdot\boldsymbol{A}^*(\boldsymbol{r})\right)\nabla G_1(\boldsymbol{r},\boldsymbol{r}') + \boldsymbol{A}^*(\boldsymbol{r})\Delta G_1(\boldsymbol{r},\boldsymbol{r}') + G_1(\boldsymbol{r},\boldsymbol{r}')\left(\nabla\times\nabla\times\boldsymbol{A}^*(\boldsymbol{r})\right)\Big)\,\mathrm{d}\boldsymbol{r} \\ = \oiint_{\Gamma_1}\Big(\left(\boldsymbol{n}\cdot\boldsymbol{A}^*(\boldsymbol{r})\right)\nabla G_1(\boldsymbol{r},\boldsymbol{r}') + \left(\boldsymbol{n}\times\boldsymbol{A}^*(\boldsymbol{r})\right)\times\nabla G_1(\boldsymbol{r},\boldsymbol{r}') + \left(\boldsymbol{n}\times(\nabla\times\boldsymbol{A}^*(\boldsymbol{r}))\right)G_1(\boldsymbol{r},\boldsymbol{r}')\Big)\,\mathrm{d}\boldsymbol{r}. \end{aligned} \tag{5.21}$$

Note that due to the Coulomb Gauge, $\nabla\cdot\boldsymbol{A}^* = 0$. Additionally, $\boldsymbol{n}\cdot\boldsymbol{A}^* = 0$ will be imposed. This yields:

$$\int_{\Omega_1}\boldsymbol{A}^*(\boldsymbol{r})\Delta G_1(\boldsymbol{r},\boldsymbol{r}') + G_1(\boldsymbol{r},\boldsymbol{r}')\left(\nabla\times\nabla\times\boldsymbol{A}^*(\boldsymbol{r})\right)\mathrm{d}\boldsymbol{r} = \oiint_{\Gamma_1}\left(\boldsymbol{n}\times\boldsymbol{A}^*(\boldsymbol{r})\right)\times\nabla G_1(\boldsymbol{r},\boldsymbol{r}') + \left(\boldsymbol{n}\times(\nabla\times\boldsymbol{A}^*(\boldsymbol{r}))\right)G_1(\boldsymbol{r},\boldsymbol{r}')\,\mathrm{d}\boldsymbol{r}. \tag{5.22}$$

Filling in the expression for ΔG_1 from Equation (5.18) in the left hand side yields

$$\int_{\Omega_1} \boldsymbol{A}^*(\boldsymbol{r})\left(j\omega\mu_1\sigma_1 G_1(\boldsymbol{r},\boldsymbol{r}') - \delta(\boldsymbol{r},\boldsymbol{r}')\right) + G_1(\boldsymbol{r},\boldsymbol{r}')\left(\nabla\times\nabla\times\boldsymbol{A}^*(\boldsymbol{r})\right)\,\mathrm{d}\boldsymbol{r} = \oiint_{\Gamma_1}\left(\boldsymbol{n}\times\boldsymbol{A}^*(\boldsymbol{r})\right)\times\nabla G_1(\boldsymbol{r},\boldsymbol{r}') + \left(\boldsymbol{n}\times(\nabla\times\boldsymbol{A}^*(\boldsymbol{r}))\right)G_1(\boldsymbol{r},\boldsymbol{r}')\,\mathrm{d}\Gamma, \quad (5.23)$$

and since Equation (5.10) holds, this is equivalent to:

$$\int_{\Omega_1} -\boldsymbol{A}^*(\boldsymbol{r})\delta(\boldsymbol{r},\boldsymbol{r}')\,\mathrm{d}\boldsymbol{r} = \oiint_{\Gamma_1}\left(\boldsymbol{n}\times\boldsymbol{A}^*(\boldsymbol{r})\right)\times\nabla G_1(\boldsymbol{r},\boldsymbol{r}') + \left(\boldsymbol{n}\times(\nabla\times\boldsymbol{A}^*(\boldsymbol{r}))\right)G_1(\boldsymbol{r},\boldsymbol{r}')\,\mathrm{d}\boldsymbol{r}. \quad (5.24)$$

The integral on the left hand side can be rewritten, using the sifting property of the Dirac delta function. In simple terms, the integral will yield the value of $\boldsymbol{A}^*$ at the point $\boldsymbol{r}'$. Note that $\boldsymbol{A}^*$ outsidethe conductor is zero. If $\boldsymbol{r}'$ lies on the surface of the conductor, a coefficient h_1, which depends on the smoothness of the surface, needs to be taken into account. For a smooth surface, this coefficient is 0.5. This leads to the following integral boundary equation of the modified vector potential:

$$h_1\boldsymbol{A}^*(\boldsymbol{r}') = -\oiint_{\Gamma_1}\left(\boldsymbol{n}\times\boldsymbol{A}^*(\boldsymbol{r})\right)\times\nabla G_1(\boldsymbol{r},\boldsymbol{r}') + \left(\boldsymbol{n}\times(\nabla\times\boldsymbol{A}^*(\boldsymbol{r}))\right)G_1(\boldsymbol{r},\boldsymbol{r}')\,\mathrm{d}\boldsymbol{r}, \quad (5.25)$$

with

$$h_1 = \begin{cases} 0 \text{ if } \boldsymbol{r} \text{ is outside } \Omega_1 \\ 1 \text{ if } \boldsymbol{r} \text{ is inside } \Omega_1 \\ \frac{1}{2} \text{ if } \boldsymbol{r} \text{ is on the (regular) surface } \Gamma_1 \end{cases}. \quad (5.26)$$

In a similar way, one can use a Green's function to derive an integral boundary equation for the free air region. For the Laplace equation, which the scalar potential φ must satisfy, the Green's function G_0 is the solution to

$$\Delta G_0(\boldsymbol{r},\boldsymbol{r}') + \delta(\boldsymbol{r},\boldsymbol{r}') = 0, \quad (5.27)$$

where once again $\boldsymbol{r}$ is the observation point, $\boldsymbol{r}'$ is the integration point, and δ denotes a Dirac function. This equation is solved by

$$G_0(\boldsymbol{r},\boldsymbol{r}') = \frac{1}{4\pi|\boldsymbol{r}-\boldsymbol{r}'|}. \quad (5.28)$$

The usual continuation is to make use of Green's second theorem. However, Green's theorem applies only to bounded regions, and the exterior problem under consideration extends to infinity. Hence it is necessary to consider a large sphere, having radius R and outer boundary Γ_V, which encompasses the the conducting region, and apply Gauss' theorem to the area V between Γ_1 and Γ_V. Let $\boldsymbol{n}_o$ be the normal vector on the outside of this sphere, and let $\boldsymbol{n}_i$ be the normal vector on the inside of this sphere. Figure 5.2 shows a sketch of this situation. Note that $\boldsymbol{n}_i$ points into Ω_1, and that therefore $\boldsymbol{n} = -\boldsymbol{n}_i$. To this bounded region Green's second theorem can be applied, which states that:

$$\int_V \left(\varphi(\boldsymbol{r})\Delta G_0(\boldsymbol{r},\boldsymbol{r}') - G_0(\boldsymbol{r},\boldsymbol{r}')\Delta\varphi(\boldsymbol{r})\right)\mathrm{d}\boldsymbol{r} = \oiint_{\Gamma_1}\left(\left(\boldsymbol{n}_i\cdot\nabla G_0(\boldsymbol{r},\boldsymbol{r}')\right)\varphi(\boldsymbol{r}) - \left(\boldsymbol{n}_i\cdot\nabla\varphi(\boldsymbol{r})\right)G_0(\boldsymbol{r},\boldsymbol{r}')\right)\mathrm{d}\boldsymbol{r} + \oiint_{\Gamma_V}\left(\left(\boldsymbol{n}_o\cdot\nabla G_0(\boldsymbol{r},\boldsymbol{r}')\right)\varphi(\boldsymbol{r}) - \left(\boldsymbol{n}_o\cdot\nabla\varphi(\boldsymbol{r})\right)G_0(\boldsymbol{r},\boldsymbol{r}')\right)\mathrm{d}\boldsymbol{r}. \quad (5.29)$$

Taking the limit $R\to\infty$, and assuming that the potential has a limiting value $\lim_{\boldsymbol{r}\to\infty} = \varphi_\infty$, it can be shown by the properties of the Green's function that the second term is equal to

$$\oint_{\Gamma_V}\left(\left(\boldsymbol{n}_o\cdot\nabla G_0(\boldsymbol{r},\boldsymbol{r}')\right)\varphi(\boldsymbol{r}) - \left(\boldsymbol{n}_o\cdot\nabla\varphi(\boldsymbol{r})\right)G_0(\boldsymbol{r},\boldsymbol{r}')\right)\mathrm{d}\boldsymbol{r} = \varphi_\infty. \quad (5.30)$$

Also, note that in the left-hand side, $\Delta\varphi = 0$ since φ satisfies the Laplace equation, and $\Delta G_0 = -\delta(\boldsymbol{r},r')$. Together, this leads to:

$$\int_V\left(-\varphi(\boldsymbol{r})\delta(\boldsymbol{r},\boldsymbol{r}')\right)\mathrm{d}\boldsymbol{r} = \oiint_{\Gamma_1}\left(\left(\boldsymbol{n}_i\cdot\nabla G_0(\boldsymbol{r},\boldsymbol{r}')\right)\varphi(\boldsymbol{r}) - \left(\boldsymbol{n}_i\cdot\nabla\varphi(\boldsymbol{r})\right)G_0(\boldsymbol{r},\boldsymbol{r}')\right)\mathrm{d}\boldsymbol{r} + \varphi_\infty. \quad (5.31)$$

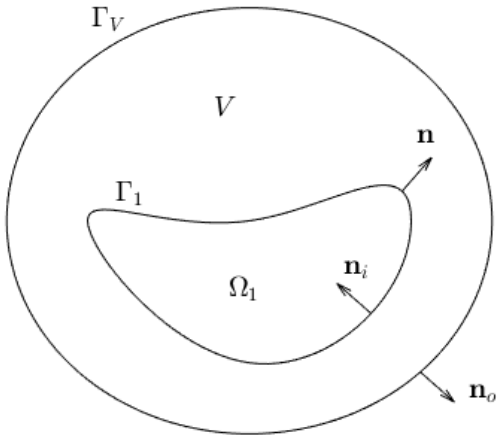

Figure 5.2: Overview of domains for exterior potential problem

Once again, this can be rewritten with a coefficient h_0, which depends on the location of the observation point. Also, $\boldsymbol{n} = -\boldsymbol{n}_i$ can be used to express the integral in terms of the same normal vector as above. Finally, the limit of the potential can be set to $\varphi_\infty = 0$. Thus the boundary integral formulation becomes:

$$h_0\varphi(\boldsymbol{r}') = \oiint_{\Gamma_1} \Big(\big(\boldsymbol{n}\cdot\nabla G_0(\boldsymbol{r},\boldsymbol{r}')\big)\varphi(\boldsymbol{r}) - \big(\boldsymbol{n}\cdot\nabla\varphi(\boldsymbol{r})\big) G_0(\boldsymbol{r},\boldsymbol{r}') \Big)\, \mathrm{d}\boldsymbol{r}, \tag{5.32}$$

where

$$h_0 = \begin{cases} 0 \text{ if } \boldsymbol{r}' \text{ is outside } \Omega_0 \\ 1 \text{ if } \boldsymbol{r}' \text{ is inside } \Omega_0 \\ \frac{1}{2} \text{ if } \boldsymbol{r}' \text{ is on the (regular) surface } \Gamma_1 \end{cases}. \tag{5.33}$$

Together with the formulation for the modified magnetic vector potential (Equation (5.25)), this yields the following system of integral boundary equations:

$$\begin{cases} h_1 \boldsymbol{A}^*(\boldsymbol{r}) &= -\oiint_{\Gamma_1} \big(\boldsymbol{n}\times\boldsymbol{A}^*(\boldsymbol{r}')\big)\times\nabla' G_1(\boldsymbol{r}',\boldsymbol{r}) + \big(\boldsymbol{n}\times(\nabla'\times\boldsymbol{A}^*(\boldsymbol{r}'))\big) G_1(\boldsymbol{r}',\boldsymbol{r})\, \mathrm{d}\boldsymbol{r}', \\ h_0\varphi(\boldsymbol{r}) &= \oiint_{\Gamma_1} \Big(\big(\boldsymbol{n}\cdot\nabla' G_0(\boldsymbol{r}',\boldsymbol{r})\big)\varphi(\boldsymbol{r}') - \big(\boldsymbol{n}\cdot\nabla'\varphi(\boldsymbol{r}')\big) G_0(\boldsymbol{r}',\boldsymbol{r}) \Big)\, \mathrm{d}\boldsymbol{r}'. \end{cases} \tag{5.34}$$

Note that we have switched the variables $\boldsymbol{r}'$ and $\boldsymbol{r}$. We will now incorporate the interface conditions. From the interface conditions in Equation (5.17), the following expressions for $\boldsymbol{n}\times\nabla\times\boldsymbol{A}^*$ and $\boldsymbol{n}\cdot\nabla\varphi$ on the interface can be used:

$$\boldsymbol{n}\times(\nabla'\times\boldsymbol{A}^*(\boldsymbol{r}')) = \mu_1\big(\boldsymbol{n}\times\boldsymbol{H}_s - \boldsymbol{n}\times\nabla'\varphi(\boldsymbol{r}')\big) \tag{5.35}$$

$$\boldsymbol{n}\cdot\nabla'\varphi(\boldsymbol{r}') = \boldsymbol{n}\cdot\boldsymbol{H}_s - \frac{1}{\mu_0}\Big(\boldsymbol{n}\cdot\big(\nabla'\times\boldsymbol{A}^*(\boldsymbol{r}')\big)\Big) \tag{5.36}$$

By filling this in in the obtained system, the potentials are linked to each other, and to the periodically varying background field:

$$\begin{cases} h_1 \boldsymbol{A}^*(\boldsymbol{r}) &= -\oiint_{\Gamma_1} \big(\boldsymbol{n}\times\boldsymbol{A}^*(\boldsymbol{r}')\big)\times\nabla' G_1(\boldsymbol{r}',\boldsymbol{r}) + \mu_1\big(\boldsymbol{n}\times\boldsymbol{H}_s - \boldsymbol{n}\times\nabla'\varphi(\boldsymbol{r}')\big) G_1(\boldsymbol{r}',\boldsymbol{r})\, \mathrm{d}\boldsymbol{r}', \\ h_0\varphi(\boldsymbol{r}) &= \oiint_{\Gamma_1} \left(\big(\boldsymbol{n}\cdot\nabla' G_0(\boldsymbol{r}',\boldsymbol{r})\big)\varphi(\boldsymbol{r}') - \left(\boldsymbol{n}\cdot\boldsymbol{H}_s - \frac{1}{\mu_0}\Big(\boldsymbol{n}\cdot\big(\nabla'\times\boldsymbol{A}^*(\boldsymbol{r}')\big)\Big)\right) G_0(\boldsymbol{r}',\boldsymbol{r}) \right)\, \mathrm{d}\boldsymbol{r}'. \end{cases} \tag{5.37}$$

Taking what is known, i.e. the terms depending only on the background field $\boldsymbol{H}_s$, to the right-hand side yields the final formulation:

$$\begin{cases} h_1 \boldsymbol{A}^*(\boldsymbol{r}) + \oiint_{\Gamma_1} \big(\boldsymbol{n} \times \boldsymbol{A}^*(\boldsymbol{r}')\big) \times \nabla' G_1(\boldsymbol{r}', \boldsymbol{r}) \, \mathrm{d}\boldsymbol{r}' - \mu_1 \oiint_{\Gamma_1} \big(\boldsymbol{n} \times \nabla' \varphi(\boldsymbol{r}')\big) G_1(\boldsymbol{r}', \boldsymbol{r}) \, \mathrm{d}\boldsymbol{r}' = -\mu_1 \oiint_{\Gamma_1} \big(\boldsymbol{n} \times \boldsymbol{H}_s\big) G_1(\boldsymbol{r}', \boldsymbol{r}) \, \mathrm{d}\boldsymbol{r}', \\ h_0 \varphi(\boldsymbol{r}) - \oiint_{\Gamma_1} \big(\boldsymbol{n} \cdot \nabla' G_0(\boldsymbol{r}', \boldsymbol{r})\big) \varphi(\boldsymbol{r}') \, \mathrm{d}\boldsymbol{r}' - \dfrac{1}{\mu_0} \oiint_{\Gamma_1} \boldsymbol{n} \cdot \big(\nabla' \times \boldsymbol{A}^*(\boldsymbol{r}')\big) G_0(\boldsymbol{r}', \boldsymbol{r}) \, \mathrm{d}\boldsymbol{r}' = -\oiint_{\Gamma_1} \big(\boldsymbol{n} \cdot \boldsymbol{H}_s\big) G_0(\boldsymbol{r}', \boldsymbol{r}) \, \mathrm{d}\boldsymbol{r}'. \end{cases} \tag{5.38}$$

5.4. Weak formulation and Galerkin's method

To implement this formulation with a boundary element method, it is necessary to convert it to a weak formulation. To this end, the equations are multiplied by suitable test functions $\boldsymbol{u}$ and v respectively, making use of the inner product on $\mathscr{H}(\mathrm{div}, \Gamma_1)$ defined in Section 3.1 for the first equation, and of the regular $\mathscr{H}^2$ inner product for the second equation:

$$\begin{cases} \big(\boldsymbol{u}(\boldsymbol{r}) \, , \, h_1 \boldsymbol{A}^*(\boldsymbol{r})\big)_{\mathscr{H}(\mathrm{div},\Gamma_1)} + \left(\boldsymbol{u}(\boldsymbol{r}) \, , \oiint_{\Gamma_1} \big(\boldsymbol{n} \times \boldsymbol{A}^*(\boldsymbol{r}')\big) \times \nabla' G_1(\boldsymbol{r}', \boldsymbol{r}) \, \mathrm{d}\boldsymbol{r}'\right)_{\mathscr{H}(\mathrm{div},\Gamma_1)} \\ \qquad - \left(\boldsymbol{u}(\boldsymbol{r}) \, , \, \mu_1 \oiint_{\Gamma_1} \big(\boldsymbol{n} \times \nabla' \varphi(\boldsymbol{r}')\big) G_1(\boldsymbol{r}', \boldsymbol{r})\right)_{\mathscr{H}(\mathrm{div},\Gamma_1)} = \left(\boldsymbol{u}(\boldsymbol{r}) \, , \, \mu_1 \oiint_{\Gamma_1} \big(\boldsymbol{n} \times \boldsymbol{H}_s\big) G_1(\boldsymbol{r}', \boldsymbol{r}) \, \mathrm{d}\boldsymbol{r}'\right)_{\mathscr{H}(\mathrm{div},\Gamma_1)}, \\ \big(v(\boldsymbol{r}) \, , \, h_0 \varphi(\boldsymbol{r})\big)_{\mathscr{H}^2(\Gamma_1)} - \left(v(\boldsymbol{r}) \, , \oiint_{\Gamma_1} \big(\boldsymbol{n} \cdot \nabla' G_0(\boldsymbol{r}', \boldsymbol{r})\big) \varphi(\boldsymbol{r}') \, \mathrm{d}\boldsymbol{r}'\right)_{\mathscr{H}^2(\Gamma_1)} \\ \qquad - \left(v(\boldsymbol{r}) \, , \, \dfrac{1}{\mu_0} \oiint_{\Gamma_1} \boldsymbol{n} \cdot \big(\nabla' \times \boldsymbol{A}^*(\boldsymbol{r}')\big) G_0(\boldsymbol{r}', \boldsymbol{r}) \, \mathrm{d}\boldsymbol{r}'\right)_{\mathscr{H}^2(\Gamma_1)} = \left(v(\boldsymbol{r}) \, , \, -\oiint_{\Gamma_1} \big(\boldsymbol{n} \cdot \boldsymbol{H}_s\big) G_0(\boldsymbol{r}', \boldsymbol{r}) \, \mathrm{d}\boldsymbol{r}'\right)_{\mathscr{H}^2(\Gamma_1)}. \end{cases} \tag{5.39}$$

Note, however, that the $\mathscr{H}(\mathrm{div}, \Gamma_1)$ inner product reduces to the regular $\mathscr{H}^2$ inner product for divergence-free functions. As will be shown in Chapter 6, the basis functions and test functions in the Galerkin approach will be divergence-free. Thus, the system can be written in the following integral form:

$$\begin{cases} \oiint_{\Gamma_1} \boldsymbol{u}(\boldsymbol{r}) \cdot h_1 \boldsymbol{A}^*(\boldsymbol{r}) \, \mathrm{d}\boldsymbol{r} + \oiint_{\Gamma_1} \boldsymbol{u}(\boldsymbol{r}) \cdot \oiint_{\Gamma_1} \big(\boldsymbol{n} \times \boldsymbol{A}^*(\boldsymbol{r}')\big) \times \nabla' G_1(\boldsymbol{r}', \boldsymbol{r}) \, \mathrm{d}\boldsymbol{r}' \, \mathrm{d}\boldsymbol{r} \\ \qquad - \oiint_{\Gamma_1} \boldsymbol{u}(\boldsymbol{r}) \cdot \mu_1 \oiint_{\Gamma_1} \big(\boldsymbol{n} \times \nabla' \varphi(\boldsymbol{r}')\big) G_1(\boldsymbol{r}', \boldsymbol{r}) \, \mathrm{d}\boldsymbol{r}' \, \mathrm{d}\boldsymbol{r} = \oiint_{\Gamma_1} \boldsymbol{u}(\boldsymbol{r}) \cdot -\mu_1 \oiint_{\Gamma_1} \big(\boldsymbol{n} \times \boldsymbol{H}_s\big) G_1(\boldsymbol{r}', \boldsymbol{r}) \, \mathrm{d}\boldsymbol{r}' \, \mathrm{d}\boldsymbol{r}, \\ \oiint_{\Gamma_1} v(\boldsymbol{r}) \cdot h_0 \varphi(\boldsymbol{r}) \, \mathrm{d}\boldsymbol{r} - \oiint_{\Gamma_1} v(\boldsymbol{r}) \cdot \oiint_{\Gamma_1} \big(\boldsymbol{n} \cdot \nabla' G_0(\boldsymbol{r}', \boldsymbol{r})\big) \varphi(\boldsymbol{r}') \, \mathrm{d}\boldsymbol{r}' \, \mathrm{d}\boldsymbol{r} \\ \qquad - \oiint_{\Gamma_1} v(\boldsymbol{r}) \cdot \dfrac{1}{\mu_0} \oiint_{\Gamma_1} \boldsymbol{n} \cdot \big(\nabla' \times \boldsymbol{A}^*(\boldsymbol{r}')\big) G_0(\boldsymbol{r}', \boldsymbol{r}) \, \mathrm{d}\boldsymbol{r}' \, \mathrm{d}\boldsymbol{r} = \oiint_{\Gamma_1} v(\boldsymbol{r}) \cdot -\oiint_{\Gamma_1} \big(\boldsymbol{n} \cdot \boldsymbol{H}_s\big) G_0(\boldsymbol{r}', \boldsymbol{r}) \, \mathrm{d}\boldsymbol{r}' \, \mathrm{d}\boldsymbol{r}. \end{cases} \tag{5.40}$$

The modified magnetic vector potential is approximated making use of edge shape functions:

$$\boldsymbol{A}^*(\boldsymbol{r}) = \sum_{j=1}^{n_e} A_j^* \boldsymbol{N}_j(\boldsymbol{r}), \tag{5.41}$$

where n_e is the number of edges, $\boldsymbol{N}_i(\boldsymbol{r})$ are the edge shape functions, and A_i^* are the coefficients. The reduced scalar potential is approximated with nodal shape functions:

$$\varphi = \sum_{j=1}^{n_n} \varphi_j \lambda_j(\boldsymbol{r}), \tag{5.42}$$

where n_n is the number of nodes, $\lambda_i(\boldsymbol{r})$ are the nodal shape functions, and φ_i are the coefficients. These shape functions are described in Chapter 6. The Galerkin approach is used, whereby the basis functions used for the approximation are also used as test function. Thus the following system is derived:

$$\begin{bmatrix} M^{11} & M^{12} \\ M^{21} & M^{22} \end{bmatrix} \begin{bmatrix} A^* \\ \varphi \end{bmatrix} = \begin{bmatrix} L^1 \\ L^2 \end{bmatrix}, \tag{5.43}$$

where:

$$M_{ij}^{11} = h_1 \oiint_{\Gamma_1} \boldsymbol{N}_i(\boldsymbol{r}) \cdot \boldsymbol{N}_j(\boldsymbol{r}) \, \mathrm{d}\boldsymbol{r} + \oiint_{\Gamma_1} \boldsymbol{N}_i(\boldsymbol{r}) \cdot \oiint_{\Gamma_1} \Big(\boldsymbol{n} \times \boldsymbol{N}_j(\boldsymbol{r}') \Big) \times \nabla G_1(\boldsymbol{r}, \boldsymbol{r}') \, \mathrm{d}\boldsymbol{r}' \, \mathrm{d}\boldsymbol{r}, \tag{5.44}$$

$$M_{ij}^{12} = -\mu_1 \oiint_{\Gamma_1} \boldsymbol{N}_i(\boldsymbol{r}) \cdot \oiint_{\Gamma_1} \Big(\boldsymbol{n} \times \nabla \lambda_j(\boldsymbol{r}') \Big) G_1(\boldsymbol{r}, \boldsymbol{r}') \, \mathrm{d}\boldsymbol{r}' \, \mathrm{d}\boldsymbol{r}, \tag{5.45}$$

$$M_{ij}^{21} = -\frac{1}{\mu_0} \oiint_{\Gamma_1} \lambda_i(\boldsymbol{r}) \oiint_{\Gamma_1} \boldsymbol{n} \cdot \Big(\nabla \times \boldsymbol{N}_j(\boldsymbol{r}') \Big) G_0(\boldsymbol{r}, \boldsymbol{r}') \, \mathrm{d}\boldsymbol{r}' \, \mathrm{d}\boldsymbol{r}, \tag{5.46}$$

$$M_{ij}^{22} = h_0 \oiint_{\Gamma_1} \lambda_i(\boldsymbol{r}) \lambda_j(\boldsymbol{r}) \, \mathrm{d}\boldsymbol{r} - \oiint_{\Gamma_1} \lambda_i(\boldsymbol{r}) \oiint_{\Gamma_1} \big(\boldsymbol{n} \cdot \nabla G_0(\boldsymbol{r}, \boldsymbol{r}') \big) \lambda_j(\boldsymbol{r}') \, \mathrm{d}\boldsymbol{r}' \, \mathrm{d}\boldsymbol{r}, \tag{5.47}$$

$$L_i^1 = -\mu_1 \oiint_{\Gamma_1} \boldsymbol{N}_i(\boldsymbol{r}) \cdot \oiint_{\Gamma_1} \big(\boldsymbol{n} \times \boldsymbol{H}_s \big) G_1(\boldsymbol{r}, \boldsymbol{r}') \, \mathrm{d}\boldsymbol{r}' \, \mathrm{d}\boldsymbol{r}, \tag{5.48}$$

$$L_i^2 = -\oiint_{\Gamma_1} \lambda_i(\boldsymbol{r}) \oiint_{\Gamma_1} \big(\boldsymbol{n} \cdot \boldsymbol{H}_s \big) G_0(\boldsymbol{r}, \boldsymbol{r}') \, \mathrm{d}\boldsymbol{r}' \, \mathrm{d}\boldsymbol{r}. \tag{5.49}$$

Solving this system yields the coefficients of the basis functions on the interface Γ_1 for both potentials. With this, we can subsequently determine the potentials everywhere in the conductor and in the free air region using the boundary element formulation.

5.5. Implementation of the Greens functions

The derived system is not a simple one by any measure. A notable difficulty is the integration of the two Greens functions:

$$G_0(\boldsymbol{r}, \boldsymbol{r}') = \frac{1}{4\pi |\boldsymbol{r} - \boldsymbol{r}'|}, \tag{5.50}$$

$$G_1(\boldsymbol{r}, \boldsymbol{r}') = \frac{1}{4\pi |\boldsymbol{r} - \boldsymbol{r}'|} e^{-jk|\boldsymbol{r} - \boldsymbol{r}'|}, \tag{5.51}$$

where k is a complex wavenumber. These Greens functions need to be integrated over a triangular domain. The difficulty lies in the fact that the integrals contain a singular point at $\boldsymbol{r} = \boldsymbol{r}'$. It turns out that this challenge can be overcome, by making use of an analytical expression for G_0, and by splitting G_1 into an analytical and a numerical (bounded) part.

Let us begin by consider G_0, for which we have an analytical expression for the case in which the singular point $\boldsymbol{r}$ lies in the integration domain. Specifically, for a triangular domain $\mathcal{T}$, the following integrals have analytical expressions:

$$\mathcal{I}_1 = \oiint_{\mathcal{T}} \frac{1}{|\boldsymbol{r} - \boldsymbol{r}'|} \, \mathrm{d}\boldsymbol{r}', \tag{5.52}$$

$$\mathcal{I}_2 = \oiint_{\mathcal{T}} \frac{\lambda_1(\boldsymbol{r}')}{|\boldsymbol{r} - \boldsymbol{r}'|} \, \mathrm{d}\boldsymbol{r}', \tag{5.53}$$

$$\nabla \mathcal{I}_2 = \oiint_{\mathcal{T}} \lambda_1(\boldsymbol{r}') \nabla \left(\frac{1}{|\boldsymbol{r} - \boldsymbol{r}'|} \right) \mathrm{d}\boldsymbol{r}', \tag{5.54}$$

where $\lambda_1(\boldsymbol{r}')$ is the first linear basis function on the element. The analytical solution is described in [13]. Note that only $\mathcal{I}_1$ and $\nabla\mathcal{I}_2$ are used in the system we have derived above. The integral $\mathcal{I}_2$ is included because it will be used for the dynamic integrals discussed below. In particular, we must find a way to evaluate the following integrals, which are associated with G_0:

$$\mathcal{G}_1 = \oiint_{\mathcal{T}} \frac{1}{|\boldsymbol{r} - \boldsymbol{r}'|} e^{-jk|\boldsymbol{r} - \boldsymbol{r}'|} \, \mathrm{d}\boldsymbol{r}', \tag{5.55}$$

$$\nabla \mathcal{G}_2 = \oiint_{\mathcal{T}} \lambda_1(\boldsymbol{r}') \nabla \left(\frac{1}{|\boldsymbol{r} - \boldsymbol{r}'|} e^{-jk|\boldsymbol{r} - \boldsymbol{r}'|} \right) \mathrm{d}\boldsymbol{r}'. \tag{5.56}$$

Instead of attempting to find an analytical expression for these integrals, we split the integral into an analytical part, and a numerical part, as is done in [13]. Let us begin by investigating $\mathcal{G}_1$. Splitting this integral into two

parts yields:

$$\begin{aligned}\mathcal{G}_1 &= \oiint_{\mathcal{T}} \frac{1}{|\boldsymbol{r}-\boldsymbol{r}'|} e^{-jk|\boldsymbol{r}-\boldsymbol{r}'|}\,\mathrm{d}\boldsymbol{r}' \\ &= \oiint_{\mathcal{T}} \frac{1}{|\boldsymbol{r}-\boldsymbol{r}'|}\,\mathrm{d}\boldsymbol{r}' + \oiint_{\mathcal{T}} \frac{1}{|\boldsymbol{r}-\boldsymbol{r}'|}\left(e^{-jk|\boldsymbol{r}-\boldsymbol{r}'|}-1\right)\mathrm{d}\boldsymbol{r}'. \end{aligned} \tag{5.57}$$

We recognize the integral $\mathcal{I}_1$ in the first term. We have an analytical expression for this term. The second term still contains a singular point at $\boldsymbol{r}' = \boldsymbol{r}$. However, it is now bounded. We will further investigate the function in the integrand, for which we will introduce the normalized coordinate system:

$$\boldsymbol{R} := k(\boldsymbol{r}-\boldsymbol{r}') \tag{5.58}$$

$$R := k|\boldsymbol{r}-\boldsymbol{r}'| \tag{5.59}$$

$$\hat{\boldsymbol{R}} = \frac{\boldsymbol{R}}{R}. \tag{5.60}$$

Denote the function in the integrand by $f(R)$:

$$f(R) := \frac{k(e^{-jR}-1)}{R}. \tag{5.61}$$

Filling in the definition of R shows that this is indeed equal to the integrand in equation (5.57). As stated before, this function tends to a finite limit as R approaches zero. Application of l'Hospital's rule yields the following value for this singularity:

$$\lim_{R\to 0} f(R) = \lim_{R\to 0}\left(\frac{k(e^{-jR}-1)}{R}\right) = \lim_{R\to 0}\left(-jk\frac{e^{-jR}}{1}\right) = -jk. \tag{5.62}$$

To linearise around $R = 0$, we use the derivative:

$$f'(R) = \frac{-k(e^{-jR}-1)}{R^2} - \frac{jke^{-jR}}{R}, \tag{5.63}$$

for which the limit as R approaches zero, using l'Hospital again, is:

$$\lim_{R\to 0} f'(R) = \lim_{R\to 0}\left(\frac{-k(e^{-jR}-1)}{R^2} - \frac{jke^{-jR}}{R}\right) \tag{5.64}$$

$$= \lim_{R\to 0}\left(\frac{jke^{-jR}}{2R} + \frac{j^2ke^{-jR}}{1}\right) \tag{5.65}$$

$$= \lim_{R\to 0}\left(\frac{-j^2ke^{-jR}}{2}\right) + j^2k \tag{5.66}$$

$$= -\frac{1}{2}k. \tag{5.67}$$

Thus for values of R close to the singularity, we can use the linearised function

$$f(R) \approx -jk - \frac{1}{2}kR, \tag{5.68}$$

or in terms of $(\boldsymbol{r}, \boldsymbol{r}')$:

$$\frac{1}{|\boldsymbol{r}-\boldsymbol{r}'|} e^{-jk|\boldsymbol{r}-\boldsymbol{r}'|} \approx -jk - \frac{1}{2}k^2|\boldsymbol{r}-\boldsymbol{r}'|. \tag{5.69}$$

With this we can evaluate the integral $\mathcal{G}_1$ numerically. For values far from the singular point, the integrand can be calculated normally. For values close to the singular point, the linearised integrand in Equation (5.69) can be used. For the singular point, the limiting value $-jk$ is used.

Now consider the integral $\nabla\mathcal{G}_2$. This integral can also be split into two parts, in a similar way as above:

$$\begin{aligned}\nabla\mathcal{G}_2 &= \oiint_{\mathcal{T}} \lambda_1(\boldsymbol{r}')\nabla\left(\frac{1}{|\boldsymbol{r}-\boldsymbol{r}'|} e^{-jk|\boldsymbol{r}-\boldsymbol{r}'|}\right)\mathrm{d}\boldsymbol{r}' \\ &= \oiint_{\mathcal{T}} \lambda_1(\boldsymbol{r}')\nabla\left(\frac{1}{|\boldsymbol{r}-\boldsymbol{r}'|}\right)\mathrm{d}\boldsymbol{r}' + \oiint_{\mathcal{T}} \lambda_1(\boldsymbol{r}')\nabla\left(\frac{1}{|\boldsymbol{r}-\boldsymbol{r}'|}\left(e^{-jk|\boldsymbol{r}-\boldsymbol{r}'|}-1\right)\right)\mathrm{d}\boldsymbol{r}'. \end{aligned} \tag{5.70}$$

We recognize $\nabla\mathcal{I}_2$, for which we have an analytical expression, in the first term. The second term is now bounded. Let us investigate the troublesome gradient in the second integral, and its linearisation around the singularity. Once again, we will use the normalized position R (as defined in equation (5.59)) and the function $f(R)$ (as defined in Equation (5.61)). We begin by determining an explicit expression for the integrand. By the chain rule, we have:

$$\nabla\left(\frac{1}{|\boldsymbol{r}-\boldsymbol{r}'|}\left(e^{-jk|\boldsymbol{r}-\boldsymbol{r}'|}-1\right)\right)=\nabla\left(f(R(\boldsymbol{r},\boldsymbol{r}'))\right)=f'(R)\nabla R(\boldsymbol{r},\boldsymbol{r}'). \tag{5.71}$$

We have determined an expression for $f'(r)$ earlier, see Equation (5.63). The gradient of $R(\boldsymbol{r},\boldsymbol{r}')$ is:

$$\begin{aligned}\nabla R(\boldsymbol{r},\boldsymbol{r}')&=\nabla\left(k|\boldsymbol{r}-\boldsymbol{r}'|\right)\\&=k\frac{\boldsymbol{r}-\boldsymbol{r}'}{|\boldsymbol{r}-\boldsymbol{r}'|}\\&=\frac{k^2(\boldsymbol{r}-\boldsymbol{r}')}{R}.\end{aligned} \tag{5.72}$$

Thus, putting the pieces together, the gradient of $R(\boldsymbol{r},\boldsymbol{r}')$ is:

$$\nabla\left(\frac{1}{|\boldsymbol{r}-\boldsymbol{r}'|}\left(e^{-jk|\boldsymbol{r}-\boldsymbol{r}'|}-1\right)\right)=\left(\frac{-k(e^{-jR}-1)}{R^2}-\frac{jke^{-jR}}{R}\right)\frac{k^2(\boldsymbol{r}-\boldsymbol{r}')}{R}. \tag{5.73}$$

In terms of $(\boldsymbol{r},\boldsymbol{r}')$, this is:

$$\nabla\left(\frac{1}{|\boldsymbol{r}-\boldsymbol{r}'|}\left(e^{-jk|\boldsymbol{r}-\boldsymbol{r}'|}-1\right)\right)=\left(\frac{-(e^{-jk|\boldsymbol{r}-\boldsymbol{r}'|}-1)}{|\boldsymbol{r}-\boldsymbol{r}'|^3}-\frac{jke^{-jk|\boldsymbol{r}-\boldsymbol{r}'|}}{|\boldsymbol{r}-\boldsymbol{r}'|^2}\right)(\boldsymbol{r}-\boldsymbol{r}'), \tag{5.74}$$

and thus the explicit expression for $\boldsymbol{\mathcal{G}}_2$ is:

$$\nabla\boldsymbol{\mathcal{G}}_2=\oiint_{\mathcal{T}}\lambda_1(\boldsymbol{r}')\nabla\left(\frac{1}{|\boldsymbol{r}-\boldsymbol{r}'|}\right)\mathrm{d}\boldsymbol{r}'+\oiint_{\mathcal{T}}\lambda_1(\boldsymbol{r}')\left(\frac{-(e^{-jk|\boldsymbol{r}-\boldsymbol{r}'|}-1)}{k|\boldsymbol{r}-\boldsymbol{r}'|^3}-\frac{je^{-jk|\boldsymbol{r}-\boldsymbol{r}'|}}{|\boldsymbol{r}-\boldsymbol{r}'|^2}\right)\begin{bmatrix}(x-x')\\(y-y')\\(z-z')\end{bmatrix}\mathrm{d}\boldsymbol{r}'. \tag{5.75}$$

We wish to find the limiting value for the singular point, and to determine the linearisation around this point. However, proceeding as we did for $\boldsymbol{\mathcal{G}}_1$ and taking the limit as R goes to zero yields:

$$\lim_{R\to0}\nabla f(R)=\lim_{R\to0}\left(\frac{-k(e^{-jR}-1)}{R^2}-\frac{jke^{-jR}}{R}\right)\hat{\boldsymbol{R}} \tag{5.76}$$

$$=\lim_{R\to0}-\frac{1}{2}k\hat{\boldsymbol{R}}. \tag{5.77}$$

Note that this limit is undefined. Thus we cannot determine the limit value. However, a volume integral over a closed ball around the singular point will equal zero, by symmetry. Hence the numerical integration of the second integral can be done by setting the integrand to zero for the singular point.

5.6. Calculating the magnetic field and the current density

Solving the system described above (Equation (5.43)) yields the coefficients describing our approximation to the potentials $\boldsymbol{A}^*$ and φ on the interface. Using the BEM formulation in Equation (5.34), the potential at each point in the domain can be calculated. With this, the fields can be calculated as well. The eddy current density inside the conductor is given by $\boldsymbol{J}=\sigma\boldsymbol{E}=-j\omega\sigma\boldsymbol{A}^*$. Thus, using the BEM formulation, we find:

$$\boldsymbol{J}(\boldsymbol{r})=j\omega\sigma\oiint_{\Gamma_1}\left(\boldsymbol{n}\times\boldsymbol{A}^*(\boldsymbol{r}')\right)\times\nabla' G_1(\boldsymbol{r}',\boldsymbol{r})+\left(\boldsymbol{n}\times(\nabla'\times\boldsymbol{A}^*(\boldsymbol{r}'))\right)G_1(\boldsymbol{r}',\boldsymbol{r})\,\mathrm{d}\boldsymbol{r}'. \tag{5.78}$$

In certain conditions, however, this expression can be simplified. This is due to the chosen edge basis functions, for which we have that $\boldsymbol{n}\times\nabla\times\boldsymbol{N}=0$ on a triangular element, where $\boldsymbol{N}$ denotes a basis function on that element. Thus the second term vanishes, and we are left with

$$\boldsymbol{J}(\boldsymbol{r})=j\omega\sigma\oiint_{\Gamma_1}\left(\boldsymbol{n}\times\boldsymbol{A}^*(\boldsymbol{r}')\right)\times\nabla' G_1(\boldsymbol{r}',\boldsymbol{r})\,\mathrm{d}\boldsymbol{r}'. \tag{5.79}$$

Note that this introduces a discrepancy, since by the boundary conditions, we have that $\boldsymbol{n} \times \nabla \times \boldsymbol{A}^* = \mu_1(\boldsymbol{n} \times \boldsymbol{H}_s - \boldsymbol{n} \times \nabla\varphi)$. This observation and this discrepancy are not noted in [30].

To calculate the magnetic flux density in air, we could proceed by making use of the BEM formulation for the scalar potential φ:

$$\boldsymbol{B}(\boldsymbol{r}) = \boldsymbol{B}_0 - \mu_0 \nabla\varphi(\boldsymbol{r}) = \boldsymbol{B}_0 - \mu_0 \nabla \oiint_{\Gamma_1} \Big(\big(\boldsymbol{n} \cdot \nabla' G_0(\boldsymbol{r}', \boldsymbol{r})\big)\, \varphi(\boldsymbol{r}') - \big(\boldsymbol{n} \cdot \nabla' \varphi(\boldsymbol{r}')\big)\, G_0(\boldsymbol{r}', \boldsymbol{r}) \Big)\, \mathrm{d}\boldsymbol{r}'. \tag{5.80}$$

However, the implementation of this expression is not straight-forward, since it will include Laplacian-like terms with the Green's functions. Instead, an expression derived from [18] and [48] can be used:

$$\boldsymbol{B}(\boldsymbol{r}) = \boldsymbol{B}_0 + \mu_0 \oiint_{\Gamma_1} (\boldsymbol{n} \times \boldsymbol{H}_s) \times \nabla' G_0(\boldsymbol{r}', \boldsymbol{r})\, \mathrm{d}\boldsymbol{r}' + \oiint_{\Gamma_1} \boldsymbol{n} \cdot (\nabla \times \boldsymbol{A}^*(\boldsymbol{r}')) \nabla' G_0(\boldsymbol{r}', \boldsymbol{r})\, \mathrm{d}\boldsymbol{r}' - \oiint_{\Gamma_1} (\boldsymbol{n} \times \nabla\varphi(\boldsymbol{r}')) \times \nabla' G_0(\boldsymbol{r}', \boldsymbol{r})\, \mathrm{d}\boldsymbol{r}' \tag{5.81}$$

Note that this equation appears wrongly in [30], where the factor μ_0 is missing in some terms.

Finally, to calculate the Joule losses, we rewrite the complex Poynting vector to find

$$P_{\text{loss}} = -\frac{1}{2} \operatorname{Re}\left(\oiint_{\partial\Gamma_1} \boldsymbol{S} \cdot \boldsymbol{n}\, \mathrm{d}\boldsymbol{r} \right) \tag{5.82}$$

$$= \operatorname{Re}\left(-\frac{j\omega}{2} \oiint_{\Gamma_1} (\boldsymbol{n} \times \boldsymbol{H}) \cdot \overline{\boldsymbol{E}}\, \mathrm{d}\boldsymbol{r}' \right) \tag{5.83}$$

$$= \operatorname{Re}\left(-\frac{j\omega}{2} \oiint_{\Gamma_1} (\boldsymbol{n} \times \boldsymbol{H}_s - \boldsymbol{n} \times \nabla\varphi(\boldsymbol{r})') \cdot \overline{\boldsymbol{A}^*}(\boldsymbol{r}')\, \mathrm{d}\boldsymbol{r}' \right), \tag{5.84}$$

where the bar indicates the complex conjugate.

6

Implementation

6.1. Nodal shape functions in 2D

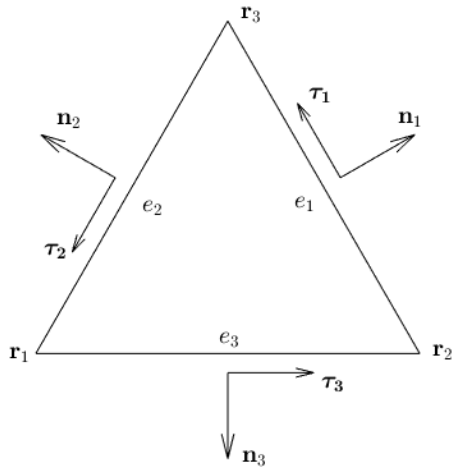

Figure 6.1: A triangular element, with tangent unit vectors and outward normal vectors.

For scalar problems, the finite element method is frequently implemented using piecewise linear basis functions, also known as nodal shape functions. A common approach is to use triangular elements. Consider a single triangular element, having vertices $\boldsymbol{r}_1 = (x_1, y_1)$, $\boldsymbol{r}_2 = (x_2, y_2)$ and $\boldsymbol{r}_3 = (x_3, y_3)$. Denote the unit length tangential vectors along each edge by $\boldsymbol{\tau}_i$:

$$\boldsymbol{\tau}_1 = \frac{\boldsymbol{r}_3 - \boldsymbol{r}_2}{\|\boldsymbol{r}_3 - \boldsymbol{r}_2\|}, \tag{6.1}$$

$$\boldsymbol{\tau}_2 = \frac{\boldsymbol{r}_1 - \boldsymbol{r}_3}{\|\boldsymbol{r}_1 - \boldsymbol{r}_3\|}, \tag{6.2}$$

$$\boldsymbol{\tau}_3 = \frac{\boldsymbol{r}_2 - \boldsymbol{r}_1}{\|\boldsymbol{r}_2 - \boldsymbol{r}_1\|}. \tag{6.3}$$

The outward normal vector on each edge will be denoted by $\boldsymbol{n}_i$. It is defined as:

$$\boldsymbol{n}_i = \boldsymbol{\tau}_i \begin{pmatrix} 0 & -1 \\ 1 & 0 \end{pmatrix}. \tag{6.4}$$

Denote by s_i the edge opposite vertex v_i. These edges are characterised by:

$$s_1 = \{\boldsymbol{r} : (\boldsymbol{r} - \boldsymbol{r}_2) \cdot \boldsymbol{n}_1 = 0\}, \tag{6.5}$$
$$s_2 = \{\boldsymbol{r} : (\boldsymbol{r} - \boldsymbol{r}_3) \cdot \boldsymbol{n}_2 = 0\}, \tag{6.6}$$
$$s_3 = \{\boldsymbol{r} : (\boldsymbol{r} - \boldsymbol{r}_1) \cdot \boldsymbol{n}_3 = 0\}. \tag{6.7}$$

See Figure 6.1 for an overview of all above-mentioned nodes and vectors.

A linear function can be interpolated on such triangular element using three nodal shape functions λ_i, $i = 1,2,3$. These shape functions have the property that they are linear, and that they satisfy:

$$\lambda_i(\boldsymbol{r}_j) = \delta_{ij}, \tag{6.8}$$

where δ_{ij} is the Kronecker delta.

The three basis functions are given by:

$$\lambda_1(\boldsymbol{r}) = \frac{(\boldsymbol{r} - \boldsymbol{r}_2) \cdot \boldsymbol{n}_1}{(\boldsymbol{r}_1 - \boldsymbol{r}_2) \cdot \boldsymbol{n}_1}, \tag{6.9}$$
$$\lambda_2(\boldsymbol{r}) = \frac{(\boldsymbol{r} - \boldsymbol{r}_3) \cdot \boldsymbol{n}_2}{(\boldsymbol{r}_2 - \boldsymbol{r}_3) \cdot \boldsymbol{n}_2}, \tag{6.10}$$
$$\lambda_3(\boldsymbol{r}) = \frac{(\boldsymbol{r} - \boldsymbol{r}_1) \cdot \boldsymbol{n}_3}{(\boldsymbol{r}_3 - \boldsymbol{r}_1) \cdot \boldsymbol{n}_3}. \tag{6.11}$$

These basis functions are shown in Figure 6.2. Note that the gradient of the basis functions is constant:

$$\nabla\big(\lambda_1(\boldsymbol{r})\big) = \frac{1}{(\boldsymbol{r}_1 - \boldsymbol{r}_2) \cdot \boldsymbol{n}_1} \boldsymbol{n}_1, \tag{6.12}$$
$$\nabla\big(\lambda_2(\boldsymbol{r})\big) = \frac{1}{(\boldsymbol{r}_2 - \boldsymbol{r}_3) \cdot \boldsymbol{n}_2} \boldsymbol{n}_2, \tag{6.13}$$
$$\nabla\big(\lambda_3(\boldsymbol{r})\big) = \frac{1}{(\boldsymbol{r}_3 - \boldsymbol{r}_1) \cdot \boldsymbol{n}_3} \boldsymbol{n}_3. \tag{6.14}$$

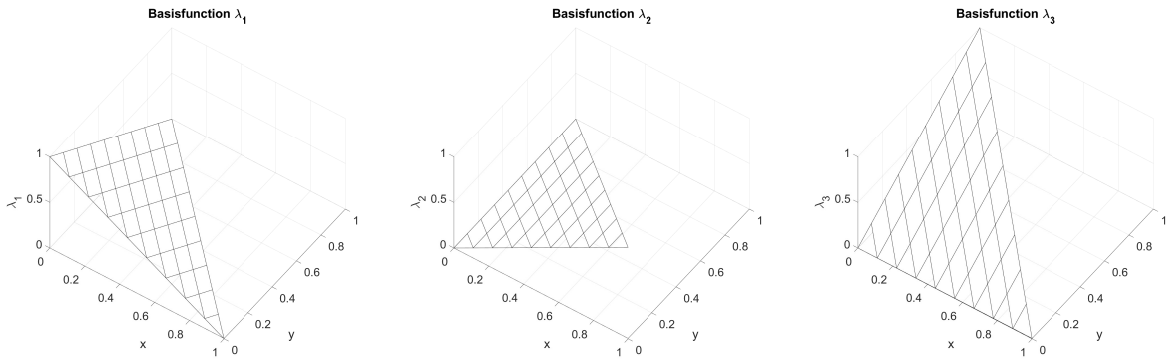

Figure 6.2: The nodal basis functions on a triangular reference element with $\boldsymbol{r}_1 = (0,0)$, $\boldsymbol{r}_1 = (1,0)$ and $\boldsymbol{r}_3 = (0,1)$.

Alternatively, it is possible to determine the basis functions for a given triangle explicitly by solving a linear system. The shape function can be written as $\lambda_i(x,y) = ax + by + c$. With the prescribed values at the nodes, i.e. Equation (6.8), the coefficients of this equation can be found. For example, for λ_1, the coefficients are found by solving:

$$\begin{pmatrix} x_1 & y_1 & 1 \\ x_2 & y_2 & 1 \\ x_3 & y_3 & 1 \end{pmatrix} \begin{pmatrix} a \\ b \\ c \end{pmatrix} = \begin{pmatrix} 1 \\ 0 \\ 0 \end{pmatrix}. \tag{6.15}$$

The matrix on the left-hand side can be inverted to find the solution:

$$\begin{pmatrix} a \\ b \\ c \end{pmatrix} = \frac{1}{2\Delta} \begin{pmatrix} y_2 - y_3 & y_3 - y_1 & y_1 - y_2 \\ x_3 - x_2 & x_1 - x_3 & x_2 - x_1 \\ x_2 y_3 - x_3 y_2 & x_3 y_1 - x_1 y_3 & x_1 y_2 - x_2 y_1 \end{pmatrix} \begin{pmatrix} 1 \\ 0 \\ 0 \end{pmatrix}, \tag{6.16}$$

where Δ is the area of the triangle. So the explicit nodal basis function λ_1 is:

$$\lambda_1(x,y) = \frac{1}{2\Delta}\big(y_2 - y_3\big)x + \big(x_3 - x_2\big)y + \big(x_2 y_3 - x_3 y_2\big), \tag{6.17}$$

which corresponds to the coefficients in the first column of the inverted matrix. The other two nodal basis functions can be found by taking the coefficients in the second and third columns, leading to:

$$\lambda_2(x,y) = \frac{1}{2\Delta}\big(y_3 - y_1\big)x + \big(x_1 - x_3\big)y + \big(x_3 y_1 - x_1 y_3\big), \tag{6.18}$$

$$\lambda_3(x,y) = \frac{1}{2\Delta}\big(y_1 - y_2\big)x + \big(x_2 - x_1\big)y + \big(x_1 y_2 - x_2 y_1\big). \tag{6.19}$$

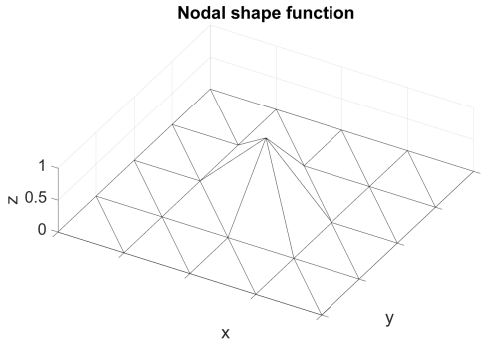

Figure 6.3: Local 'tent' shape function.

The local basis functions described above are defined on a single element. To define global shape functions, the local shape functions are combined. If continuity is enforced, this yields the familiar 'tent' functions as shown in Figure 6.3. This global basis function is associated with a single vertex, on which it is equal to one. On all other vertices, it is equal to zero. On each element, it is linear, and thus globally it is piecewise linear.

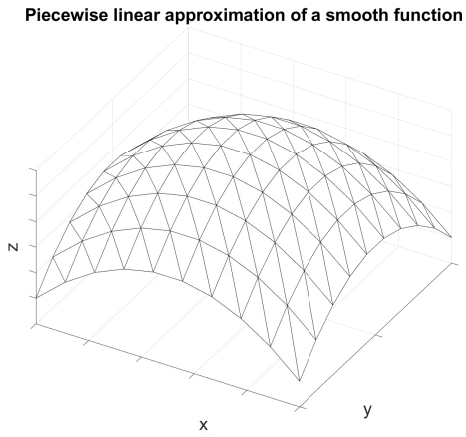

Figure 6.4: Linear combinations of nodal shape functions can be used to find a piecewise linear approximation of a smooth function.

To approximate a function, linear combinations of these basis functions can be used. An example is shown in Figure 6.4.

6.2. Edge elements in 2D

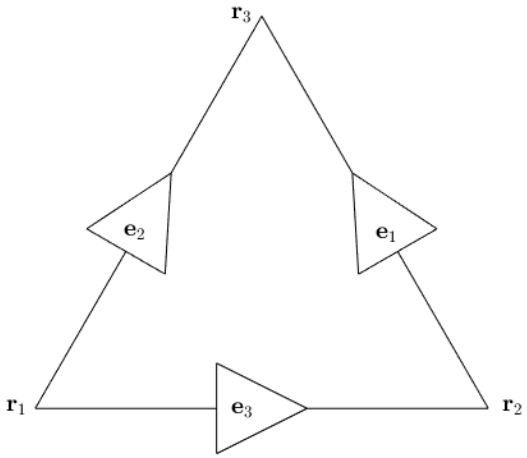

Figure 6.5: Reference directions for triangular edge element

For vector equations, one might expect that it is possible to simply approximate the solution by expanding each component using nodal shape function. This, however, leads to nonphysical solutions [7]. Instead, edge elements can be used. These elements, introduced by Nedelec in [28], consist of vector basis functions, and have the useful property that their tangential components are continuous over element boundaries, while their normal components are allowed to be discontinuous. To define the local edge element basis functions, the nodes and edges of a triangle are numbered as in Figure 6.5. Note that the edges are assigned a reference direction, which is oriented from lower index to higher index. The local edge element basis functions are defined using the nodal basis functions [7]:

$$\boldsymbol{N}_1 = \lambda_2 \nabla \lambda_3 - \lambda_3 \nabla \lambda_2, \tag{6.20}$$

$$\boldsymbol{N}_2 = \lambda_1 \nabla \lambda_3 - \lambda_3 \nabla \lambda_1, \tag{6.21}$$

$$\boldsymbol{N}_3 = \lambda_1 \nabla \lambda_2 - \lambda_2 \nabla \lambda_1. \tag{6.22}$$

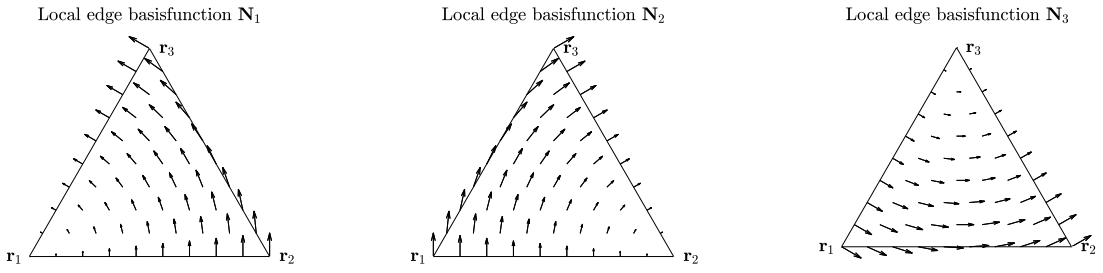

Figure 6.6: Local edge basis functions on a triangle.

These basis functions are shown in Figure 6.6. From visual inspection, it seems that the tangential component of edge basis function i is constant on edge s_i, and zero on all other edges. This property allows for the construction of fields with continuous tangential components over element boundaries, as described above. This property will now be shown mathematically for the first edge basis function $\boldsymbol{N}_1$. Consider the basis function $\boldsymbol{N}_1$, evaluated at a point $\boldsymbol{r}$ on edge s_1, and take the dot product with the tangent vector (as in

Figure 6.1):

$$\boldsymbol{N}_1(\boldsymbol{r})\cdot\boldsymbol{\tau}_1 = \big(\lambda_2(\boldsymbol{r})\nabla\lambda_3(\boldsymbol{r}) - \lambda_3(\boldsymbol{r})\nabla\lambda_2(\boldsymbol{r})\big)\cdot\boldsymbol{\tau}_1 \tag{6.23}$$

$$= \left(\frac{(\boldsymbol{r}-\boldsymbol{r}_3)\cdot\boldsymbol{n}_2}{(\boldsymbol{r}_2-\boldsymbol{r}_3)\cdot\boldsymbol{n}_2}\nabla\left(\frac{(\boldsymbol{r}-\boldsymbol{r}_1)\cdot\boldsymbol{n}_3}{(\boldsymbol{r}_3-\boldsymbol{r}_1)\cdot\boldsymbol{n}_3}\right) - \frac{(\boldsymbol{r}-\boldsymbol{r}_1)\cdot\boldsymbol{n}_3}{(\boldsymbol{r}_3-\boldsymbol{r}_1)\cdot\boldsymbol{n}_3}\nabla\left(\frac{(\boldsymbol{r}-\boldsymbol{r}_3)\cdot\boldsymbol{n}_2}{(\boldsymbol{r}_2-\boldsymbol{r}_3)\cdot\boldsymbol{n}_2}\right)\right)\cdot\boldsymbol{\tau}_1 \tag{6.24}$$

$$= \frac{1}{\big((\boldsymbol{r}_2-\boldsymbol{r}_3)\cdot\boldsymbol{n}_2\big)\big((\boldsymbol{r}_3-\boldsymbol{r}_1)\cdot\boldsymbol{n}_3\big)}\Big(\big((\boldsymbol{r}-\boldsymbol{r}_3)\cdot\boldsymbol{n}_2\big)\boldsymbol{n}_3 - \big((\boldsymbol{r}-\boldsymbol{r}_1)\cdot\boldsymbol{n}_3\big)\boldsymbol{n}_2\Big)\cdot\boldsymbol{\tau}_1. \tag{6.25}$$

Since $\boldsymbol{r}$ on e_1, it can be parametrised as $\boldsymbol{r} = \boldsymbol{r}_2 + k\boldsymbol{\tau}_1$ for some scalar k. Filling this in yields:

$$\boldsymbol{N}_1(\boldsymbol{r})\cdot\boldsymbol{\tau}_1 = \frac{1}{\big((\boldsymbol{r}_2-\boldsymbol{r}_3)\cdot\boldsymbol{n}_2\big)\big((\boldsymbol{r}_3-\boldsymbol{r}_1)\cdot\boldsymbol{n}_3\big)}\Big(\big((\boldsymbol{r}_2+k\boldsymbol{\tau}_1-\boldsymbol{r}_3)\cdot\boldsymbol{n}_2\big)\boldsymbol{n}_3 - \big((\boldsymbol{r}_2+k\boldsymbol{\tau}_1-\boldsymbol{r}_1)\cdot\boldsymbol{n}_3\big)\boldsymbol{n}_2\Big)\cdot\boldsymbol{\tau}_1. \tag{6.26}$$

Rearranging the terms yields:

$$\boldsymbol{N}_1(\boldsymbol{r})\cdot\boldsymbol{\tau}_1 = \frac{1}{\big((\boldsymbol{r}_2-\boldsymbol{r}_3)\cdot\boldsymbol{n}_2\big)\big((\boldsymbol{r}_3-\boldsymbol{r}_1)\cdot\boldsymbol{n}_3\big)}\Big(\big((\boldsymbol{r}_2-\boldsymbol{r}_3)\cdot\boldsymbol{n}_2\big)(\boldsymbol{n}_3\cdot\boldsymbol{\tau}_1) + (k\boldsymbol{\tau}_1\cdot\boldsymbol{n}_2)(\boldsymbol{n}_3\cdot\boldsymbol{\tau}_1)$$
$$- \big((\boldsymbol{r}_2-\boldsymbol{r}_1)\cdot\boldsymbol{n}_3\big)(\boldsymbol{n}_2\cdot\boldsymbol{\tau}_1) - (k\boldsymbol{\tau}_1\cdot\boldsymbol{n}_3)(\boldsymbol{n}_2\cdot\boldsymbol{\tau}_1)\Big). \tag{6.27}$$

Note that $(\boldsymbol{r}_2-\boldsymbol{r}_1)\cdot\boldsymbol{n}_3$, and that the terms containing k cancel each other out, leading to the following constant tangential component on the boundary:

$$\boldsymbol{N}_1(\boldsymbol{r})\cdot\boldsymbol{\tau}_1 = \frac{1}{\big((\boldsymbol{r}_2-\boldsymbol{r}_3)\cdot\boldsymbol{n}_2\big)\big((\boldsymbol{r}_3-\boldsymbol{r}_1)\cdot\boldsymbol{n}_3\big)}\Big(\big((\boldsymbol{r}_2-\boldsymbol{r}_3)\cdot\boldsymbol{n}_2\big)\boldsymbol{n}_3\Big)\cdot\boldsymbol{\tau}_1, \tag{6.28}$$

As expected, the edge basis function $\boldsymbol{N}_1$ has a constant tangential component on boundary e_1.

For the other edges, the edge basis function should have a tangential component which is equal to zero, since the field seems to be perpendicular to the edge in Figure 6.6. This is proven by examining $\boldsymbol{N}_1(\boldsymbol{r})\cdot\boldsymbol{\tau}_2$ with $(\boldsymbol{r})$ on s_2:

$$\boldsymbol{N}_1(\boldsymbol{r})\cdot\boldsymbol{\tau}_2 = \big(\lambda_2(\boldsymbol{r})\nabla\lambda_3(\boldsymbol{r}) - \lambda_3(\boldsymbol{r})\nabla\lambda_2(\boldsymbol{r})\big)\cdot\boldsymbol{\tau}_2 \tag{6.29}$$

$$= -\lambda_3(\boldsymbol{r})\nabla\big(\lambda_2(\boldsymbol{r})\big)\cdot\boldsymbol{\tau}_2 \tag{6.30}$$

$$= -\lambda_3(\boldsymbol{r})\nabla\left(\frac{(\boldsymbol{r}-\boldsymbol{r}_3)\cdot\boldsymbol{n}_2}{(\boldsymbol{r}_2-\boldsymbol{r}_3)\cdot\boldsymbol{n}_2}\right)\cdot\boldsymbol{\tau}_2 \tag{6.31}$$

$$= -\frac{\lambda_3(\boldsymbol{r})}{(\boldsymbol{r}_2-\boldsymbol{r}_3)\cdot\boldsymbol{n}_2}\boldsymbol{n}_2\cdot\boldsymbol{\tau}_2 \tag{6.32}$$

$$= 0. \tag{6.33}$$

Here the fact that $\lambda_2(\boldsymbol{r}) = 0$ for $\boldsymbol{r}$ on s_2 has been used, as well as the fact that $\boldsymbol{n}_2\cdot\boldsymbol{\tau}_2 = 0$. As expected, the dot product is zero, and hence the field has a tangential component equal to zero on the edge s_2. In a similar fashion, examining $\boldsymbol{N}_1(\boldsymbol{r})\cdot\boldsymbol{\tau}_3$ with $(\boldsymbol{r})$ on s_3 yields:

$$\boldsymbol{N}_1(\boldsymbol{r})\cdot\boldsymbol{\tau}_3 = \big(\lambda_2(\boldsymbol{r})\nabla\lambda_3(\boldsymbol{r}) - \lambda_3(\boldsymbol{r})\nabla\lambda_2(\boldsymbol{r})\big)\cdot\boldsymbol{\tau}_3 \tag{6.34}$$

$$= \lambda_2(\boldsymbol{r})\nabla\lambda_3(\boldsymbol{r})\cdot\boldsymbol{\tau}_3 \tag{6.35}$$

$$= \lambda_2(\boldsymbol{r})\nabla\frac{(\boldsymbol{r}-\boldsymbol{r}_1)\cdot\boldsymbol{n}_3}{(\boldsymbol{r}_3-\boldsymbol{r}_1)\cdot\boldsymbol{n}_3}\cdot\boldsymbol{\tau}_3 \tag{6.36}$$

$$= \lambda_2(\boldsymbol{r})\frac{1}{(\boldsymbol{r}_3-\boldsymbol{r}_1)\cdot\boldsymbol{n}_2}\boldsymbol{n}_3\cdot\boldsymbol{\tau}_3 \tag{6.37}$$

$$= 0, \tag{6.38}$$

where the fact that $\lambda_3(\boldsymbol{r}) = 0$ for $\boldsymbol{r}$ on s_3 has been used, as well as the fact that $\boldsymbol{n}_3\cdot\boldsymbol{\tau}_3 = 0$. Thus it has been shown that the edge basis function $\boldsymbol{N}_1$ has a constant tangential component on edge s_1, and zero tangential component on the remaining edges s_2 and s_3. This can be shown in a completely analogous way for the other basis functions $\boldsymbol{N}_2$ and $\boldsymbol{N}_3$, and their respective edges.

Another useful property of the edge basis functions, is that their curl is constant, i.e. that $\nabla \times \boldsymbol{N}_i$ is constant. This can be shown by rewriting the expression for the basis function using the vector identities. For $\boldsymbol{N}_1$, for example:

$$\begin{aligned}
\nabla \times \boldsymbol{N}_1 &= \nabla \times \left(\lambda_2 \nabla \lambda_3 - \lambda_3 \nabla \lambda_2\right) && (6.39)\\
&= \nabla \times (\lambda_2 \nabla \lambda_3) - \nabla \times (\lambda_3 \nabla \lambda_2) && (6.40)\\
&= \lambda_2 \nabla \times \nabla \lambda_3 + \nabla \lambda_2 \times \nabla \lambda_3 - (\lambda_3 \nabla \times \nabla \lambda_2 + \nabla \lambda_3 \times \nabla \lambda_2) && (6.41)\\
&= \nabla \lambda_2 \times \nabla \lambda_3 - \nabla \lambda_3 \times \nabla \lambda_2 && (6.42)\\
&= 2\left(\nabla \lambda_2 \times \nabla \lambda_3\right). && (6.43)
\end{aligned}$$

Note that the fact that the cross product is anticommutative, i.e. $\boldsymbol{A} \times \boldsymbol{B} = -(\boldsymbol{B} \times \boldsymbol{A})$, has been used. Since the gradient of the basis function is constant, as was shown earlier, this result implies that the curl of $\boldsymbol{N}_1$ is constant. The same result can be found in an analogous way for the other edge basis functions $\boldsymbol{N}_2$ and $\boldsymbol{N}_3$.

A consequence of the result for the curl of the edge basis functions, is that the cross product of the element normal vector with the curl of the edge basis function is zero. To verify this, recall that $\nabla \lambda_2 = C_2 \boldsymbol{n}_2$ for a constant C_2, as shown in the previous section in Equation (6.13), and similarly $\nabla \lambda_3 = C_3 \boldsymbol{n}_3$ for a constant C_3. Thus $\nabla \lambda_2 \times \nabla \lambda_3 = C_2 C_3 (\boldsymbol{n_2} \times \boldsymbol{n_3})$. These two normals lie in the plane of the element, and as such we have that $\boldsymbol{n} = C(\boldsymbol{n}_2 \times \boldsymbol{n}_3)$ for some constant C. Putting this together, we find that

$$\begin{aligned}
\boldsymbol{n} \times (\nabla \times \boldsymbol{N}_1) &= \boldsymbol{n} \times (2\left(\nabla \lambda_2 \times \nabla \lambda_3\right)) && (6.44)\\
&= \boldsymbol{n} \times (2 C_2 C_3 (\boldsymbol{n_2} \times \boldsymbol{n_3})) && (6.45)\\
&= \boldsymbol{n} \times (2 C_2 C_3 C \boldsymbol{n}) && (6.46)\\
&= \boldsymbol{0}. && (6.47)
\end{aligned}$$

Here we have used that $\boldsymbol{n} \times \boldsymbol{n} = \boldsymbol{0}$.

Finally, consider the divergence of the edge basis functions. In implementations where a Coulomb gauge is imposed, it is beneficial for the basis functions to be divergence free, since this ensures that the resulting field will be adhere to the Coulomb gauge. The edge basis functions are in fact divergence free, as can be seen by rewriting:

$$\begin{aligned}
\nabla \cdot \boldsymbol{N}_1 &= \nabla \cdot \left(\lambda_2 \nabla \lambda_3 - \lambda_3 \nabla \lambda_2\right) && (6.48)\\
&= \nabla \cdot \left(\lambda_2 \nabla \lambda_3\right) - \nabla \cdot \left(\lambda_3 \nabla \lambda_2\right) && (6.49)\\
&= \lambda_2 \nabla \cdot \left(\nabla \lambda_3\right) + \left(\nabla \lambda_2\right) \cdot \left(\nabla \lambda_3\right) - \lambda_3 \nabla \cdot \left(\nabla \lambda_2\right) - \left(\nabla \lambda_3\right) \cdot \left(\nabla \lambda_2\right) && (6.50)\\
&= \left(\nabla \lambda_2\right) \cdot \left(\nabla \lambda_3\right) - \left(\nabla \lambda_3\right) \cdot \left(\nabla \lambda_2\right) = 0. && (6.51)
\end{aligned}$$

Here the vector identity $\nabla \cdot \left(\phi \boldsymbol{A}\right) = \phi \nabla \cdot \boldsymbol{A} + \left(\nabla \phi\right) \cdot \boldsymbol{A}$ has been used, as well as the fact that the gradient of the nodal basis functions is constant, and hence $\nabla \cdot \left(\nabla \lambda_i\right) = 0$. A similar derivation shows that the other basis functions are also divergence-free.

Two local edge basis functions combined form a global edge function, associated with the edge on which the local basis functions have a tangential component. This is shown in Figure 6.7. A characteristic of this edge $\boldsymbol{e}$ is that the circulation of the basis function $\boldsymbol{N}_e$ along the edge is equal to one:

$$\int_{\boldsymbol{e}} \boldsymbol{N}_e \cdot \, \mathrm{d}\boldsymbol{l} = 1. \tag{6.52}$$

Thus, similar to how the nodal shape functions are associated with a single node on which they are equal to one (and zero on all other nodes), the edge basis functions are associated with a single edge, on which their circulation is equal to one (and zero on all other edges).

6.3. Meshing of the domain

One of the motivations for choosing a boundary element method was the fact that only the interface between the regions needs to be meshed. This is advantageous for several reasons. One of these reasons is that finding an optimal mesh is a complex puzzle of its own, which increases in difficulty for 3D space. The interface, being a 2D surface, is slightly easier to work with. An excellent introduction to finite element meshes is given in [37]. What constitutes a 'good' mesh is very dependent on the problem under consideration. In general, it

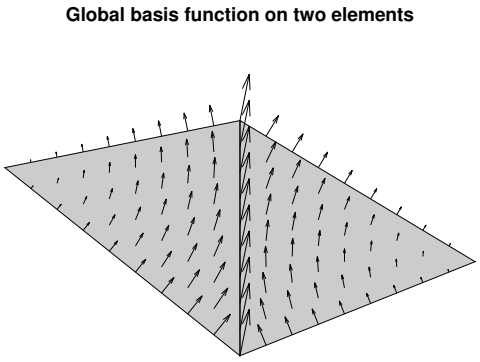

Figure 6.7: A global edge basisfunction on two elements. This edge function is associated with the edge between the triangles, on which its circulation is zero. The circulation along all other edges is one, and the function is zero on all other elements.

is best to avoid very large angles, as is shown in the celebrated paper by Babuška and Aziz [4]. One method to do this is Delauney triangulation. For a given set of points, a Delauney triangulation is a mesh such that no point is within the circumcircle of any triangle (i.e. the circle containing all three vertices of the triangle). This tends to avoid sliver triangles with extreme proportions.

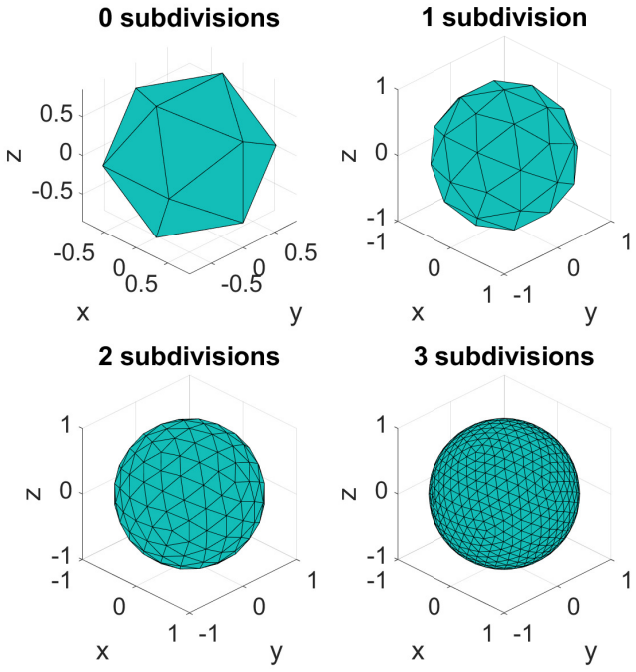

Figure 6.8: Overview of icosahedral meshes with varying amount of subdivisions. Note that due to the way the meshes are generated, the number of elements increases exponentially.

For our purposes, the meshing of the surface of a sphere, we could make use of Delauney triangulation for a discrete collection of points. However, given the symmetry and simplicity of the geometry, we instead choose for the easier option of approximating the sphere by a regular convex icosahedron. The MATLAB script which was used for this can be found in [44]. It creates a unit sphere consisting of regular triangles, with a given number of subdivisions. The first four subdivisions are shown in Figure 6.8.

Refinements	0	1	2	3
Vertices	12	42	162	642
Edges	30	120	480	1920
Elements	20	80	320	1280

Table 6.1: Number of vertices, edges and elements for each refinement step of the icosahedral mesh.

6.4. Numerical integration on reference triangle

The integrals in the BEM formulation necessitate numerical integration. For this, a Gauss quadrature scheme will be used. The Gauss quadrature rules were determined using a MATLAB script which can be found in [20]. For the situations in which both the inner and the outer integral were approximated numerically, it is necessary to choose different Gauss points. As such, two quadrature rules were implemented, with degree 9 and with degree 10. The points for these quadrature rules are shown in Figure 6.9. It is important to note that the rules contain no identical points, and that for both rules, no points lie on an edge or vertex of the reference triangle.

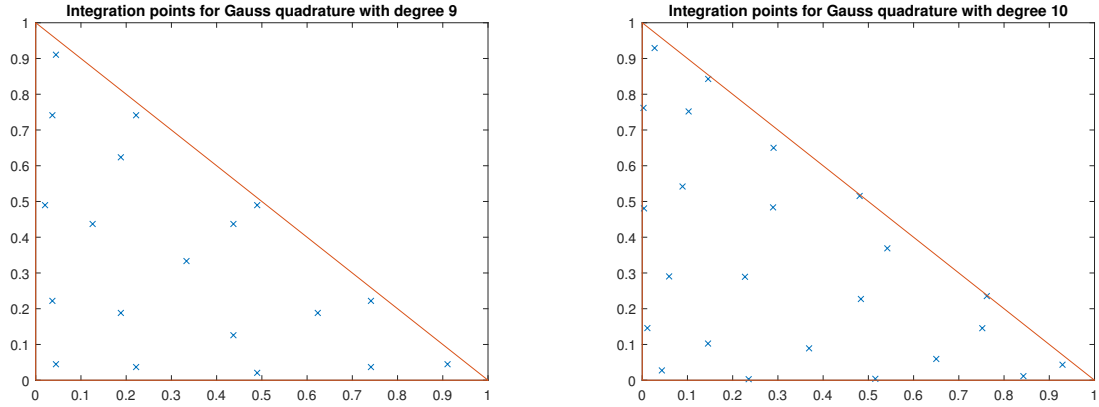

Figure 6.9: Gauss quadrature rules of degree 9 and degree 10.

7

Numerical results

The BEM method as described in Chapters 5 and 6 was implemented in MATLAB. In this chapter, some results of this implementation will be given. The results will be compared to the analytical solution as derived in Section 3.2 for the sphere.

7.1. Results for a sphere

The BEM implementation which has been developed in MATLAB takes as input a geometry G, and a set of system parameters consisting of the relative permeability μ_r, the conductivity of the object σ, and the source field $\boldsymbol{B}_0$. The source field is assumed to be time-harmonic, with a frequency f. In the test case of a sphere, the symmetry of the problem allows us to set the background field in the positive $\boldsymbol{z}$-direction without loss of generality, assuming that the discretisation is symmetric as well. An example of a discretised sphere is shown in Figure 7.1. This sphere, which has $n_{\text{ref}} = 2$ mesh refinements, consists of 192 vertices, 320 elements, and 480 edges.

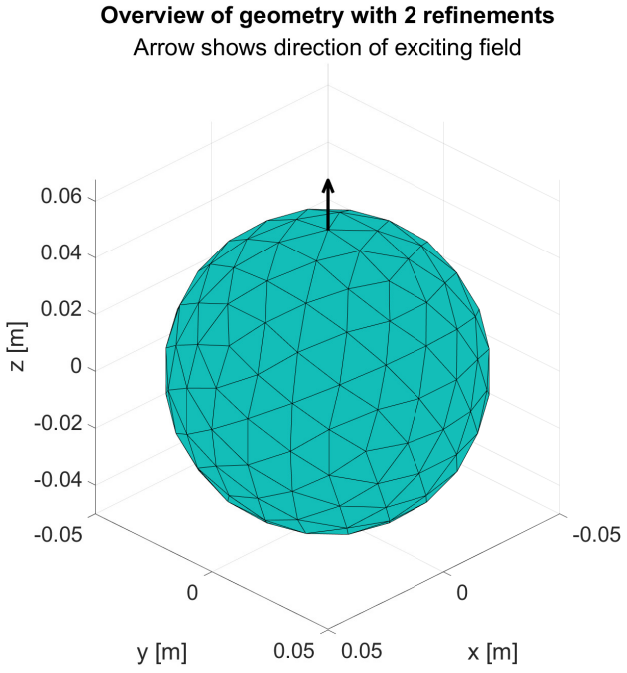

Figure 7.1: A discretised sphere, with $n_{\text{ref}} = 2$ mesh refinements. The sphere has a radius of $r_0 = 0.05\,\text{m}$.

The solution consists of a modified magnetic vector potential $\boldsymbol{A}^*$ and a reduced scalar potential φ. The BEM implementation calculates these potentials restricted on the interface between the object and the free

space region. Subsequently, the fields everywhere in the domain can be calculated making use of the Green's functions. With these two potentials, the magnetic flux density or eddy current density can then be calculated. The steps are shown in Figure 7.2

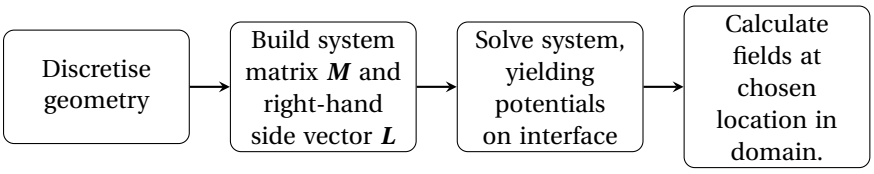

Figure 7.2: An overview of the steps in the BEM implementation

Building the system matrix is the most time-consuming part of the process. The sphere with two mesh refinements as shown in Figure 7.1 leads to a computation time of roughly four hours, on an AMD Ryzen 7 PRO 4750U processor with 1.70GHz and 16GB RAM. However, it should be noted that the implementation is very naive, and preference was given to a clear and readable script over an efficient script. Thus, much could be optimised by replacing `for` loops by vector calculations.

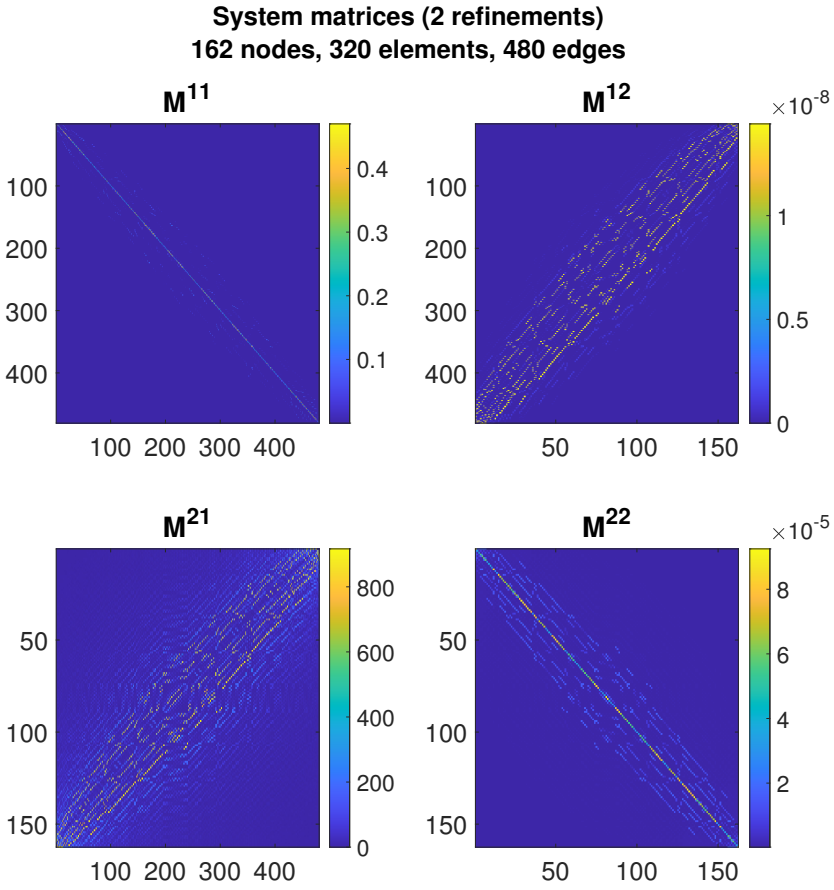

Figure 7.3: Visualisation of system matrix $\boldsymbol{M}$ for the sphere. It is split according to the submatrices defined in the derivation of the method. Note the diagonal dominance of the matrices containing the self-interactions.

A visualisation of the system matrix $\boldsymbol{M}$ is shown in Figure 7.3. The matrix is split up into the submatrices as defined in the derivation of the method in section 5.4. The first submatrix, $\boldsymbol{M}^{11}$, contains the terms where both the test function and the basis function are edge basis functions. This self-interaction matrix shows a clear diagonal dominance, which is numerically favourable. Similarly, we see a siagonally dominant structure in the $\boldsymbol{M}^{22}$ submatrix, which contains the self-terms for the nodal basis functions. The other submatrices $\boldsymbol{M}^{12}$

and $\boldsymbol{M}^{21}$ contain the relation between edge basis functions and nodal shape functions (and vice versa). The structure which is apparent here is completely dependent on node ordering. It seems that the node ordering used by the `icosahedron` script and the subsequent ordering used to define the edges yields a coherent structure where high node numbers correspond to low edge numbers. However, there is probably still room for improvement here. Finally, one might note that there is a large difference in magnitude between the submatrices. Upon investigation of the formulae for the entries of the submatrices, we find a factor of μ_1 in $\boldsymbol{M}^{12}$, and a factor of $1/\mu_0$ in $\boldsymbol{M}^{21}$. Given the magnitude of μ_0 and μ_1, which are of order 10^{-7}, this seems to explain part of the discrepancy. However, this still leaves unexplained why the submatrix $\boldsymbol{M}^{22}$ is so much smaller than the other submatrices.

Solving the system was done with the default MATLAB solver, i.e. the backslash operator. The system matrix is full-rank, but has a large condition number of $k_{\text{cond}} = 3.0317 \times 10^{11}$. The solving is done very quickly, and has a low residual (of order 10^{-14}).

Once the system has been solved, the potentials on the interface can be used to determine the eddy current distribution inside the sphere as well as the magnetic flux density outside the sphere. These are the actual results we are interested in, since these are the physical quantities which are used in magnetic signature reduction.

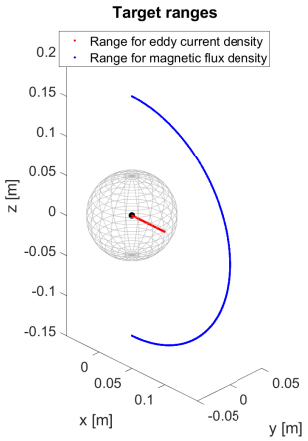

Figure 7.4: Target ranges for eddy current density (red) and magnetic flux density (blue). The red points lie on the $y = 0, z = 0$ axis. The blue points lie in the $y = 0$ plane, at a distance $r = 3r_0$ from the origin.

Below, the results are given for a discretised sphere of radius $r_0 = 0.05m$ with two mesh refinements. The system parameters are

$$\begin{aligned} B_0 &= 1\,\text{T} \\ f &= 50\,\text{Hz} \\ \mu_r &= 20 \\ \sigma &= 10\,\text{MS}\,\text{m}^{-1} \end{aligned}$$

which are the same parameters as were used for the analytical solution in section 3.2, to facilitate comparison of results. Let us begin by investigating the eddy current density $\boldsymbol{J}$ inside the sphere. Once again, this will be calculated for a range of points between the centre and the interface, on the line $y = 0, z = 0$, as is shown in Figure 7.4, which is reprinted here for ease of reference.

Let us begin by considering the eddy current distribution. The results of the approximation are shown in Figure 7.5. The black lines show the numerical approximation, and the red lines show the analytical solution. From a qualitative perspective, the numerical approximation is very acceptable. The eddy currents consist mainly of a azimuthal component, which for this range of points equates to a component in the y-direction. The skin depth effect is visible, with eddy current strength being strongest near the interface. Moreover, the shape of the real and imaginary components correspond well to the shape of the analytical solution.

Upon inspecting the magnitude of the fields, we note that the approximation yields weaker eddy current density than expected from the analytical solution. It seems that a constant scaling factor is missing. Empirically, this scaling factor was found to be roughly 2. An example of the resultant eddy current density using

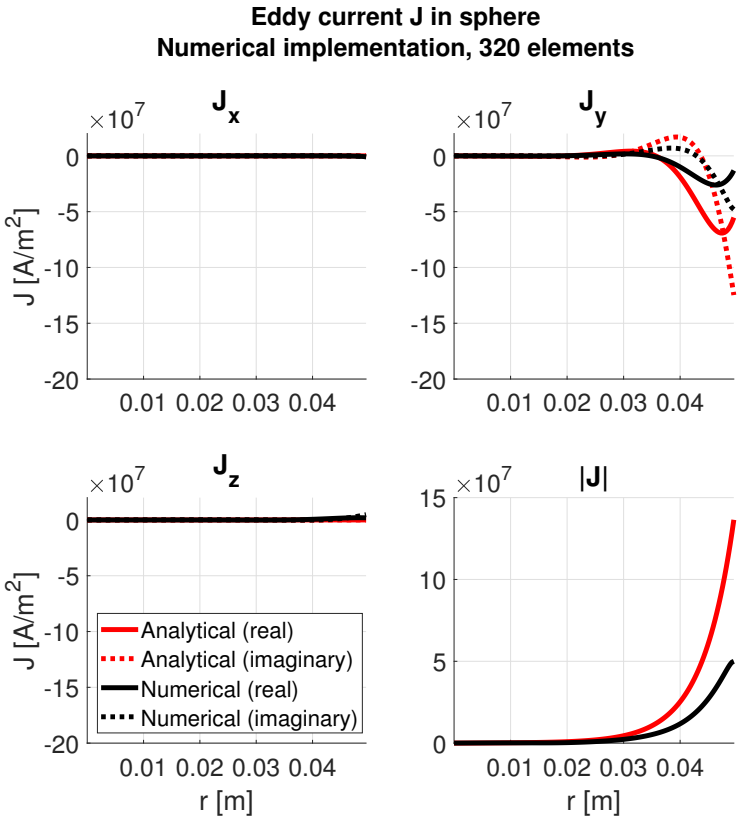

Figure 7.5: Approximated eddy current distribution in sphere.

a scaling factor of $\sqrt{2\pi}$ is shown in Figure 7.6, which seems like an excellent approximation. However, it is unclear if and why this scaling factor is indeed necessary, nor have we rigorously determined its value. Possibly, there is a bug in the implementation. An alternative explanation is that there is a difference between the analytical solution and the numerical approximation in the scaling used for Fourier transformations.

Now let us investigate the approximated magnetic flux density, shown in Figure 7.7. Once again, the approximation is qualitatively very similar to the analytical solution. The y-component is zero, and the x- and z-components have the same shape as the analytical solution, for both the real and imaginary parts. The strength of the field is greatest near the poles, at $\theta = 0$ and $\theta = \pi$, and weakest near the equator. The error for the magnetic field is much smaller than was the case for the eddy current density. The fact that the fields are not the exact same strength could be explained by the coarseness of the discretisation, or the degree of the quadrature rules used.

The Joule losses were also approximated numerically. The analytical Joule losses for the system under consideration are 5.839×10^4 J. For the numerical approximation, the Joule losses were found to be:

$$\begin{aligned} \text{0 refinements:} \quad & P_{\text{loss}} = 5.477 \times 10^4 \text{J} \\ \text{1 refinement:} \quad & P_{\text{loss}} = 2.143 \times 10^4 \text{J} \\ \text{2 refinement:} \quad & P_{\text{loss}} = 3.247 \times 10^4 \text{J} \end{aligned}$$

It seems that the approximation is too inaccurate to determine any meaningful results in terms of Joule losses.

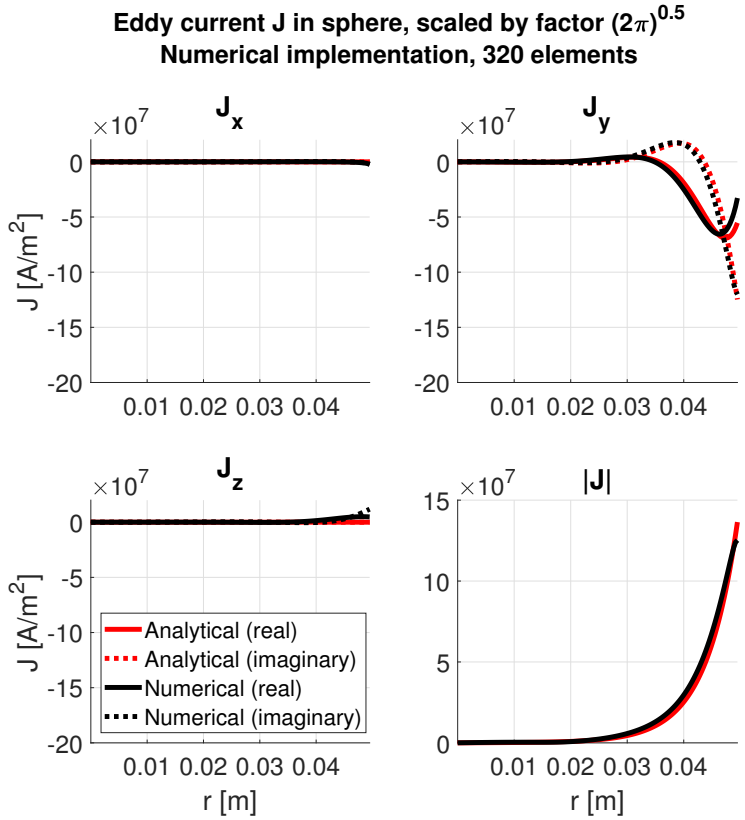

Figure 7.6: Approximated eddy current distribution in sphere, scaled by a factor $\sqrt{2\pi}$.

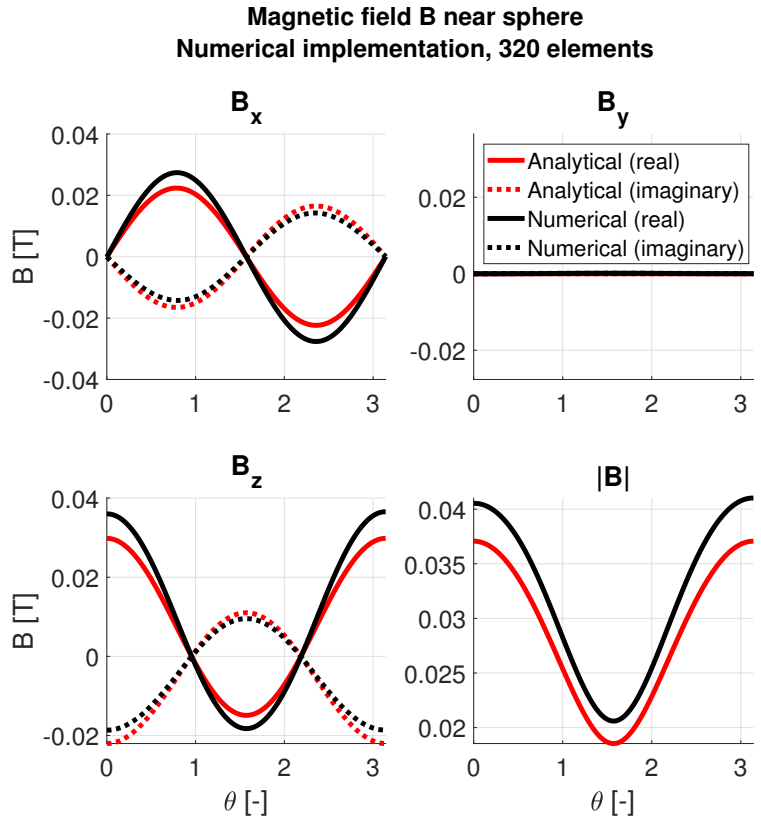

Figure 7.7: Approximated magnetic flux density near sphere.

To quantify the accuracy of the approximation, the absolute and relative error compared to the analytical solution have been calculated. Figure 7.8 shows the absolute error of both fields. For the eddy current density, the absolute error is not a very good metric due to the range of the analytical solution. For the magnetic flux density, we see that the absolute error for the geometry with no refinements is much higher than for the case of one or two refinements. Surprisingly, however, there is not much difference between the errors of one and two refinements.

The relative error for both fields is shown in Figure 7.9. For the current density, the relative error blows up as the current density goes to zero near the centre of the sphere. However, restricting the range of the relative error, we see that the geometry with more elements performs much better than the geometries with less refinements. Taking into account the empirical scaling factor would strongly reduce the relative error. For the magnetic flux density, we once again see that no refinements performs worse, but one and two refinements perform roughly equally. Here too an empirical scaling factor may improve peformance, given the fact that the relative error is roughly constant across the range for these geometries.

Refinements	0	1	2
RMSE of $\boldsymbol{J}$	2.06e7	1.91e7	1.97e7
RMSE of $\boldsymbol{B}$	0.0124	0.0057	0.0059

Table 7.1: Root-mean-squared-error for eddy current density and magnetic flux density.

The root-mean-squared-error for both cases is shown in Table 7.1. The errors are in line with what was seen in the plots.

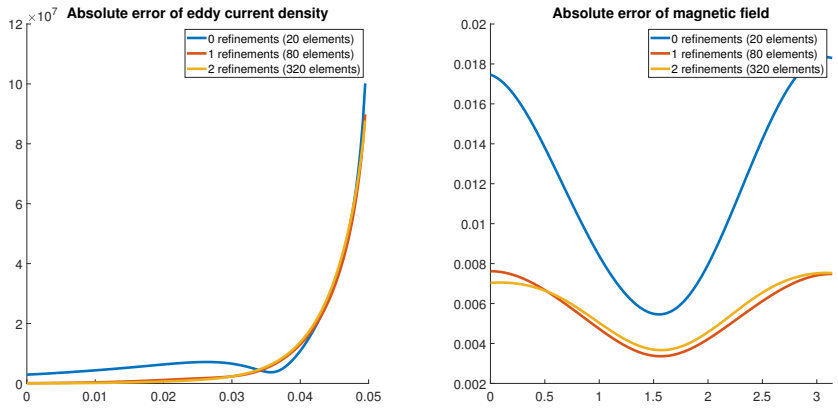

Figure 7.8: Absolute error for eddy current density and magnetic flux density approximations.

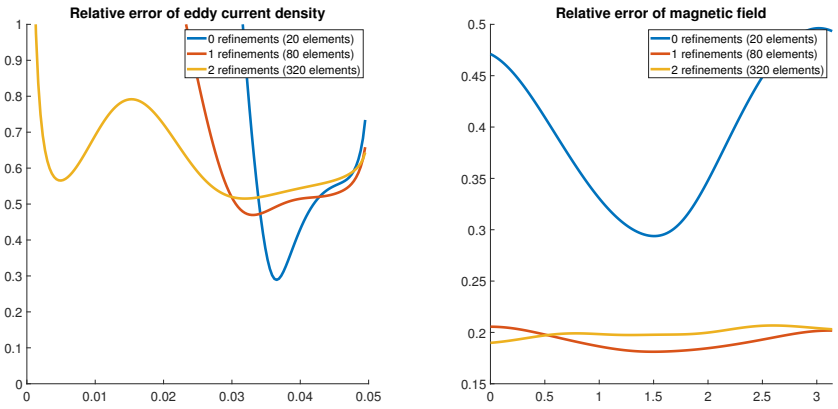

Figure 7.9: Relative error for eddy current density and magnetic flux density approximations.

7.2. Ellipsoid

Having verified that the model is reasonably accurate for the magnetic fields, at least in a qualitative sense, we now turn our attention to some geometries which more strongly resemble a ship. To begin, we will consider an ellipsoid. The geometry is shown in Figure 7.10, on the left. The ellipsoid has a length of 8 m, and a height and width of 1 m. It consists of 80 elements, and was created by scaling the sphere geometry. As such, the meshing is not necessarily optimal, with element size varying from the middle to the ends of the geometry. Also shown in the figure, on the right, is a sensor array. This sensor array is located at a depth of 5 m below the center of the ellipsoid. On the array, the magnetic signature of the ellipsoid will be visible.

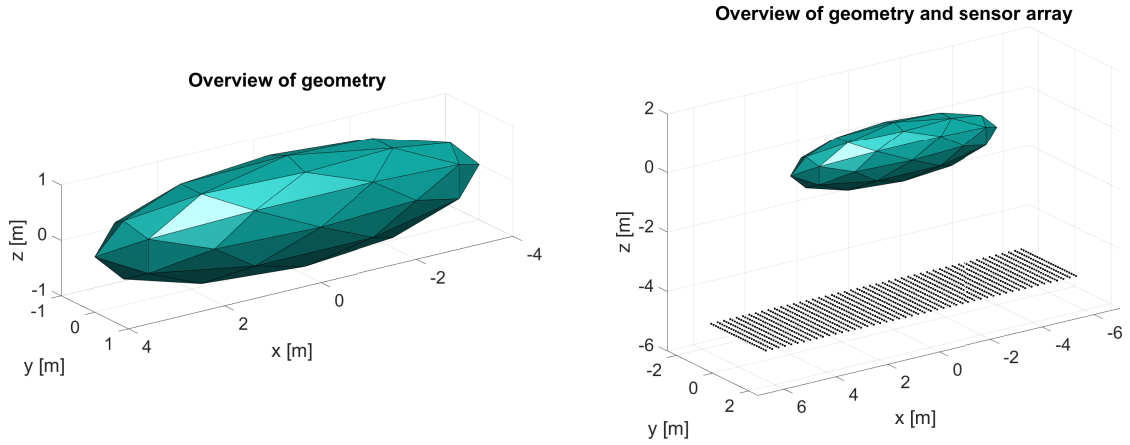

Figure 7.10: Geometry and sensor array for ellipsoid

The parameters for the eddy current simulation with the ellipsoid were chosen to resemble a realistic scenario, with a magnetic field roughly as strong as the Earth magnetic field, a relative permeability similar to that of steel, and a low frequency (albeit in the upper ranges of what is to be expected for sea-surface motion). The parameters are:

$$\begin{aligned} B_0 &= 40\,\mu\text{T}, \\ f &= 1\,\text{Hz}, \\ \mu_r &= 100, \\ \sigma &= 10\,\text{MS}\,\text{m}^{-1}. \end{aligned}$$

The excitation field was applied once in each of the cardinal directions. The results are shown for x-excitation in Figure 7.11, for y-excitation in Figure 7.12, and for z-excitation in Figure 7.13.

The results show that the ellipsoid causes a dipole-like field. The real and imaginary components are opposite in sign, and the imaginary component is slightly weaker than the real component. This is very similar to what was seen for the analytical solution.

As an extra verification, a non-conductive ellipsoid and a non-magnetic ellipsoid were simulated. The resultant magnetic signatures are shown in Figure 7.14. For the non-conductive ellipsoid, no eddy currents should be generated. Therefore one expects to find a pure magnetic dipole field (due to the induced magnetism), with no imaginary component. As can be seen in the plot, this is indeed the case. The imaginary component is negligible. For the non-magnetic sphere, there should be no induced magnetism, but only an eddy current field. In the plot, we find that the imaginary and real components now have the same sign distribution. For the real part, the sign is opposite to that of the non-conducting sphere. In other words, the eddy current field is oriented such that it opposes the magnetic field, as expected by Lenz' Law. The overall strength of the field is lower than in the magnetic case.

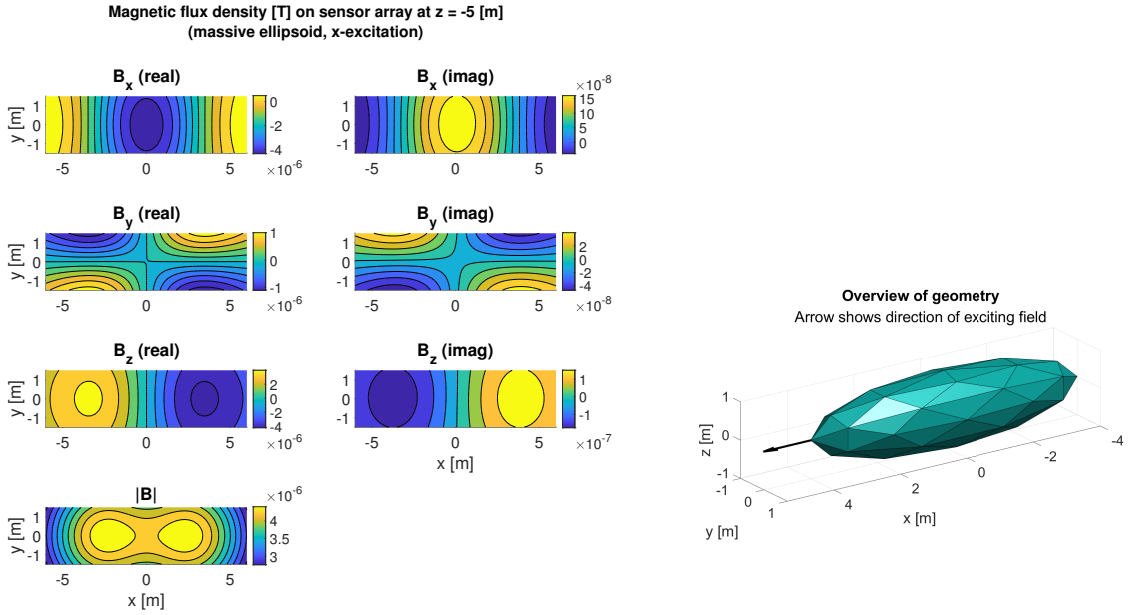

Figure 7.11: *Left:* Magnetic signature on sensor array for ellipsoid subjected to an excitation field in the x-direction. *Right:* Geometry and field direction.

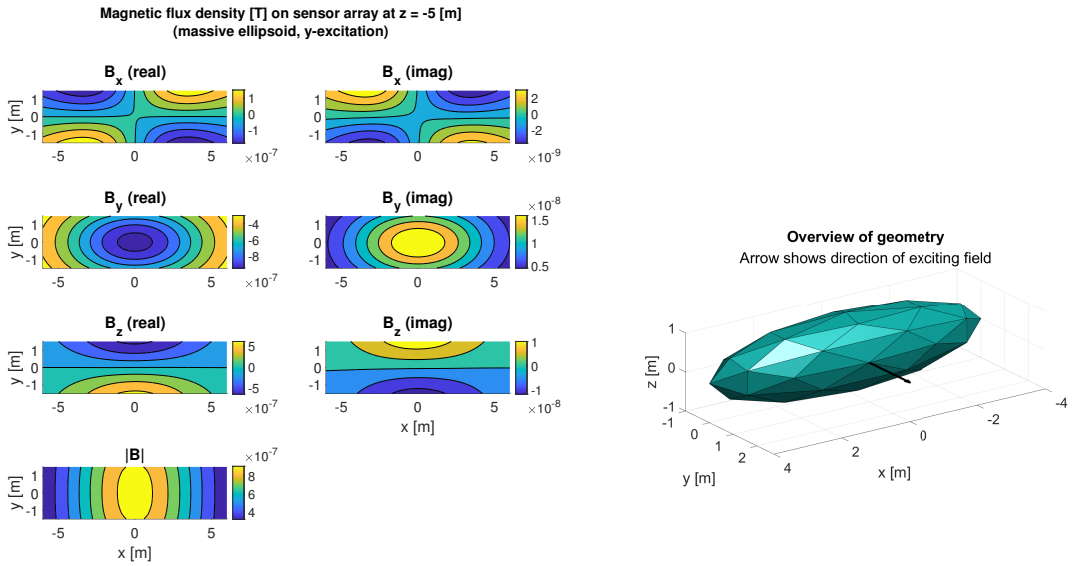

Figure 7.12: *Left:* Magnetic signature on sensor array for ellipsoid subjected to an excitation field in the y-direction. *Right:* Geometry and field direction.

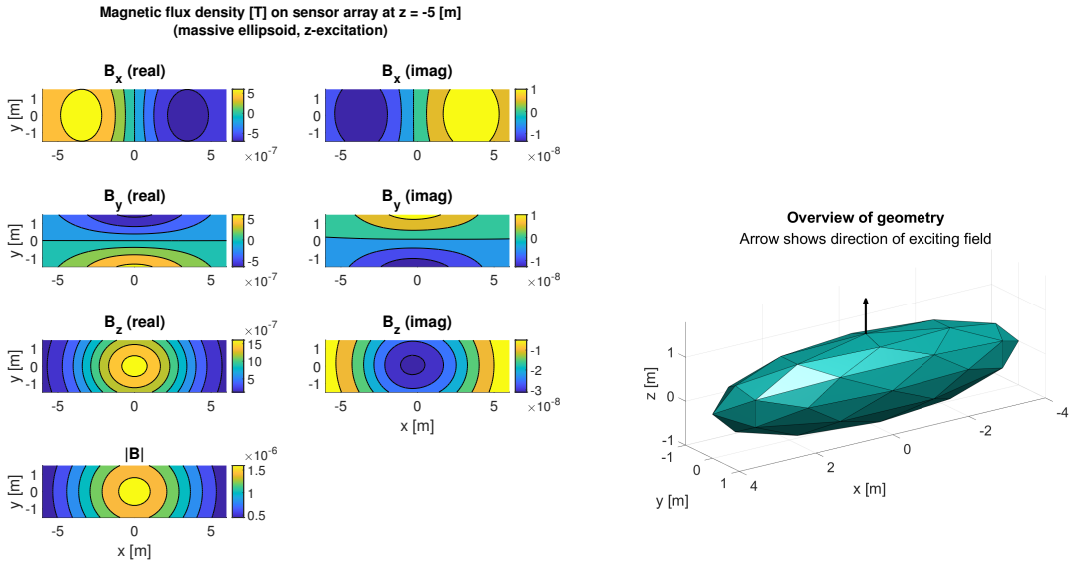

Figure 7.13: *Left:* Magnetic signature on sensor array for ellipsoid subjected to an excitation field in the z-direction. *Right:* Geometry and field direction.

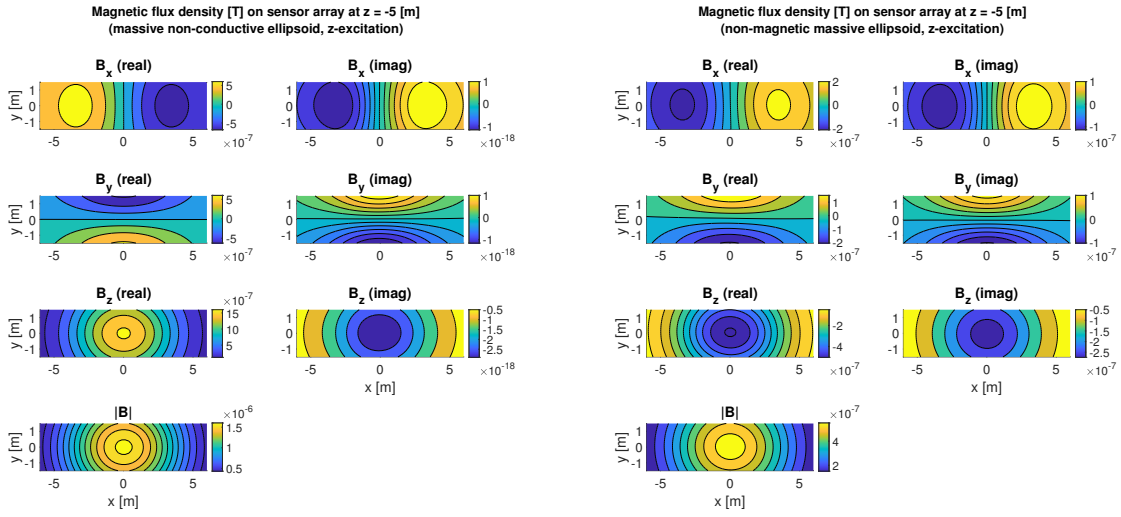

Figure 7.14: *Left:* Magnetic signature on sensor array for non-conductive ellipsoid subjected to an excitation field in the z-direction. *Right:* Magnetic signature on sensor array for non-magnetic ellipsoid subjected to an excitation field in the z-direction.

7.3. Half ellipsoid shell

The final geometry under consideration is a half ellipsoid shell. The geometry is shown in Figure 7.15. It was created by first creating a spherical shell, with an outer radius of 1 m and an inner radius of 0.9 m, and subsequently scaling this shell in the x-direction. Therefore the thickness of the shell is not uniform: it is 10 cm thick at its thinnest point, and 40 cm thick at its thickest point. The mesh consists of 100 elements. The magnetic signature was measured on a sensor array at a depth of 5 m below the half ellipsoid shell.

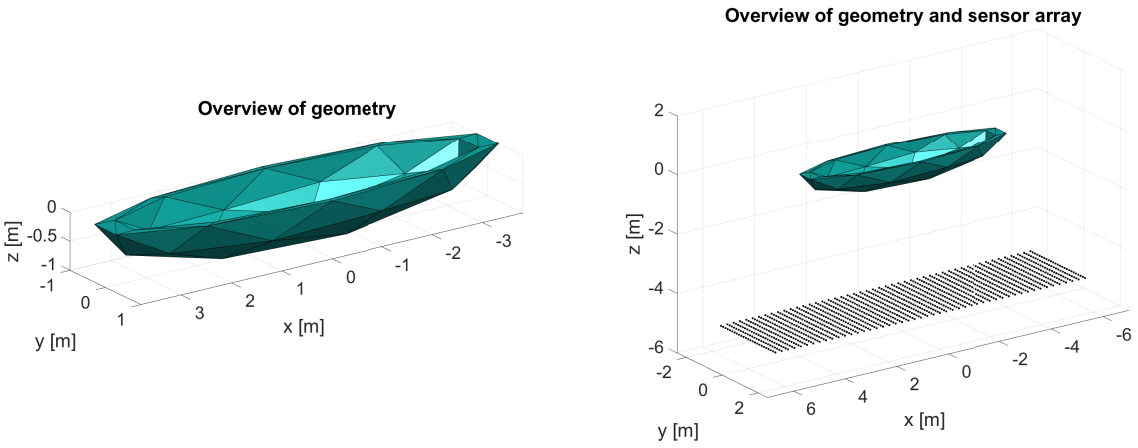

Figure 7.15: Geometry and sensor array for hollow ellipsoid

The same parameters as before were used for the eddy current simulations:

$$\begin{aligned} B_0 &= 40\,\mu\mathrm{T}, \\ f &= 1\,\mathrm{Hz}, \\ \mu_r &= 100, \\ \sigma &= 10\,\mathrm{MS\,m^{-1}}. \end{aligned}$$

The excitation field was applied in each of the cardinal directions.

The results are shown for x-excitation in Figure 7.16, for y-excitation in Figure 7.17, and for z-excitation in Figure 7.18.

The observed fields are no longer symmetric about the x- and y-axes. This is surprising, since the geometry itself is symmetric. In the case of x-excitation, for example, the strongest point of magnetic field is found near $x = -2.5$. The y-excitation and z-excitation do show a maximum in magnetic field strength near the centre of the sensor array. An interesting feature of the signatures is the diagonal slant in the strength of the fields.

It can also be observed that the strength of the fields does not differ much between the hollow ellipsoid and the massive ellipsoid. One possible explanation for this is that the eddy currents for the massive ellipsoid are concentrated near the edge due to the skin effect, and that thus there is little difference between the fields they generate and the fields generated by the eddy currents in the hollow ellipsoid.

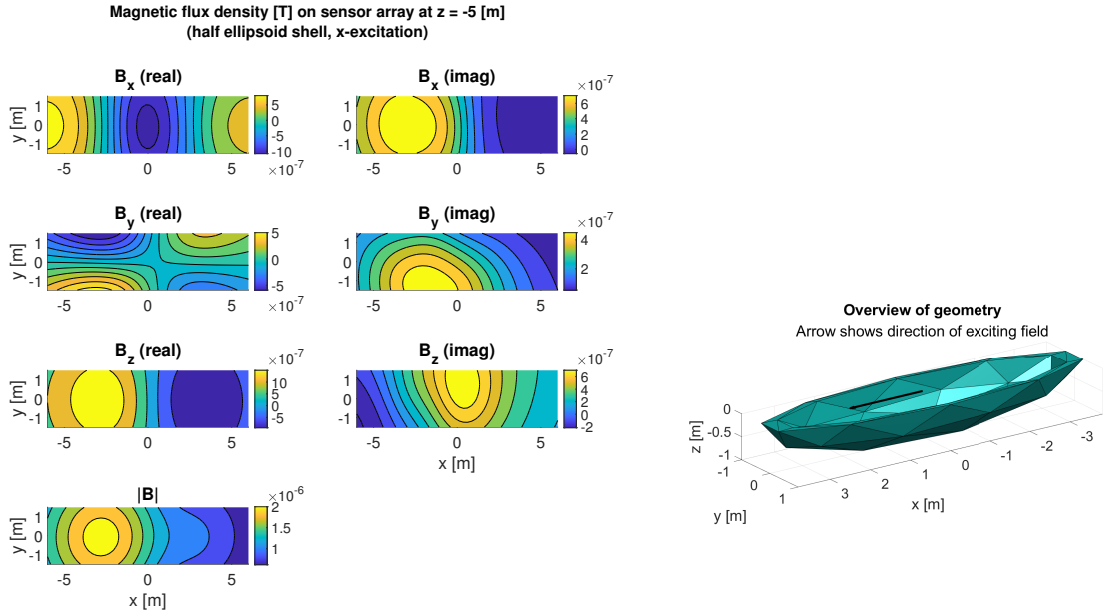

Figure 7.16: *Left:* Magnetic signature on sensor array for ellipsoid subjected to an excitation field in the x-direction. *Right:* Geometry and field direction.

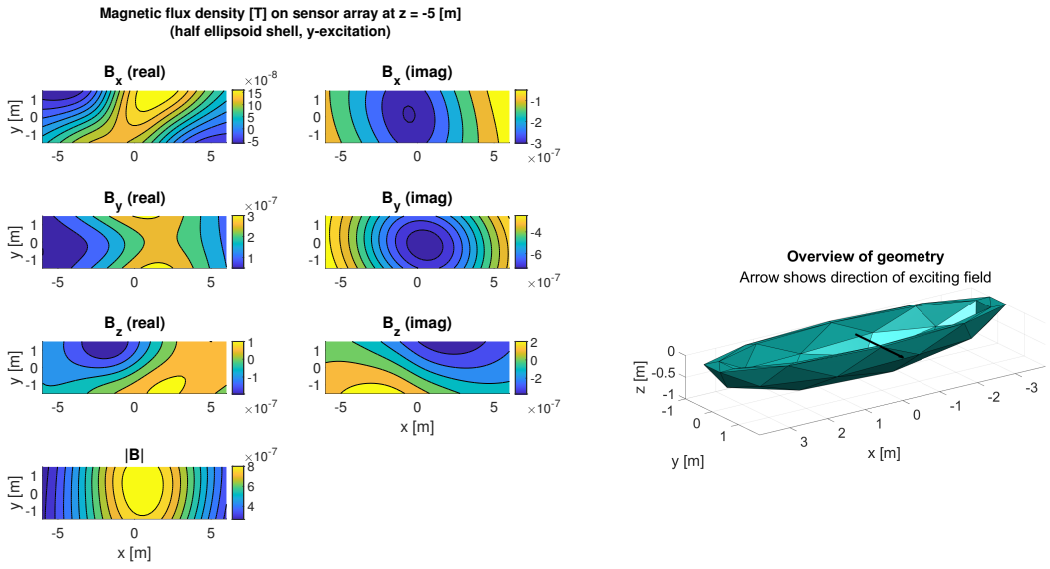

Figure 7.17: *Left:* Magnetic signature on sensor array for ellipsoid subjected to an excitation field in the y-direction. *Right:* Geometry and field direction.

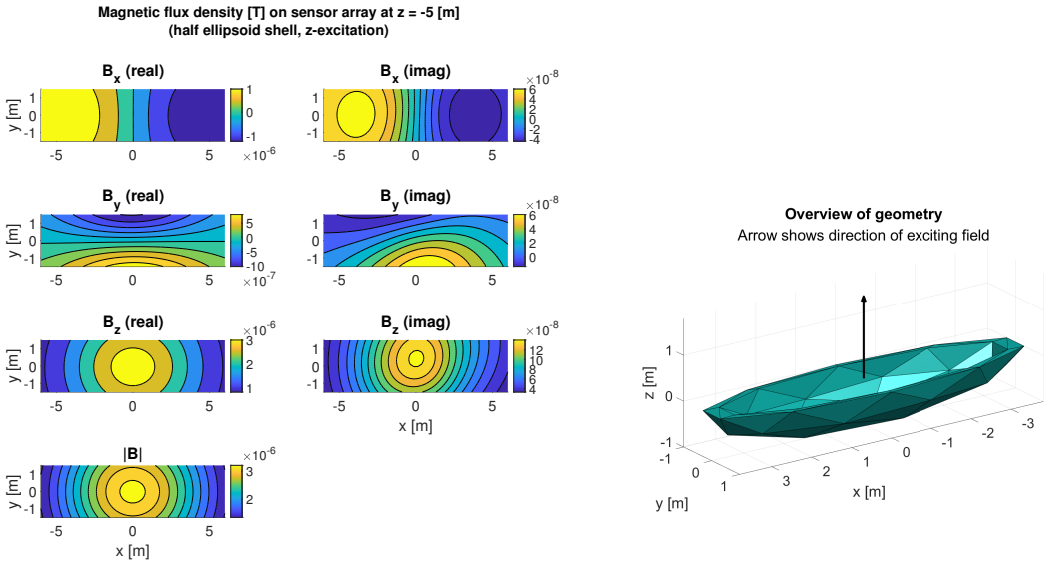

Figure 7.18: *Left:* Magnetic signature on sensor array for ellipsoid subjected to an excitation field in the z-direction. *Right:* Geometry and field direction.

8

Conclusion and recommendations for future research

The goal of this research project is to investigate and develop a modelling method for eddy current fields in the context of degaussing systems of naval vessels. Two main research questions arise from this:

- How can eddy current effects be modelled?
- How can the model be validated?

In the following subsections a short summary will be given of our findings pertaining to these research questions. Subsequently, recommendations for further research will be given, as well as an outlook of how these results may be of use for degaussing systems.

8.1. Modelling the eddy current problem

8.1.1. Analytical solution for sphere

The initial focus of the research performed has been a spherical object which is conductive and magnetic, and which is excited by a time-harmonic background field. For this situation, the Maxwell equations (derived and described in Chapter 2) are adapted: displacement currents are neglected (the quasi-magnetostatic approach) and the equations are transformed to the phasor domain (due to the constant frequency of the exciting field). This leads to the following governing equations of the eddy current problem:

$$\nabla \times \boldsymbol{E} = -j\omega \boldsymbol{B} \tag{8.1}$$

$$\nabla \times \boldsymbol{H} = \boldsymbol{J}_f, \tag{8.2}$$

$$\nabla \cdot \boldsymbol{D} = \boldsymbol{0} \tag{8.3}$$

$$\nabla \cdot \boldsymbol{B} = \boldsymbol{0}, \tag{8.4}$$

The materials are governed by the constitutive relationship $\boldsymbol{B} = \mu \boldsymbol{H}$ and by Ohm's law, $\boldsymbol{J} = \sigma \boldsymbol{E}$.

Before implementing a numerical model, the problem was solved analytically for a spherical geometry. For a sphere with radius r_0 magnetic permeability μ, and electrical conductivity σ, which is excited by a periodic background field with angular frequency ω and strength B_0 in the z-direction, the eddy current density $\boldsymbol{J}$ in the sphere is described by

$$\boldsymbol{J}(r,\theta) = -j\omega\sigma \boldsymbol{A} = -j\omega\sigma \sin\theta C j_1(kr)\hat{\boldsymbol{\varphi}}, \quad (r \leq r_0), \tag{8.5}$$

and the magnetic flux density $\boldsymbol{B}$ in and around the sphere is described by

$$\boldsymbol{B}(r,\theta) = \begin{cases} 2C\cos\theta r^{-1} j_1(kr)\hat{\boldsymbol{r}} - C\sin\theta r^{-1}\left(kr\, j_0(kr) - j_1(kr)\right)\hat{\boldsymbol{\theta}}, & (r \leq r_0) \\ \cos\theta\left(B_0 + \left(2Cr_0^2 j_1(kr_0) - B_0 r_0^3\right) r^{-3}\right)\hat{\boldsymbol{r}} - \sin\theta\left(B_0 - \left(Cr_0^2 j_1(kr_0) - \dfrac{B_0 r_0^3}{2}\right) r^{-3}\right)\hat{\boldsymbol{\theta}}, & (r > r_0), \end{cases} \tag{8.6}$$

where

$$k := -(1-j)\sqrt{\frac{\omega\mu\sigma}{2}}, \qquad C := \frac{3B_0 r_0}{2\mu_r^{-1} kr_0 j_0(kr_0) - 2\mu_r^{-1} j_1(kr_0) + 2j_1(kr_0)}. \tag{8.7}$$

These expressions show that the eddy currents are oriented azimuthally, since only a φ-component is present. This is in line with the physics of the situation, since by Lenz' Law the eddy currents will be oriented in such a way that the field they generate opposes the change in background field. Since the background field is changing in the z-direction, the azimuthally oriented eddy currents will create an opposing field in the z-direction.

The expression for the magnetic flux density is slightly more complicated. Upon rewriting to Cartesian coordinates, however, one finds that the field generated by the eddy currents is in fact a magnetic dipole field, with dipole moment

$$\boldsymbol{m} = \frac{4\pi}{\mu_0}\left(Cr_0^2 j_1(kr_0) - \frac{B_0 r_0^3}{2}\right). \tag{8.8}$$

8.1.2. BEM implementation

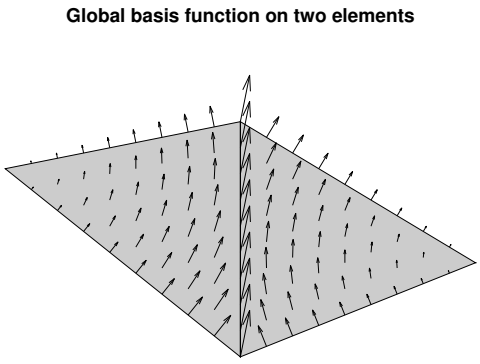

Figure 8.1: A global edge basisfunction on two elements. This edge function is associated with the edge between the triangles, on which its circulation is zero. The circulation along all other edges is one, and the function is zero on all other elements.

Several different formulations exist for the eddy current problem, using various scalar and vector potentials (see Chapter 4). The modified magnetic vector potential $\boldsymbol{A}^*$, introduced by [12], is claimed to have minimum degrees of freedom while still being numerically stable. This formulation, which uses a magnetic scalar potential for the air region, was chosen to be implemented. For the implementation method, preference was given to a boundary element method (BEM). With a BEM, only the surface of the conductor needs to be meshed and approximated. The fields at any point in space can then be determined using the approximated potentials on the surface. The chosen implementation is described in [30]. Chapters 5 and 6 give a a detailed explanation of the method as implemented. In summary, the numerical implementation works as follows:

1. For a conducting and magnetic object in an air region, the modified magnetic vector potential $\boldsymbol{A}^*$ and reduced scalar magnetic potential φ formulation is derived from the Maxwell equations under eddy current assumptions.

2. Using the free space Green's functions for the vector Helmholtz equation (for the $\boldsymbol{A}^*$ potential) and for the Laplace equation (for the φ potential), a BEM formulation is derived.

3. The interface conditions, and thereby the forcing background field, are used to link the BEM formulations.

4. The potentials on the interface are approximated using basis functions, and the Galerkin approach is used to determine the coefficients of the basis functions.

5. Using the potentials on the interface, the magnetic flux density and the eddy current density can be calculated at any point with the BEM formulation.

A notable feature of the implementation is that the scalar potential is approximated using nodal shape functions, whereas the vector potential is approximated using edge shape functions. These edge shape functions are constructed such that their tangential component is continuous across element boundaries, while their normal component is allowed to be discontinuous. An edge shape function is shown in Figure 8.1.

8.2. Validating the model

First, the numerical method was compared to the analytical solution for the sphere. A set of system parameters was chosen:

$$\begin{aligned} r_0 &= 0.05\,\mathrm{m} \\ B_0 &= 1\,\mathrm{T} \\ f &= 50\,\mathrm{Hz} \\ \mu_r &= 20 \\ \sigma &= 10\,\mathrm{MS\,m^{-1}} \end{aligned}$$

The resultant magnetic flux density and eddy current density fields are visualized in Figure 8.2. As expected due to the magnetic dipole-character of the eddy current field, the field is strongest near the top (positive z-direction) and bottom (negative z-direction) of the sphere, and weakest around the middle.

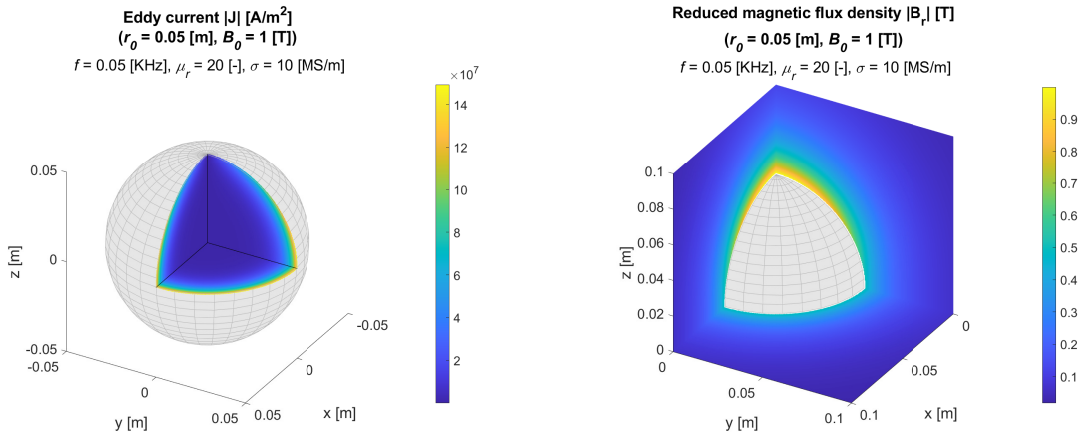

Figure 8.2: Eddy current distribution $\boldsymbol{J}$ inside sphere, and reduced magnetic flux density $\boldsymbol{B}_r$ around sphere. Parameters: $r_0 = 0.05\,\mathrm{m}$, $B_0 = 1\,\mathrm{T}$, $f = 50\,\mathrm{Hz}$, $\mu_r = 20$, $\sigma = 10\,\mathrm{MS\,m^{-1}}$.

The numerical method was implemented in MATLAB, as described in Chapters 5 and 6. The conductor was meshed using triangular elements, on which the potentials were approximated by solving a linear system which was built using the BEM formulation. Figure 8.3 shows the results for a sphere with 320 elements, compared to the analytical solution. The system parameters for this sphere are:

The implementation gives fields which resemble the analytical solution very well, at least qualitatively. The eddy current density $\boldsymbol{J}$ consists only of an azimuthal component, as expected, and moreover shows the correct distribution of real part and imaginary part. However, the eddy current density is off by a scaling factor. This scaling factor seems to be constant for all points, but it is unclear if the scaling factor is constant for other sets of parameters as well. The magnetic flux density $\boldsymbol{B}$ also shows the correct shape of each component, and moreover is a closer fit in terms of field strength, although a scaling factor may still improve the result.

With this it was validated that the model gives a reasonably insight into the shape of the magnetic field surrounding an object. As a first step towards the modelling of a ship geometry, the magnetic signature of a

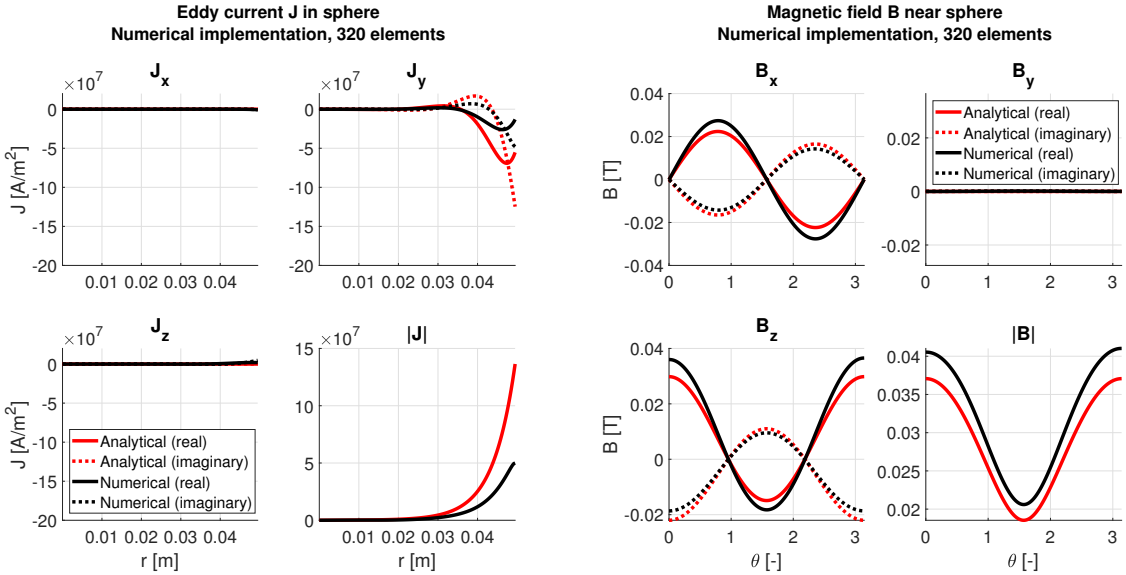

Figure 8.3: Approximated eddy current distribution in sphere (fixed $\theta = 0.5\pi$, $\varphi = 0$, varying r), and approximated reduced magnetic flux density near sphere (fixed $r = 3r_0$, $\varphi = 0$, varying θ).

half ellipsoid shell was approximated. The system parameters for the hollow ellipsoid shell are:

$$\begin{aligned} B_0 &= 40\,\mu\text{T}, \\ f &= 1\,\text{Hz}, \\ \mu_r &= 100, \\ \sigma &= 10\,\text{MS}\,\text{m}^{-1}. \end{aligned}$$

The results of this are shown in Figure 8.4. The geometry is shown on the right, as well as the location of the sensor array on which the magnetic signature is calculated. The figures on the left show the components of the magnetic flux density due to the eddy currents. These results are promising, since they show that the method is capable of determining the magnetic signature of an object which is 'thin'.

8.3. Recommendations fur future research and outlook for degaussing systems

With the above results, the two research questions are answered, and a first step towards integration of eddy currents in a degaussing system is made. However, the model is not quite ready to be used for degaussing purposes yet. It lacks some realism in its assumptions, and moreover, it is computationally expensive and quite slow. As such, it is not fit for real-time modelling of shipboard eddy current fields. Nonetheless, the results of the model are promising, and with more development the model may prove its use in a degaussing context. In this section, recommendations for future work on the model will be given. Following this, some recommendations will be given on how this can contribute to future degaussing systems.

The BEM model which was implemented in this research project shows decent results, with fields which resemble the analytical solution qualitatively. However, an exact correspondence with the analytical solution is not yet observable. Our expectation is that the implementation still needs to be improved or adapted. This should be the first step if one chooses to continue with this model. It should be possible for the implementation to yield exact results for the analytical solution. A bug may still be present in the code, due to which eddy current density magnitude is off by a scaling factor.

The MATLAB implementation itself also has room for improvement. By optimising the code, it should be possible to greatly reduce computation time. For example, many computations are done iteratively, which could instead be programmed using vectorial calculations. Also, the multi-core capabilities of modern processors could be used to allow for parallel computation of the submatrices in the system.

Once a perfectly functioning implementation has been achieved, the next step would be to continue testing different geometries, eventually progressing to a ship-like geometry. Note that this may constitute a non-

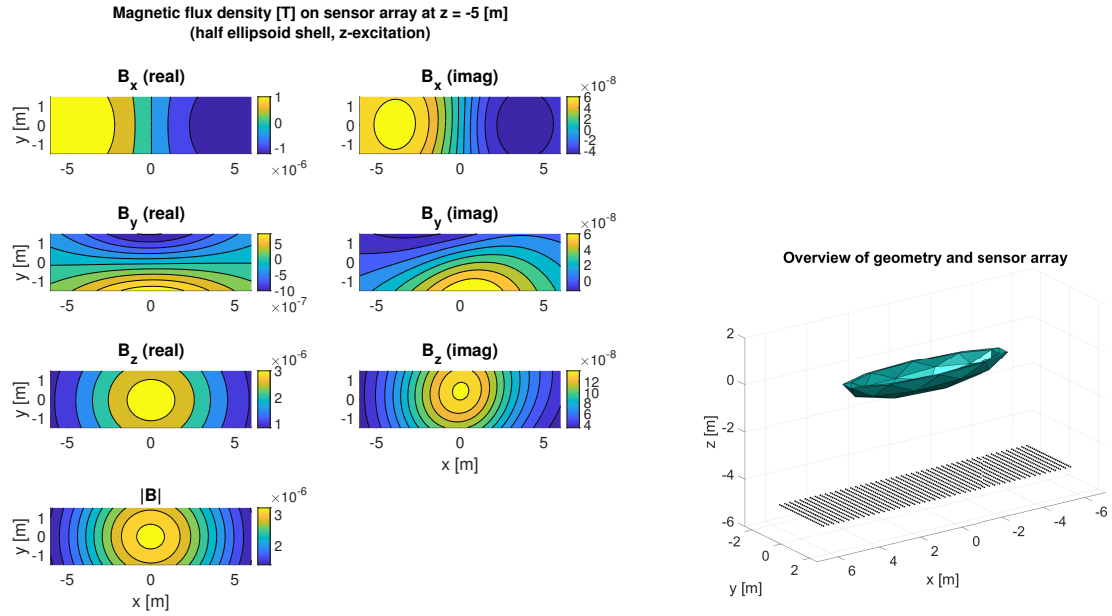

Figure 8.4: *Left:* Magnetic signature on sensor for ellipsoid subjected to an excitation field in the z-direction. *Right:* Geometry and sensor array.

simply connected domain, which the model can not handle. However, by considering only half the domain and making use of the symmetry of the problem, a solution may still be obtainable. The BEM can also be expanded to take into account multiple conducting regions. Another challenge may arise due to the thin geometry: this may lead to ill-conditioned matrices. The degree to which this is an issue is hard to predict, although perhaps a regularisation method could alleviate this somewhat. In addition, thinner geometries may necessitate higher-degree Gauss quadrature rules, thereby increasing computation time.

The results for different geometries must be validated somehow. Using an experimental set-up consisting of multiple coils in each of the cardinal directions (a Helmholtz cage), it is possible to simulate any magnetic field. Using a scale model of the geometry in this Helmholtz cage would yield a dataset against which the model can be validated. Alternatively, the data from experimental trials such as [27] and [31] could be used to validate the model.

Aside from using a more realistic geometry, it is also necessary to implement a more realistic background field. The current time-harmonic field which has been used in this research is nonphysical. A better approach would be to determine the roll, pitch and yaw angles and periods, set up a rotation matrix, and determine the frequencies from that. This is not trivial, and it may prove necessary to adapt the model somewhat to take this more complicated background field into account.

So far, the material has been assumed to be linearly magnetic. However, in practice, the vessel may be ferromagnetic. This brings an additional layer of complexity to the problem. It is unclear if this model is capable of dealing with a ferromagnetic material. Probably, this will be far from trivial.

With each of the steps described above, the model will come closer to being usable in a degaussing context. In the best case, the model will be able to determine the eddy current field due to the rolling motion of a ship in real-time. If this goal proves to be too ambitious due to computational complexity, the model may still be able to be worthwhile. The system matrices could be calculated in advance for various system parameters and movement frequencies. With this library of system matrices, one would only need to calculate the right-hand side vector for the background field, which is far less expensive. Should this still prove to slow, then perhaps a complete library of eddy current signatures for various situations may be considered. These fields, either calculated on the fly or pre-calculated, can then be taken into account by the degaussing algorithm. Hopefully, this will lead to even safer naval vessels in the future.

A

Spherical coordinates

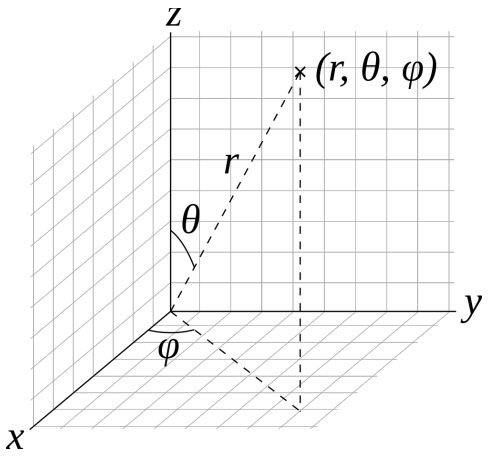

Figure A.1: Spherical coordinate system (r,θ,φ) as used in physics (ISO 80000-2:2019 convention). Image from Wikimedia Commons (Public Domain)

In many situations, it is desireable to express a problem in spherical coordinates, so that one can take advantage of some symmetries. As is the convention in physics, a point is expressed in spherical coordinates as (r,θ,φ). Here r is the radial distance, θ the polar angle, and φ is the azimuthal angle, as shown in Figure A.1. To convert a point (x,y,z) from Cartesian coordinates to spherical coordinates, the following formulae are used:

$$r = \sqrt{x^2 + y^2 + z^2}, \tag{A.1}$$

$$\theta = \arctan\left(\frac{\sqrt{x^2+y^2}}{z}\right), \qquad 0 \le \theta \le \pi, \tag{A.2}$$

$$\varphi = \arctan\left(\frac{y}{x}\right), \qquad -\pi \le \varphi \le \pi. \tag{A.3}$$

Note that the inverse tangent in $\arctan\left(y/x\right)$ must take into account the correct quadrant of (x,y). The single argument inverse tangent can not discern diametrically opposite directions. Thus it is necessary to use the two-argument inverse tangent, $\mathrm{atan2}(y,x)$.

To obtain Cartesian coordinates from a point with spherical coordinates (r,θ,φ), the following formulae are used:

$$x = r\sin\theta\cos\varphi, \tag{A.4}$$

$$y = r\sin\theta\sin\varphi, \tag{A.5}$$

$$z = r\cos\theta. \tag{A.6}$$

For integration and differentiation in spherical coordinates, the local orthogonal unit vectors will be useful:

$$\hat{\boldsymbol{r}} = \sin\theta\cos\varphi\hat{\boldsymbol{x}} + \sin\theta\sin\varphi\hat{\boldsymbol{y}} + \cos\theta\hat{\boldsymbol{z}}, \tag{A.7}$$

$$\hat{\boldsymbol{\theta}} = \cos\theta\cos\varphi\hat{\boldsymbol{x}} + \cos\theta\sin\varphi\hat{\boldsymbol{y}} - \sin\theta\hat{\boldsymbol{z}}, \tag{A.8}$$

$$\hat{\boldsymbol{\varphi}} = -\sin\varphi\hat{\boldsymbol{x}} + \cos\varphi\hat{\boldsymbol{y}}. \tag{A.9}$$

The cross product of these unit vectors is:

$$\hat{\boldsymbol{r}} \times \hat{\boldsymbol{\theta}} = \hat{\boldsymbol{\varphi}}, \tag{A.10}$$

$$\hat{\boldsymbol{\theta}} \times \hat{\boldsymbol{\varphi}} = \hat{\boldsymbol{r}}, \tag{A.11}$$

$$\hat{\boldsymbol{\varphi}} \times \hat{\boldsymbol{r}} = \hat{\boldsymbol{\theta}}. \tag{A.12}$$

This can be checked by filling in the orthogonal unit vectors.

The line element $\mathrm{d}\boldsymbol{r}$ for a displacement from (r,θ,φ) to $(r+\mathrm{d}r,\theta+\mathrm{d}\theta,\varphi+\mathrm{d}\varphi)$ is given by

$$\mathrm{d}\boldsymbol{r} = \mathrm{d}r\,\hat{\boldsymbol{r}} + r\,\mathrm{d}\theta\hat{\boldsymbol{\theta}} + r\sin\theta\,\mathrm{d}\varphi\hat{\boldsymbol{\varphi}}. \tag{A.13}$$

The surface element for a surface spanning from θ to $\theta+\mathrm{d}\theta$ and from φ to $\varphi+\mathrm{d}\varphi$ (at a constant radius) is given by

$$\mathrm{d}\boldsymbol{a} = r^2\sin\theta\,\mathrm{d}\theta\,\mathrm{d}\varphi. \tag{A.14}$$

With this, one can find the following expressions for the gradient, divergence, curl, the Laplacian and the vector Laplacian in spherical coordinates:

$$\nabla f = \frac{\partial f}{\partial r}\hat{\boldsymbol{r}} + \frac{1}{r}\frac{\partial f}{\partial\theta}\hat{\boldsymbol{\theta}} + \frac{1}{r\sin\theta}\frac{\partial f}{\partial\varphi}\hat{\boldsymbol{\varphi}} \tag{A.15}$$

$$\nabla\cdot\boldsymbol{A} = \frac{1}{r^2}\frac{\partial}{\partial r}\left(r^2A_r\right) + \frac{1}{r\sin\theta}\frac{\partial}{\partial\theta}\left(\sin\theta A_\theta\right) + \frac{1}{r\sin\theta}\frac{\partial A_\varphi}{\partial\varphi}, \tag{A.16}$$

$$\nabla\times\boldsymbol{A} = \frac{1}{r\sin\theta}\left(\frac{\partial}{\partial\theta}\left(A_\varphi\sin\theta\right) - \frac{\partial A_\theta}{\partial\varphi}\right)\hat{\boldsymbol{r}} + \frac{1}{r}\left(\frac{1}{\sin\theta}\frac{\partial A_r}{\partial\varphi} - \frac{\partial}{\partial r}\left(rA_\varphi\right)\right)\hat{\boldsymbol{\theta}} + \frac{1}{r}\left(\frac{\partial}{\partial r}\left(rA_\theta\right) - \frac{\partial A_r}{\partial\theta}\right)\hat{\boldsymbol{\varphi}}, \tag{A.17}$$

$$\nabla^2 f = \frac{1}{r^2}\frac{\partial}{\partial r}\left(r^2\frac{\partial f}{\partial r}\right) + \frac{1}{r^2\sin\theta}\frac{\partial}{\partial\theta}\left(\sin\theta\frac{\partial f}{\partial\theta}\right) + \frac{1}{r^2\sin^2\theta}\frac{\partial^2 f}{\partial\varphi^2}, \tag{A.18}$$

$$\begin{aligned}\nabla^2\boldsymbol{A} = {}& \left(\nabla^2A_r - \frac{2A_r}{r^2} - \frac{2}{r^2\sin\theta}\frac{\partial\left(A_\theta\sin\theta\right)}{\partial\theta} - \frac{2}{r^2\sin\theta}\frac{\partial A_\varphi}{\partial\varphi}\right)\hat{\boldsymbol{r}} + \left(\nabla^2A_\theta - \frac{A_\theta}{r^2\sin^2\theta} + \frac{2}{r^2}\frac{\partial A_r}{\partial\theta} - \frac{2\cos\theta}{r^2\sin^2\theta}\frac{\partial A_\varphi}{\partial\varphi}\right)\hat{\boldsymbol{\theta}} \\ & + \left(\nabla^2A_\varphi - \frac{A_\varphi}{r^2\sin^2\theta} + \frac{2}{r^2\sin\theta}\frac{\partial A_r}{\partial\varphi} + \frac{2\cos\theta}{r^2\sin^2\theta}\frac{\partial A_\theta}{\partial\varphi}\right)\hat{\boldsymbol{\varphi}}.\end{aligned} \tag{A.19}$$

B

Helmholtz's Theorem

Helmholtz's theorem, or the Helmholtz decomposition, is an important mathematical result which states that a vector field can be uniquely split into an irrotational (curl-free) and solenoidal (divergence-free) part. The statement is given below; a proof can be found in many textbooks, for example in [3, p. 671].

Let $\boldsymbol{F}(\boldsymbol{x})$ be a sufficiently smooth three-dimensional field, which decays sufficiently fast at infinity. Then $\boldsymbol{F}(\boldsymbol{x})$ can be decomposed into:

$$\boldsymbol{F}(\boldsymbol{x}) = -\nabla\phi(\boldsymbol{x}) + \nabla \times \boldsymbol{V}(\boldsymbol{x}), \tag{B.1}$$

where

$$\phi(\boldsymbol{x}) = \frac{1}{4\pi}\int \frac{\nabla \cdot \boldsymbol{F}(\boldsymbol{x}')}{|\boldsymbol{x}-\boldsymbol{x}'|}\,\mathrm{d}\boldsymbol{x}', \tag{B.2}$$

and

$$\boldsymbol{V}(\boldsymbol{x}) = \frac{1}{4\pi}\int \frac{\nabla \times \boldsymbol{F}(\boldsymbol{x}')}{|\boldsymbol{x}-\boldsymbol{x}'|}\,\mathrm{d}\boldsymbol{x}'. \tag{B.3}$$

Note that $-\nabla\phi(\boldsymbol{x})$ is irrotational, since the curl of gradient is zero, and that $\nabla \times \boldsymbol{V}(\boldsymbol{x})$ is solenoidal, since the divergence of curl is also zero. Note moreover that $\boldsymbol{V}(\boldsymbol{x})$ is itself also divergence free.

An important consequence is that if one has the divergence $\nabla \cdot \boldsymbol{F}(\boldsymbol{x})$ and curl $\nabla \times \boldsymbol{F}(\boldsymbol{x})$ of a vector field $\boldsymbol{F}(\boldsymbol{x})$, then the field can be uniquely determined.

C

Potential theory

In electromagnetics, it is often useful to express a field using a potential. For example, in electrostatics, one finds that the electric field $\boldsymbol{\mathcal{E}}$ can be expressed as the gradient of a scalar potential V:

$$\boldsymbol{\mathcal{E}} = -\nabla V. \tag{C.1}$$

Similarly, the magnetic field $\boldsymbol{\mathcal{B}}$ was found to be the curl of a vector potential $\boldsymbol{A}$:

$$\boldsymbol{\mathcal{B}} = \nabla \times \boldsymbol{A}. \tag{C.2}$$

Not all vector fields can be expressed with a potential. Certain conditions must be met, which will be stated and derived in this appendix. Such proofs can be found in many textbooks. The first proof follows the common method of using path independence, whereas the second proof given below follows [2, p.170].

C.1. Scalar potential

Let $\boldsymbol{F}$ be a vector field on a simply connected three-dimensional domain. Then the following statements are equivalent:

1. The field $\boldsymbol{F}$ has zero curl, i.e. $\nabla \times \boldsymbol{F} = \boldsymbol{0}$.
2. For any closed loop C, one has $\oint_C \boldsymbol{F} \cdot \mathrm{d}\boldsymbol{r} = 0$.
3. The field $\boldsymbol{F}$ can be expressed as the negative gradient of a scalar potential φ, i.e. $\boldsymbol{F} = -\nabla\varphi$.

Begin by proving that the first two statements are equivalent. Let C be a closed loop in the domain, bounding a surface S. If (1) holds, then integrating over the surface yields

$$\int_S (\nabla \times \boldsymbol{F}) \cdot \mathrm{d}\boldsymbol{S} = 0. \tag{C.3}$$

Applying Stoke's theorem yields

$$\oint_C \boldsymbol{F} \cdot \mathrm{d}\boldsymbol{r} = 0, \tag{C.4}$$

as stated in (2). The reverse, (2) implies (1), can be shown in the same way.

It will now be shown that (2) and (3) are equivalent. Assume that (2) holds, and define $\varphi(\boldsymbol{r}) = -\int_C \boldsymbol{F}(\boldsymbol{r}') \cdot \mathrm{d}\boldsymbol{r}'$, where C is a path from a fixed point $\boldsymbol{r}_0$ to $\boldsymbol{r}$. Note that this integral is independent of the path taken between the points. This can be verified by taking another path C_2, and combining C and $-C_2$ to form a closed curve, from which by (2) it follows that $\int_C \boldsymbol{F}(\boldsymbol{r}') \cdot \mathrm{d}\boldsymbol{r}' = \int_{C_2} \boldsymbol{F}(\boldsymbol{r}') \cdot \mathrm{d}\boldsymbol{r}'$. Hence the definition of φ is well-defined.

Now consider a perturbation $\boldsymbol{r} \mapsto \delta\boldsymbol{r}$, $C \mapsto C + \delta C$. Then

$$\varphi(\boldsymbol{r} + \delta\boldsymbol{r}) = \varphi(\boldsymbol{r}) + \nabla\varphi \cdot \delta\boldsymbol{r} + \mathcal{O}(|\delta\boldsymbol{r}|), \tag{C.5}$$

and

$$\varphi(\boldsymbol{r}+\delta\boldsymbol{r})-\varphi(\boldsymbol{r}) = -\int_{C+\delta C}\boldsymbol{F}(\boldsymbol{r}')\cdot\mathrm{d}\boldsymbol{r}'+\int_{C}\boldsymbol{F}(\boldsymbol{r}')\cdot\mathrm{d}\boldsymbol{r}' \tag{C.6}$$

$$= -\int_{\delta C}\boldsymbol{F}(\boldsymbol{r}')\cdot\mathrm{d}\boldsymbol{r}' \tag{C.7}$$

$$= -\boldsymbol{F}(\boldsymbol{r})\cdot\delta\boldsymbol{r}+\mathcal{O}(|\delta\boldsymbol{x}|). \tag{C.8}$$

Comparing these two equations, one finds that $\boldsymbol{F}=-\nabla\varphi$, as in statement (3).

To prove that (3) implies (2), simply take the curl of both sides of the equation, and note that the curl of a gradient is always zero. This implies that (1) must hold, and therefore (2) as well.

Note that the potential is defined with respect to a reference point $\boldsymbol{r}_0$, at which the potential is zero.

C.2. Vector potential

Let $\boldsymbol{B}$ be a solenoidal vector field, i.e. $\nabla\cdot\boldsymbol{B}=0$. Then $\boldsymbol{B}$ can be described as the curl of a vector potential $\boldsymbol{A}$:

$$\boldsymbol{B}=\nabla\times\boldsymbol{A}. \tag{C.9}$$

To prove this, a construction of $\boldsymbol{A}$ will be given. Define $\boldsymbol{A}$ as

$$\boldsymbol{A}=\hat{\boldsymbol{y}}\int_{x_0}^{x}B_z(x,y,z)\;\mathrm{d}x+\hat{\boldsymbol{z}}\left(\int_{y_0}^{y}B_x(x_0,y,z)\;\mathrm{d}y-\int_{x_0}^{x}B_y(x,y,z)\;\mathrm{d}x\right). \tag{C.10}$$

Begin by evaluating the y-component of $\nabla\times\boldsymbol{A}$, which yields:

$$(\nabla\times\boldsymbol{A})_y=\frac{\partial A_x}{\partial z}-\frac{\partial A_z}{\partial x} \tag{C.11}$$

$$=0-\frac{\partial}{\partial x}\left(\int_{y_0}^{y}B_x(x_0,y,z)\;\mathrm{d}y-\int_{x_0}^{x}B_y(x,y,z)\;\mathrm{d}x\right) \tag{C.12}$$

$$=\frac{\partial}{\partial x}\left(\int_{x_0}^{x}B_y(x,y,z)\;\mathrm{d}x\right) \tag{C.13}$$

$$=B_y. \tag{C.14}$$

Similarly, one finds for the z-component of $\nabla\times\boldsymbol{A}$:

$$(\nabla\times\boldsymbol{A})_z=\frac{\partial A_y}{\partial x}-\frac{\partial A_x}{\partial y} \tag{C.15}$$

$$=\frac{\partial}{\partial x}\left(\int_{x_0}^{x}B_z(x,y,z)\;\mathrm{d}x\right)-0 \tag{C.16}$$

$$=B_z. \tag{C.17}$$

Finally, checking the x-component yields:

$$(\nabla\times\boldsymbol{A})_x=\frac{\partial A_z}{\partial y}-\frac{\partial A_y}{\partial z} \tag{C.18}$$

$$=\frac{\partial}{\partial y}\left(\int_{y_0}^{y}B_x(x_0,y,z)\;\mathrm{d}y-\int_{x_0}^{x}B_y(x,y,z)\;\mathrm{d}x\right)-\frac{\partial}{\partial z}\int_{x_0}^{x}B_z(x,y,z)\;\mathrm{d}x \tag{C.19}$$

$$=B_x(X_0,y,z)-\int_{x_0}^{x}\left(\frac{\partial B_y(x,y,z)}{\partial y}+\frac{\partial B_z(x,y,z)}{\partial z}\right)\mathrm{d}x. \tag{C.20}$$

Note that since $\boldsymbol{B}$ is solenoidal, one has

$$\frac{\partial B_x(x,y,z)}{\partial x}+\frac{\partial B_y(x,y,z)}{\partial y}+\frac{\partial B_z(x,y,z)}{\partial z}=0. \tag{C.21}$$

With this, the second term above can be rewritten, which leads to

$$(\nabla \times \boldsymbol{A})_x = B_x(x_0, y, z) + \int_{x_0}^{x} \frac{\partial B_x(x, y, z)}{\partial x}\, \mathrm{d}x \tag{C.22}$$

$$= B_x(x_0, y, z) + B_x(x, y, z) - B_x(x_0, y, z) \tag{C.23}$$

$$= B_x(x, y, z). \tag{C.24}$$

Thus, as desired, one finds that $\boldsymbol{B} = \nabla \times \boldsymbol{A}$. Note that this vector potential is by no means unique. Generally, there are many different vector potentials which can be constructed for a solenoidal field. To guarantee uniqueness, a condition on the divergence of $\boldsymbol{A}$ must be imposed. This is called a gauge. A common gauge is the Coulomb gauge, which is $\nabla \cdot \boldsymbol{A} = 0$.

D

The Green's function

D.1. Motivation

Green's functions area powerful tool for solving differential equations. By determining the Green's function, the problem can be solved easily for any forcing right-hand side. It relies on the principle of superposition: by determining the response to a unit impulse, and viewing the forcing function as many unit impulses, one can find the solution. To understand how this works, it is illustrative to first consider a linear system of equations:

$$A\boldsymbol{x} = \boldsymbol{b}. \tag{D.1}$$

Instead of solving this system by a common linear algebra method, rewrite the right-hand side so it is represented as the sum:

$$\boldsymbol{b} = b_1\boldsymbol{e}_1 + \cdots + b_n\boldsymbol{e}_n, \tag{D.2}$$

where $\boldsymbol{e}_i$ are unit vectors. Now consider n separate problems:

$$A\boldsymbol{x} = \boldsymbol{e}_i, \quad i = 1, \ldots, n. \tag{D.3}$$

Each of these problems has a solution $\boldsymbol{x}_i$. Note that the subscript does not refer to the component of the vector in this case. Since the entire system is linear, the solution to the problem is simply:

$$\boldsymbol{x} = b_1\boldsymbol{x}_1 + \cdots + b_n\boldsymbol{x}_n. \tag{D.4}$$

Thus, by knowing the vectors $\boldsymbol{x}_1, \ldots, \boldsymbol{x}_n$, it is easy to find the solution for any right-hand side $\boldsymbol{b}$. Of course, these vectors are simply the columns of the inverse A^{-1}. However, this idea of solving for a unit impulse and then applying the principle of superposition carries over to the differential equations at hand.

Consider a one-dimensional problem of the following form: find $u(x)$ such that

$$Lu = f, \quad x \in [0, l], \tag{D.5}$$

where L is a linear differential operator, and f is a forcing function, and subject to some specified boundary conditions. The Green's function $G(x, x_0)$ is found by solving

$$L^\dagger G = \delta(x - x_0). \tag{D.6}$$

Here, $\delta(x - x_)$ is the Dirac delta function. It represents a unit impulse at $x = x_0$. In other words, it is zero everywhere, except at x_0, where it is 'infinite'. Of course, there is no function which satisfies this, and as such the Dirac delta function is really a distribution, which makes sense only under integration:

$$\int_{-\infty}^{\infty} \delta(x - x_0)\ \mathrm{d}x = 1. \tag{D.7}$$

There are many ways of constructing the Dirac delta function. For example,

$$\delta(x - x_0) = \lim_{\xi \to 0} \begin{cases} \dfrac{1}{2\xi} & x_0 - \xi < x < x_0 + \xi \\ 0 & \text{elsewhere} \end{cases} \tag{D.8}$$

A useful property of the Dirac delta function is the sifting property. Taking the inner product of the Dirac delta function with another function $f(x)$ yields the value of f at x_0. In other words, the delta function 'sifts' out the value at x_0. To see this, consider:

$$\langle f(x), \delta(x-x_0)\rangle = \int_{-\infty}^{\infty} f(x)\delta(x-x_0)\ \mathrm{d}x \tag{D.9}$$

$$= \lim_{\xi\to 0}\int_{x_0-\xi}^{x_0+\xi} \frac{f(x)}{2\xi}\ \mathrm{d}x \tag{D.10}$$

$$= \lim_{\xi\to 0}\frac{1}{2\xi}\int_{x_0-\xi}^{x_0+\xi} f(x)\ \mathrm{d}x \tag{D.11}$$

$$= \lim_{\xi\to 0}\frac{1}{2\xi} 2\xi f(\tilde{x})\ \mathrm{d}x \tag{D.12}$$

$$= f(x_0), \tag{D.13}$$

where the mean-value theorem yields $\tilde{x}$, which is then squeezed to x_0 as $\xi \to 0$.

With this property, the usefulness of the Green's function becomes apparent. Considering D.6, and taking the inner product of both sides with the Green's function G, one finds:

$$\langle Lu, G\rangle = \langle f, G\rangle. \tag{D.14}$$

Filling in the adjoint of L in the left-hand side, and using D.5, then yields

$$\langle u, L^\dagger G\rangle = \langle f, G\rangle \tag{D.15}$$

$$\langle u, \delta(x-x_0)\rangle = \langle f, G\rangle. \tag{D.16}$$

Finally, by the sifting property, this yields

$$u(x_0) = \langle f, G\rangle. \tag{D.17}$$

Thus, noting that the variables x and x_0 can be interchanged, the solution at any point x_0 can be found:

$$u(x_0) = \int_0^l f(x)G(x,x_0)\ \mathrm{d}x. \tag{D.18}$$

Thus, by knowing the Green's function, one can solve the problem for any forcing function $f(x)$ with a simple integration. This technique can be applied to higher-dimensional problems as well. Note that it in the some derivations, a different sign convention is chosen, i.e. the Green's function satisfies

$$L^\dagger G = -\delta(x-x_0). \tag{D.19}$$

D.2. Derivation of the Green's function G_0 for the Laplace Equation

The Laplace equation in three dimensions is given by

$$\Delta u(\boldsymbol{x}) = 0. \tag{D.20}$$

Thus the Green's function $G_0(\boldsymbol{x}, \boldsymbol{x}_0)$ must satisfy

$$\Delta G_0(\boldsymbol{x}, \boldsymbol{x}_0) = -\delta(\boldsymbol{x}-\boldsymbol{x}_0). \tag{D.21}$$

Due to the symmetry of the Laplace equation, which is unchanged by a coordinate change, the Green's function is expected to depend solely on the distance to the source point, given by $r = |\boldsymbol{x}-\boldsymbol{x}_0|$. Let Ω be a sphere centered on $\boldsymbol{x}_0$ and with radius r. Denote the surface of the sphere by $\partial\Omega$. Integrating the equation over this sphere yields

$$\int_\Omega \Delta G_0(\boldsymbol{x}, \boldsymbol{x}_0)\ \mathrm{d}\boldsymbol{x} = \int_\Omega -\delta(\boldsymbol{x}-\boldsymbol{x}_0)\ \mathrm{d}\boldsymbol{x}. \tag{D.22}$$

The right-hand side is equal to -1 by the properties of the Dirac delta function. The left hand side can be rewritten using Gauß' theorem:

$$\int_\Omega \Delta G_0(\boldsymbol{x}, \boldsymbol{x}_0)\ \mathrm{d}\boldsymbol{x} = \int_{\partial\Omega} \nabla G_0(\boldsymbol{x}, \boldsymbol{x}_0)\cdot \boldsymbol{n}\ \mathrm{d}S \tag{D.23}$$

$$= \int_{\partial\Omega} \frac{\partial G_0(\boldsymbol{x}, \boldsymbol{x}_0)}{\partial \boldsymbol{n}}\ \mathrm{d}S \tag{D.24}$$

$$= \frac{\partial G_0(\boldsymbol{x}, \boldsymbol{x}_0)}{\partial \boldsymbol{n}} 4\pi r^2. \tag{D.25}$$

Equating the left- and right-hand side then yields:

$$\frac{\partial G_0(\boldsymbol{x},\boldsymbol{x}_0)}{\partial \boldsymbol{n}} 4\pi r^2 = -1 \tag{D.26}$$

$$\Rightarrow \frac{\partial G_0(\boldsymbol{x},\boldsymbol{x}_0)}{\partial \boldsymbol{n}} = \frac{-1}{4\pi r^2} \tag{D.27}$$

$$\Rightarrow G_0(\boldsymbol{x},\boldsymbol{x}_0) = \frac{1}{4\pi r} = \frac{1}{4\pi|\boldsymbol{x}-\boldsymbol{x}_0|}. \tag{D.28}$$

This is the free space Green's function for the Laplace Equation.

D.3. Derivation of the Green's function G_1 for the Helmholtz equation

The derivation of the free space Green's is slightly more involved than the derivation above. As such, it will not be reproduced here. Instead, the reader is referred to one of the textbooks covering this topic, such as for example [24, p. 791].

The free space Green's function for the Helmholtz equation is found to be:

$$G_1(\boldsymbol{r},\boldsymbol{r}') = \frac{1}{4\pi|\boldsymbol{r}-\boldsymbol{r}'|} e^{-jk|\boldsymbol{r}-\boldsymbol{r}'|}. \tag{D.29}$$

E

Function spaces

To describe and solve eddy current problems, a strong mathematical foundation is necessary. The following description of the function spaces and operators involved is adapted from [40], which gives a complete overview of the mathematics required for these types of problems.

Several well-known function spaces which will be used are given here. Let Ω denote a measurable domain, which in this context generally will be three dimensional. The space of infinitely differentiable functions with compact support is denoted by $\mathscr{D}(\Omega)$. The Lebesgue spaces $\mathscr{L}^p(\Omega)$ are defined as the space of all measurable functions[1] for which

$$\int_\Omega |u|^p \, \mathrm{d}\boldsymbol{x} < \infty \qquad \text{for } 1 \le p < \infty, \tag{E.1}$$

$$\sup_{\boldsymbol{x}\in\Omega} |u| < \infty \qquad \text{for } p = \infty. \tag{E.2}$$

The Lebesgue spaces are Banach spaces, equipped with the standard norms:

$$\|u\|_{\mathscr{L}^p(\Omega)} := \left(\int_\Omega |u|^p \, \mathrm{d}\boldsymbol{x} \right)^{\frac{1}{p}} \qquad \text{for } 1 \le p < \infty, \tag{E.3}$$

$$\|u\|_{\mathscr{L}^\infty(\Omega)} := \sup_{\boldsymbol{x}\in\Omega} |u| \qquad \text{for } p = \infty. \tag{E.4}$$

The Sobolev space $\mathscr{W}^{m,p}(\Omega)$ is the subspace of $\mathscr{L}^p(\Omega)$ for which the first m derivatives are also in $\mathscr{L}^p(\Omega)$:

$$\mathscr{W}^{m,p}(\Omega) := \left\{ u \in \mathscr{L}^p(\Omega) : \frac{\partial^{|\alpha|} u}{\partial x_1^{\alpha_1} \partial x_2^{\alpha_2} \partial x_3^{\alpha_3}} \in \mathscr{L}^p(\Omega),\ |\alpha| \le m \right\}, \tag{E.5}$$

where $|\alpha| = \alpha_1 + \alpha_2 + \alpha_3$ and each α is non-negative. The Sobolev spaces are Banach spaces, with the following norms:

$$\|u\|_{\mathscr{W}^{m,p}(\Omega)} := \left(\sum_{|\alpha|\le m} \left\| \frac{\partial^{|\alpha|} u}{\partial x_1^{\alpha_1} \partial x_2^{\alpha_2} \partial x_3^{\alpha_3}} \right\|^p_{\mathscr{L}^p(\Omega)} \right)^{\frac{1}{p}} \qquad \text{for } 1 \le p < \infty, \tag{E.6}$$

$$\|u\|_{\mathscr{W}^{m,\infty}(\Omega)} := \sup_{|\alpha|\le m} \left\| \frac{\partial^{|\alpha|} u}{\partial x_1^{\alpha_1} \partial x_2^{\alpha_2} \partial x_3^{\alpha_3}} \right\|_{\mathscr{L}^\infty(\Omega)} \qquad \text{for } p = \infty. \tag{E.7}$$

The case when $p = 2$ is special, since in this case the Lebesgue and Sobolev spaces become Hilbert spaces, with the standard inner product. The Hilbert space $\mathscr{W}^{m,2}(\Omega)$ will be denoted by $\mathscr{H}^m(\Omega)$. Finally, for

In the context of electromagnetism, the div and $\boldsymbol{curl}$ operators are regularly used, as can be seen in Maxwell's equations. For this, the spaces $\mathscr{H}(\mathrm{div},\Omega)$ and $\mathscr{H}(\boldsymbol{curl},\Omega)$ are useful. These space $\mathscr{H}(\mathrm{div},\Omega)$ is defined as:

$$\mathscr{H}(\mathrm{div},\Omega) := \{ u \in \mathscr{L}^2(\Omega) : \nabla \cdot u \in \mathscr{L}^2(\Omega) \}, \tag{E.8}$$

[1] Note that strictly speaking, the Lebesgue spaces are spaces of function equivalence classes, not functions, and as such the essential supremum must be used for the infinity-norm.

which is a Hilbert space, with inner product defined as

$$(\boldsymbol{u},\boldsymbol{v})_{\mathscr{H}(\mathrm{div},\Omega)} \coloneqq \int_\Omega \boldsymbol{u}\cdot\overline{\boldsymbol{v}}\,\mathrm{d}\boldsymbol{x} + \int_\Omega \nabla\cdot\boldsymbol{u}\,\nabla\cdot\overline{\boldsymbol{v}}\,\mathrm{d}\boldsymbol{x}, \tag{E.9}$$

and its norm defined as

$$\|\boldsymbol{v}\|_{\mathscr{H}(\mathrm{div},\Omega)} \coloneqq (\|\boldsymbol{v}\|^2_{\mathscr{L}^2(\Omega)} + \|\nabla\cdot\boldsymbol{v}\|^2_{\mathscr{L}^2(\Omega)})^{\frac{1}{2}}. \tag{E.10}$$

Similarly, the space $\mathscr{H}(\boldsymbol{curl},\Omega)$ is defined as

$$\mathscr{H}(\boldsymbol{curl},\Omega) \coloneqq \{u\in\mathscr{L}^2(\Omega) : \nabla\times u\in\mathscr{L}^2(\Omega)\}, \tag{E.11}$$

which is a Hilbert space, with inner product defined as

$$(\boldsymbol{u},\boldsymbol{v})_{\mathscr{H}(\boldsymbol{curl},\Omega)} \coloneqq \int_\Omega \boldsymbol{u}\cdot\overline{\boldsymbol{v}}\,\mathrm{d}\boldsymbol{x} + \int_\Omega \nabla\times\boldsymbol{u}\cdot\nabla\times\overline{\boldsymbol{v}}\,\mathrm{d}\boldsymbol{x}, \tag{E.12}$$

and its norm defined as

$$\|\boldsymbol{v}\|_{\mathscr{H}(\boldsymbol{curl},\Omega)} \coloneqq (\|\boldsymbol{v}\|^2_{\mathscr{L}^2(\Omega)} + \|\nabla\times\boldsymbol{v}\|^2_{\mathscr{L}^2(\Omega)})^{\frac{1}{2}}. \tag{E.13}$$

So far, the spaces have been defined on an arbitrary measurable space Ω. For the case of eddy current problems, the domain generally consists of a conductive object in a non-conductive region, both three-dimensional. From now on, let Ω now denote the domain of a conductive material, and denote by Γ the boundary of Ω, which is assumed to be smooth and with outward unit normal $\boldsymbol{n}$. For the moment, it is assumed that Ω is open, bounded and connected. Let Ω_{ext} denote the non-conductive domain, that is the complement of the closure of Ω, i.e. $\Omega_{\mathrm{ext}} = \mathbb{R}^3\setminus\overline{\Omega}$.

For functions which are discontinuous over the boundary Γ, it is necessary to denote the inner and outer restriction. Consider a function u, defined in $\mathbb{R}^3$, of which the restriction to Ω is continuous (and which admits a continuous extension on Γ). The inner restriction of u to Γ is denoted by u^-, and similarly the outer restriction of u to Γ is denoted by u^+, i.e. for $\boldsymbol{x}\in\Gamma$:

$$u^-(\boldsymbol{x}) = \lim_{\delta\downarrow 0} u(\boldsymbol{x}-\delta\boldsymbol{n}(\boldsymbol{x})), \tag{E.14}$$

$$u^+(\boldsymbol{x}) = \lim_{\delta\downarrow 0} u(\boldsymbol{x}+\delta\boldsymbol{n}(\boldsymbol{x})). \tag{E.15}$$

The jump between the inner and outer restriction is denoted by $[u]_\Gamma \coloneqq u^+ - u^-$.

This description of space as consisting of a conductive and non-conductive region, combined with the function spaces defined above, facilitates a useful description of the interface conditions between the conductive and non-conductive region. For a vector function $\boldsymbol{u}:\mathbb{R}^3\mapsto\mathbb{C}^3$:

- If $\boldsymbol{u}|_\Omega\in\mathscr{H}(\mathrm{div},\Omega)$ and $\boldsymbol{u}|_{\Omega_{\mathrm{ext}}}\in\mathscr{H}(\mathrm{div},\Omega_{\mathrm{ext}})$, then $\boldsymbol{u}\in\mathscr{H}(\mathrm{div},\mathbb{R}^3)$ if and only if $[\boldsymbol{u}\cdot\boldsymbol{n}]_\Gamma = 0$.
- If $\boldsymbol{u}|_\Omega\in\mathscr{H}(\boldsymbol{curl},\Omega)$ and $\boldsymbol{u}|_{\Omega_{\mathrm{ext}}}\in\mathscr{H}(\boldsymbol{curl},\Omega_{\mathrm{ext}})$, then $\boldsymbol{u}\in\mathscr{H}(\boldsymbol{curl},\mathbb{R}^3)$ if and only if $[\boldsymbol{u}\times\boldsymbol{n}]_\Gamma = 0$.

The following characterisations of the kernel of the div and $\boldsymbol{curl}$ operators will also be of use in modelling the Maxwell Equations:

- If $\boldsymbol{u}\in\mathscr{H}(\mathrm{div},\mathbb{R}^3)$ such that $\nabla\cdot\boldsymbol{u}=0$, then there exists a vector $\boldsymbol{v}\in\mathscr{W}^1(\mathbb{R}^3)$ such that $\boldsymbol{u}=\nabla\times\boldsymbol{v}$. Applying the Coulomb Gauge, $\nabla\cdot\boldsymbol{v}=0$, ensures that $\boldsymbol{v}$ is unique.
- If $\boldsymbol{u}\in\mathscr{H}(\boldsymbol{curl},\mathbb{R}^3)$ such that $\nabla\times\boldsymbol{u}=0$, then there exists a unique $\phi\in\mathscr{W}^1(\mathbb{R}^3)$ such that $\boldsymbol{u}=\nabla\phi$.

Bibliography

[1] M. Abramowitz, I. A. Stegun, and R. H. Romer. *Handbook of mathematical functions with formulas, graphs, and mathematical tables*. American Association of Physics Teachers, 1988.

[2] G. B. Arfken and H. Weber. *Mathematical methods for physicists*. Academic Press Harcourt Brace Jovanovich, San Diego, 1967.

[3] A. Babin and A. Figotin. *Neoclassical Theory of Electromagnetic Interactions*. Springer, 2016.

[4] I. Babuška and A. K. Aziz. On the angle condition in the finite element method. *SIAM Journal on numerical analysis*, 13(2):214–226, 1976.

[5] O. Biro and K. Preis. On the use of the magnetic vector potential in the finite-element analysis of three-dimensional eddy currents. *IEEE Transactions on magnetics*, 25(4):3145–3159, 1989.

[6] M. Birsan and R. Tan. The effect of roll and pitch motion on ship magnetic signature. *Journal of Magnetics*, 21(4):503–508, 2016.

[7] A. Bondeson, T. Rylander, and P. Ingelström. *Computational Electromagnetics*. Springer, 2012.

[8] A. Bossavit. The computation of eddy-currents, in dimension 3, by using mixed finite elements and boundary elements in association. *Mathematical and Computer Modelling*, 15(3-5):33–42, 1991.

[9] A. Buffa, H. Ammari, and J. Nédélec. A justification of eddy currents model for the Maxwell equations. *SIAM Journal on Applied Mathematics*, 60(5):1805–1823, 2000.

[10] C. J. Carpenter. Comparison of alternative formulations of 3-dimensional magnetic-field and eddy-current problems at power frequencies. In *Proceedings of the Institution of Electrical Engineers*, volume 124, pages 1026–1034. IET, 1977.

[11] J. M. D. Coey. *Magnetism and Magnetic Materials*. Cambridge University Press, 2009.

[12] C. Emson and J. Simkin. An optimal method for 3-D eddy currents. *IEEE Transactions on Magnetics*, 19 (6):2450–2452, 1983.

[13] R. D. Graglia. On the numerical integration of the linear shape functions times the 3-d green's function or its gradient on a plane triangle. *IEEE transactions on antennas and propagation*, 41(10):1448–1455, 1993.

[14] D. J. Griffiths. *Introduction to Electrodynamics (Fourth Edition)*. Cambridge University Press, 2017.

[15] J. J. Holmes. *Exploitation of a Ship's Magnetic Field Signatures*. Morgan & Claypool, 2006.

[16] J. J. Holmes. *Modeling a Ship's Ferromagnetic Signatures*. Morgan & Claypool, 2007.

[17] J. J. Holmes. *Reduction of a Ship's Magnetic Field Signatures*. Morgan & Claypool, 2008.

[18] K. Ishibashi. A least residual approach for 3-d eddy current analysis by bem. *IEEE transactions on magnetics*, 29(2):1512–1515, 1993.

[19] J. D. Jackson. *Classical Electrodynamics (Third Edition)*. Wiley, 1999.

[20] E. Kubatko. Matlab central file exchange: quadtriangle, 2021. URL `https://nl.mathworks.com/matlabcentral/fileexchange/72131-quadtriangle`.

[21] F. Matsuoka and A. Kameari. Calculation of three dimensional eddy current by FEM-BEM coupling method. *IEEE Transactions on Magnetics*, 24(1):182–185, 1988.

[22] G. Meunier, J. Guichon, O. Chadebec, B. Bannwarth, L. Krähenbühl, and C. Guérin. Unstructured–PEEC method for thin electromagnetic media. *IEEE Transactions on Magnetics*, 56(1):1–5, 2019.

[23] T. Morisue and M. Fukumi. 3-d eddy current calculations using the magnetic vector potential. *IEEE Transactions on magnetics*, 24(1):106–109, 1988.

[24] P. M. Morse and H. Feshbach. Methods of theoretical physics. *American Journal of Physics*, 22(6):410–413, 1954.

[25] G. Mur. Edge elements, their advantages and their disadvantages. *IEEE transactions on magnetics*, 30(5): 3552–3557, 1994.

[26] J. R. Nagel. Induced eddy currents in simple conductive geometries: mathematical formalism describes the excitation of electrical eddy currents in a time-varying magnetic field. *IEEE Antennas and Propagation Magazine*, 60(1):81–88, 2017.

[27] NATO STO Technical Report. Signature management system for underwater signatures of surface ships, TR-SET-166, 2015.

[28] J. Nédélec. Mixed finite elements in R3. *Numerische Mathematik*, 35(3):315–341, 1980.

[29] Q. Phan, G. Meunier, O. Chadebec, J. Guichon, and B. Bannwarth. BEM-FEM formulation based on magnetic vector and scalar potentials for eddy current problems. In *2019 19th International Symposium on Electromagnetic Fields in Mechatronics, Electrical and Electronic Engineering (ISEF)*, pages 1–2. IEEE, 2019.

[30] Q. Phan, G. Meunier, O. Chadebec, J. Guichon, and B. Bannwarth. 3d eddy currents computation by bem using the modified magnetic vector potential and the reduced magnetic scalar potential. *International Journal of Numerical Modelling: Electronic Networks, Devices and Fields*, 33(5):e2642, 2020.

[31] P. Polański and F. Szarkowski. Simulations and measurements of eddy current magnetic signatures. *Scientific Journal of Polish Naval Academy*, 215(4):77–102, 2018.

[32] Z. Ren, F. Bouillault, A. Razek, and J. C. Vérité. Comparison of different boundary integral formulations when coupled with finite elements in three dimensions. *IEE Proceedings A (Physical Science, Measurement and Instrumentation, Management and Education, Reviews)*, 135(8):501–507, 1988.

[33] Z. Ren, F. Bouillault, A. Razek, A. Bossavit, and J. C. Vérité. A new hybrid model using electric field formulation for 3-d eddy current problems. *IEEE Transactions on magnetics*, 26(2):470–473, 1990.

[34] P. Robert, M. Ito, and T. Takahashi. Numerical solution of three dimensional transient eddy current problems by the a-phi method. *IEEE transactions on magnetics*, 28(2):1166–1169, 1992.

[35] P. R. Rony. The electromagnetic levitation of metals. 1964.

[36] M. E. Royak, I. M. Stupakov, and N. S. Kondratyeva. Coupled vector fem and scalar bem formulation for eddy current problems. In *2016 13th International Scientific-Technical Conference on Actual Problems of Electronics Instrument Engineering (APEIE)*, volume 2, pages 330–335. IEEE, 2016.

[37] J. Shewchuck. What is a good linear finite element. *Interpolation, Conditioning, Anisotropy, and Quality Measures. (unpublished extended version)*, 2002. URL `https://people.eecs.berkeley.edu/~jrs/papers/elemj.pdf`.

[38] D. H. Staelin. *Electromagnetics and applications*. Massachusetts Institute of Technology, 2011.

[39] S. P. Thompson. *Polyphase electric currents and alternate-current motors*. Spon & Chamberlain, 1900.

[40] R. Touzani and J. Rappaz. *Mathematical Models for Eddy Currents and Magnetostatics*. Springer, 2014.

[41] H. Tsuboi and M. Tanaka. Three-dimensional eddy current analysis by the boundary element method using vector potential. *IEEE transactions on magnetics*, 26(2):454–457, 1990.

[42] H. Unz. Scalar-vector analog of green's theorem. *IRE Transactions on Antennas and Propagation*, 6(3): 300–300, 1958.

[43] I. Vágó. On the interface and boundary conditions of electromagnetic fields. *Periodica Polytechnica Electrical Engineering (Archives)*, 38(2):79–94, 1994.

[44] W.O.C. Ward. Matlab central file exchange: icosphere, 2015. URL `https://nl.mathworks.com/matlabcentral/fileexchange/50105-icosphere`.

[45] J. P. Webb. Edge elements and what they can do for you. *IEEE Transactions on magnetics*, 29(2):1460–1465, 1993.

[46] E. X. Xu and J. Simkin. Total and reduced magnetic vector potentials and electrical scalar potential for eddy current calculation. *IEEE transactions on magnetics*, 40(2):938–940, 2004.

[47] A. Zangwill. *Modern electrodynamics*. Cambridge University Press, 2013.

[48] D. Zheng. Three-dimensional eddy current analysis by the boundary element method. *IEEE transactions on Magnetics*, 33(2):1354–1357, 1997.